Intercellular transport of RNA can limit heritable epigenetic changes

Authors: Nathan Shugarts[1], Andrew L. Yi[1], Winnie M. Chan[1], Julia A. Marré[1], Aishwarya Sathya[1], and Antony M. Jose[1*]

Affiliations:

[1]Department of Cell Biology and Molecular Genetics, University of Maryland, College Park, MD 20742, USA.

*Correspondence to: amjose@umd.edu

Abstract: RNAs in circulation carry sequence-specific regulatory information between cells in animal, plant, and host-pathogen systems. Double-stranded RNA (dsRNA) delivered into the extracellular space of the nematode *C. elegans* accumulates within the germline and reaches progeny. Here we provide evidence for spatial, temporal, and substrate specificity in the transport of dsRNA from parental circulation to progeny. Temporary loss of dsRNA transport resulted in the persistent accumulation of mRNA from a germline gene. The expression of this gene varied among siblings and even between gonad arms within one animal. Perturbing RNA regulation of the gene created new epigenetic states that lasted for many generations. Thus, one role for the transport of dsRNA into the germline in every generation is to limit heritable changes in gene expression.

One Sentence Summary: RNA from parental circulation reduces heritable changes in gene expression.

Main text: RNAs released into circulation can act as intercellular messages that are used for gene regulation in distant cells. Specific examples include secretion of exosomal small RNAs in response to pathogenic fungal infection in *Arabidopsis* (*1*), virus-like proteins with their coding mRNAs in developing *Drosophila* (*2*) and mice (*3*), microRNAs from adipose tissue in mice (*4*), and small RNAs from the epididymis in mice (*5-8*). Such extracellular RNAs have also been

detected in humans, but their roles in gene regulation remain unclear despite their use as a diagnostic tool for diseases (reviewed in (*9*)). Furthermore, the recent development of double-stranded RNA (dsRNA)-based drugs (reviewed in (*10-11*)) that can silence genes of matching sequence through RNA interference (*12*) has heightened interest in understanding the import of dsRNA into cells. A conserved dsRNA-selective importer, SID-1 (*13-15*), is required for the import of extracellular dsRNA into the cytosol of any cell in the nematode *C. elegans*. SID-1 has two homologs in mammals – SIDT1 and SIDT2. Although entry of ingested dsRNA into cells through SIDT1 (*16*), which can enhance dsRNA uptake when overexpressed *in vitro* (*17*), and entry of viral dsRNA through SIDT2 (*18*) have been reported in mice, alternative roles for these mammalian homologs in the uptake of cholesterol have also been proposed (*19*).

Secretion of dsRNA from *C. elegans* tissues that express dsRNA has been inferred based upon the SID-1-dependent silencing of matching genes in other tissues (*13, 20*). Secreted dsRNA from neurons can silence genes of matching sequence in most somatic cells (*21*) and within the germline (*22*). Extracellular dsRNA delivered into parental circulation by injection or ingestion also enters the germline and can cause silencing of matching genes in progeny (*12, 23-26*). Such intergenerational transport of RNA is an attractive mechanism for explaining gene-specific effects in progeny that could occur in response to changes in somatic tissues of parents. However, which conditions induce transport of dsRNA into the germline, when during development this transport occurs, and what the regulatory consequences are for such intercellular transport of dsRNA are all unknown.

Here we use oxidative damage in neurons expressing dsRNA or exposure to bacteria expressing dsRNA to demonstrate that dsRNA from parental circulation causes maximal silencing of germline gene expression during later development and in the proximal germline.

Entry into the parental germline and subsequent transport in progeny occurs through two different intergenerational routes with distinct substrate specificities. Loss of dsRNA import through SID-1 alters the expression of a germline gene, inducing large changes in expression that can persist for many generations despite the restoration of dsRNA transport in descendants. The expression of this gene can vary between gonad arms and perturbing its RNA regulation can result in either reduced or increased expression. These changes in gene expression last for many generations, suggesting that loss of dsRNA transport induces new heritable epigenetic states.

Oxidative damage in neurons expressing dsRNA enhances silencing in the germline by neuronal dsRNA

To modulate the secretion of dsRNA from somatic cells into parental circulation during development, we adapted an approach for damaging somatic cells (*27*). Specifically, we generated animals that express the mini singlet oxygen generator (miniSOG) protein in neurons and exposed them to blue light. While animals expressing miniSOG from a single-copy transgene did not show an appreciable defect when compared with wild-type animals, those expressing miniSOG from a multi-copy transgene were paralyzed (Fig. S1A and S1B, *top*) and had visibly damaged neurons (Fig. S1B, *bottom*). Using this system, we induced oxidative damage in the neurons of animals that expressed dsRNA under the control of a neuronal promoter and evaluated silencing of target genes with matching sequence expressed in other tissues (Fig. 1A). By exposing animals to blue light for 60 minutes at different times during development (Fig. S1C), we observed SID-1-dependent enhancement in the silencing of the hypodermal gene *bli-1* in the adult stage by neuronal *bli-1*-dsRNA, with maximal silencing when oxidative damage occurred during mid-to-late larval development (Fig. S1D, light exposure from 42 to 66 hours post L4-stage of parent; Fig. S1E, ~2-fold increase from 14.9% to 29.1% in a

background with **e**nhanced **R**NA **i**nterference (*eri-1(-)*) and ~6-fold increase from ~1.6% to ~9.8% in a wild-type background). A similar period of maximal SID-1-dependent enhancement of silencing was also observed when neurons expressing *gfp*-dsRNA were damaged and silencing of a two-gene operon that expresses two fluorescent proteins, mCherry::H2B and GFP::H2B, in the germline was measured (Fig. 1B, Fig. 1C, Fig. 1D, Fig. S1F – 48 to 60 hours post L4-stage of parent, *sid-1(-)* allele (*jam80[non]*) depicted in Fig. S2). While silencing of *gfp::h2b* was observed throughout the germline, silencing of the other cistron *mCherry::h2b* was often restricted to regions of the germline. Silencing of *mCherry::h2b* was most frequent in the proximal germline and was not observed in any other region without silencing in the proximal germline (proximal germline - 57%, distal germline - 47%, sperm - 29%, Fig. 1D), likely due to reduction of *mCherry::h2b::gfp::h2b* pre-mRNA (*28*). The pattern of *mCherry::h2b* silencing is similar to the spatial pattern observed for the RME-2-dependent entry of dsRNA delivered into the parental circulation (*25*) and is consistent with the pattern of mRNA degradation in the germline by extracellular dsRNA (*29*).

These results suggest two insights into the transport of dsRNA from neurons to other tissues: (1) oxidative damage of neurons during particular periods in development increases the amount of dsRNA and/or changes the kinds of dsRNA in circulation either because of specific enhancement of secretion or nonspecific spillage; and (2) there is a preference for the entry of neuronal dsRNA into the proximal germline. These temporal and/or spatial preferences for silencing could be because of unknown characteristics of the exported neuronal dsRNA (e.g., modifications, lengths, structures, etc.) that influence import or subsequent silencing – a hypothesis that is also supported by the different requirements for silencing by neuronal *gfp*-

dsRNA compared to other sources of *gfp*-dsRNA (*21*). Alternatively, these preferences could reflect universal constraints for any extracellular dsRNA in *C. elegans*.

Requirements for the entry of extracellular dsRNA into the germline vary during development

Another convenient method for the delivery of extracellular dsRNA into *C. elegans* at various times during larval development is the expression of dsRNA in the bacteria that worms ingest as food (*23*). To determine when ingested dsRNA can enter the germline and cause silencing, we exposed developing animals with a ubiquitously expressed protein (GTBP-1) tagged with GFP to bacteria that express *gfp*-dsRNA. Silencing was detectable within the germline from the second larval stage (L2) onwards (Fig. 1E, Fig. S3A), but exposure to ingested dsRNA beyond the fourth larval stage (L4) (Fig. 1F) or, alternatively, injection of dsRNA into the 1-day old adult germline (Fig. S3B) was required for silencing in the germline of 3-day old adults. The need for exposure to dsRNA during late development to observe persistent silencing suggests recovery of expression within the germline despite detectable silencing until the L4-stage. Combined with the need for exposure to dsRNA after the L4 stage for silencing in progeny (*25-26*), these observations suggest that heritable RNA silencing is not effectively initiated during early development of the germline despite dsRNA entry and subsequent silencing. However, a 24-hour pulse of dsRNA exposure beginning at the L4 stage was sufficient for heritable silencing (Fig. S4A) (*25*). This early window for heritable silencing likely relies on entry of dsRNA into the proximal germline because (1) silencing of a somatic gene in progeny after parental ingestion of dsRNA required RME-2 (Fig. S4A), which is enriched in the proximal germline (Fig. S4B) (*30*); and (2) some *gtbp-1::gfp* animals exposed to *gfp*-dsRNA until the first day of adulthood showed selective silencing in the proximal germline (Fig. S3C).

Together, these results reveal three periods of germline development that can be broadly distinguished based on silencing in response to ingested and neuronal dsRNA: (1) from the first larval to the third larval stage when exposure to dsRNA does not result in maximal silencing within the germline in adults; (2) from the fourth larval stage to early adulthood when entry of dsRNA primarily occurs in the proximal germline through RME-2; and (3) later adulthood when entry can be independent of RME-2 (Fig. S4A) (*26*) and germline silencing by ingested dsRNA is maximal.

Different forms of dsRNA from parental circulation require different members of the transport pathway in developing progeny for silencing

When exposing animals to dsRNA expressed in bacteria, the forms of dsRNA made and processed in bacteria cannot be easily controlled. Microinjection of dsRNA into the pseudocoelom (*12*, *25*) provides a way to deliver particular forms of extracellular dsRNA into *C. elegans*, but can be most easily performed only using L4-staged and adult animals. We examined differences, if any, in the entry of *in vitro* transcribed dsRNA into the germline during these two stages as evidenced by silencing in progeny. Silencing was comparable regardless of whether wild-type or *rme-2(-)* parents were injected as L4-staged or adult animals (Fig. 2A, Fig. S4C, *left*; also reported for adults in (*26*)), although a weak requirement for RME-2 was discernable when lower concentrations of dsRNA were used (Fig. S4C, *right*). The difference in RME-2 requirement between ingested dsRNA and injected dsRNA could reflect parental circulation accumulating different amounts of dsRNA (e.g., more upon injection than upon ingestion) and/or different kinds of dsRNA (e.g., because of modifications in bacteria or upon transit through the intestine). However, these possibilities could not be easily distinguished because sensitive northern blotting (*31*) revealed that both bacterial and *in vitro* transcribed dsRNA consist of a

complex mix of dsRNAs (Fig. S4D, Fig. S4E, Fig. S4F; consistent with (*32-33*)), hereafter called mixed dsRNA. In contrast, when synthesized *gfp*-dsRNA of a defined length (50 bp) with a fluorescent label was injected into circulation in adult animals, no entry into the germline was observed in the absence of RME-2 (*25*). We found that silencing of *unc-22* in progeny by similarly synthesized but unlabeled 50-bp *unc-22*-dsRNA with a 5'-OH delivered into parental circulation also showed a strong requirement for RME-2 compared to mixed dsRNA (Fig. 2A). Further comparison between the two forms of dsRNA revealed that silencing in progeny by 50-bp dsRNA injected into parental circulation was detectably less efficient in somatic cells (Fig. 2B, Fig. S5A, Fig. S5B, *left*), even when ~14X more 50-bp dsRNA was delivered into parental circulation (Fig. S5B, *right*), and was also less efficient in the germline (Fig. 2B, Fig. S5A, Fig. S5C). Given that both 50-bp dsRNA and mixed dsRNA rely on the nuclear Argonaute HRDE-1 (*34*) for silencing within the germline (Fig. S5A, Fig. S5C) and can silence independent of the nuclear Argonaute NRDE-3 (*28*) in somatic cells (Fig. S5A, Fig. S5C), the observed difference in the extent of silencing could be the result of differences in the stability and/or intergenerational transport of 50-bp dsRNA versus mixed dsRNA. One relevant feature shared by mixed dsRNA generated in bacteria or *in vitro*, in addition to the diversity of lengths (Fig. S4), is that both forms contain 5' triphosphates. In support of the impact of 5' phosphates on transport and/or silencing, addition of 5' monophosphates to synthesized 50-bp dsRNA injected into parental circulation reduced the dependence on RME-2 for silencing in progeny (Fig. S4G, Fig. S4H). Thus, the requirements for entry into the germline and subsequent silencing vary for different lengths and/or chemical forms of dsRNA.

Fluorescently labeled 50-bp dsRNA delivered into parental circulation localized within intestinal cells in progeny (Fig. 2C, *top left*), as has been observed for vitellogenin proteins (*35*)

and fluorescent dyes (*36*). Accumulation of fluorescently-labeled dsRNA was also detected at the apical membrane of the intestine, which could reflect exocytosis of dsRNA into the lumen of developing intestinal cells. However, separation of the fluorescent label from dsRNA catalyzed by cellular enzymes cannot be excluded. Therefore, to dissect differences, if any, between the transport of short dsRNA (synthesized 50-bp with 5'OH) and mixed dsRNA (mixture transcribed *in vitro* using ~1 kb DNA template) we injected *unc-22*-dsRNA into animals with mutations in genes that play roles in the import of dsRNA. We found that maternal SID-1 was required for silencing by short dsRNA in progeny (Fig. 2C, *bottom*, left bars), suggesting that the SID-1-dependent entry of short dsRNA into the cytosol likely occurs in the injected parent or during early development in progeny. Uptake of dsRNA from the intestinal lumen requires SID-2, a transmembrane protein located in the apical membranes of intestinal cells (*37-38*). We found that SID-2 was not required for most silencing in progeny by short or mixed dsRNA injected into parental circulation (Fig. 2C, *top right* and *bottom*). Exit of dsRNA from intracellular vesicles requires SID-5, a transmembrane protein located in endolysosomal membranes (*39*). Silencing in wild-type animals was comparable to silencing in *sid-5(-)* animals (Fig. 2C, *top right*). However, when animals that lacked SID-1 were injected, SID-5 was required in progeny for silencing by mixed dsRNA from parental circulation (Fig. 2C, *bottom*, right bars; as also reported in (*26*)). Since dsRNA is expected to be present in vesicles upon entry through RME-2 in the absence of SID-1 (*25-26*), this observation suggests that SID-5 is required for the release of mixed dsRNA from inherited vesicles in progeny.

In summary, extracellular dsRNA can enter the germline in parents and be transmitted to progeny through two routes with different substrate selectivity. One route is preferentially used by short dsRNA and relies on RME-2-mediated endocytosis of dsRNA into oocytes, where early

exit from vesicles is required for silencing in progeny as evidenced by the need for maternal SID-1 (Fig. 2D, blue). The other route appears to exclude short dsRNA, but allows mixed dsRNA entry into the cytosol in the parental germline through SID-1 and exit from inherited vesicles in progeny through a process that requires both zygotic SID-1 and SID-5 (Fig. 2D, grey) (*26*).

Expression of SID-1 is consistent with a role in intergenerational transport of extracellular dsRNA but could be differentially regulated across cell types

Analysis of dsRNA transport into the germline and to progeny suggests developmental variation in the expression pattern of SID-1. Previous attempts at observing SID-1 localization relied on multi-copy transgenes (*13*), which can become silenced within the germline (*40*) and could produce a variety of tagged and untagged proteins (*41*). When using multi-copy transgenes to express a SID-1 fusion protein tagged at the C-terminus with DsRed or GFP (Fig. S6A) under the control of a promoter that drives expression within body-wall muscles, we observed intracellular localization of SID-1::DsRed or SID-1::GFP (Fig. S6B, *top*) along with rescue of gene silencing by ingested dsRNA in body-wall muscles (Fig. S6B, *bottom*). However, similar tagging to express SID-1 fusion proteins from either a single-copy transgene expressed in the germline (SID-1::DsRed) or the endogenous locus (SID-1::wrmScarlet) did not enable gene silencing by ingested dsRNA (Fig. S6C), suggesting that the C-terminal fusions of SID-1 were likely non-functional and that apparent function when using multi-copy transgenes reflects production of untagged variants. In support of our rationale, a recent prediction of SID-1 structure (*42*) suggests that the C-terminus is sequestered, a feature that may be disrupted by the addition of C-terminal fluorophores, potentially leading to misfolded proteins that are degraded. Consistently, we found that internal tagging of the *sid-1* gene using Cas9-mediated genome

editing to express SID-1::mCherry (Fig. 3A) resulted in a fusion protein with detectable function (Fig. 3B, Fig. S6D). Therefore, we analyzed fluorescence from this fusion protein expressed from the endogenous locus under the control of native regulatory sequences (Fig. 3C, Fig. 3D, Fig. S6E, Fig. S6F, Fig. S6G). Fluorescence from SID-1::mCherry progressively increased during development with tissue-specific enrichments in the developing embryo (Fig. 3C, *left*, Fig. S6G), becoming ubiquitous in hatched L1 larvae (Fig. 3C, *middle*). SID-1::mCherry was not easily detectable in the germline during larval development (Fig. 3C, *middle* and *right*), but was visible in the proximal and distal regions of the adult germline (Fig. 3D). Similarly, endogenous RME-2 was most abundant in the proximal oocytes of the adult germline (Fig. S4B) (*30*). These expression patterns are consistent with the entry of most dsRNA from circulation of adult parents into the proximal germline (*25*) and the activity of transport mechanisms in developing embryos (Fig. 2).

To determine if acute induction of SID-1 expression would be sufficient for the import of dsRNA into different cell types, we engineered the endogenous *sid-1* gene to transcribe a fusion transcript with an aptamer-regulated ribozyme (Fig. S7A, *left*) that cleaves itself when not bound to tetracycline (Fig. S7A, *right*) (based on (*43*)). Exposing these animals to tetracycline enabled silencing by dsRNA in somatic tissues (hypodermis: Fig. S7B, *left*; body-wall muscles: Fig. S7B, *right*) but not in the germline (Fig. S7C, Fig. S7D, Fig. S7E, Fig. S7F), indicative of stabilization of *sid-1* mRNA, production of SID-1 protein, and subsequent dsRNA import in somatic cells but not in the germline. Yet, similar tagging of the ubiquitously expressed gene *gtbp-1::gfp* results in detectable rescue of expression within the germline by tetracycline (Fig. S7G). A possible explanation for the poor rescue of SID-1 activity within the germline is that post-transcriptional mechanisms targeting *sid-1* mRNA in the germline but not the soma interfere with tetracycline-

dependent stabilization of the *sid-1* transcript (e.g., piRNA-based regulation of *sid-1* mRNA (*44-45*)).

Further improvements in tagging SID-1 protein, potentially guided by structure, and *sid-1* transcript, potentially guided by post-transcriptional regulatory interactions, could enable deeper analysis of dsRNA transport between cells. Nevertheless, the developmentally regulated expression observed for both SID-1 and RME-2 in the germline is consistent with intergenerational or transgenerational effects regulated by dsRNA from parental circulation after development of the adult germline.

Temporary loss of SID-1 results in a large increase in mRNA from a germline gene that lasts for many generations

To understand how transport of extracellular dsRNA into the germline might be used for endogenous gene regulation across generations, we searched for *sid-1*-dependent changes in gene expression that could be heritable (Fig. 3, Fig. S2, Fig. S8, Fig. S9, Fig. S10). We initially analyzed polyA+ RNAs extracted from wild-type, *sid-1(qt9)*, *sid-1(tm2700)*, and *sid-1(tm2700); tmIs1005[sid-1(+)]* animals and found that comparisons between samples with similar genetic backgrounds did not result in a consistent list of SID-1-dependent genes (Fig. S8). Strains with similar genotypes (*sid-1(+)* or *sid-1(-)*) did not cluster together when using principal component analysis (Fig. S8A), suggesting that other differences in genetic background could obscure or misrepresent differences between *sid-1(+)* and *sid-1(-)* animals. To ameliorate this problem we used Cas9-mediated genome editing to delete the entire *sid-1* coding sequence (*del*) or introduce a nonsense mutation (*non*) in cohorts of the same wild-type animals. When comparing polyA+ RNA from this wild type with that of the newly generated *sid-1(jam113[del])* (Fig. 3A, Fig. 3B, Fig. S9A) or *sid-1(jam80[non])* (Fig. 3A, Fig. 3B, Fig. 3E) animals, we found that 26 genes were

significantly ($q < 0.05$) misregulated in *sid-1(jam113[del])* (Fig. S9B) and 6 in *sid-1(jam80[non])* (Fig. 3F, *left*), both including *sid-1*. However, the most upregulated gene in *sid-1(jam113[del])*, *F14F9.5*, was likely perturbed as a consequence of disrupting regulation near the *sid-1* locus through deletion of DNA and not because of loss of SID-1 function because this change was only observed in the deletion mutant *sid-1(jam113[del])* and not in the newly generated nonsense mutant *sid-1(jam80[non])* (Fig. S9D, *left*), despite both mutants being equally defective for silencing by ingested dsRNA (Fig. 3B). Nevertheless, we could detect two genes that were upregulated in both *sid-1(jam113[del])* and *sid-1(jam80[non])* animals (red in Fig. 3F, *left*, Fig. S9B): the identical loci *W09B7.2*/*F07B7.2* (Fig. S9D, *middle*) and *Y102A5C.36* (Fig. S9D, *right*) - each expressed within the germline (Fig. S10, *left*) and regulated by endogenous small RNAs (Fig. S10, *middle* and *right*). While spliced mRNA levels measured at a later generation using RT-qPCR demonstrated that both transcripts were upregulated in *sid-1(jam80[non])* animals compared to wild-type animals as expected (Fig. 3G), no upregulation was detectable in *sid-1(jam113[del])* animals (Fig. S9C), potentially because of complex effects caused by deleted DNA (e.g., *F14F9.5* overexpression) that are independent of SID-1 function. To determine if changes in *W09B7.2*/*F07B7.2* and *Y102A5C.36* expression were heritable, we reverted the *sid-1* nonsense mutation to wild-type sequence using Cas9-mediated genome editing. This immediately restored most silencing by ingested dsRNA, reaching wild-type levels of SID-1 function within two generations (Fig. S11, Fig. 3B) with concomitant recovery of *sid-1* mRNA to wild-type levels (Fig. 3G, *left*). In contrast, changes in both *W09B7.2*/*F07B7.2* and *Y102A5C.36* expression persisted (Fig. 3F, *right*) even after a year of passaging revertants (i.e., after >100 generations, Fig. 3G, *middle* and *right*). Since the change in *W09B7.2*/*F07B7.2*

mRNA was large (Fig. 3G, *middle*, ~8-fold), we focused on heritable changes in the expression of this gene in this study and hereafter refer to this ***s**id-1-**d**ependent **g**ene (sdg)* as *sdg-1*.

Expression of *sdg-1* can vary within an animal and perturbing its RNA regulation creates new epigenetic states that last for many generations

To facilitate analysis of SDG-1 expression, we tagged both loci that express SDG-1 with *mCherry* coding sequences lacking piRNA-binding sites (*mCherryΔpi*) (*46-47*) (Fig. S12A, Fig. S12B), thereby preventing possible silencing of *mCherry* as a foreign sequence. Consistently, expression of SDG-1::mCherry was detectable by fluorescence microscopy and remained detectable for many generations (Fig. 4A, Fig. S12C). The expression of *sdg-1::mCherryΔpi* mRNA was ~16-fold higher than *sdg-1* mRNA (Fig. S12D), potentially because of the additional introns included in *mCherryΔpi* (*48-49*) and/or other unknown factors. Fluorescence from SDG-1::mCherry was observed in the germline of adult animals (Fig. 4A, *top left*), in early embryos (Fig. 4A, *right* and *bottom left*), and in potentially extracellular punctae near the proximal germline (Fig. 4A, *top left* and *right*). Intriguingly, SDG-1::mCherry dynamically entered the nucleus from the cytoplasm before fertilization (Fig. 4A, *right*, Movie S1) and before early cell divisions in the developing embryo (Fig. 4A, *bottom left*, Movie S2, Movie S3). Additional recent observations suggest that SDG-1 is a regulated protein that could itself play a role in RNA-based regulation within the germline: (1) the dynamic subcellular localization of the SDG-1 protein in the -1 oocyte is similar to that of the essential Argonaute CSR-1b (*50*); (2) the SDG-1 protein interacts with PID-2 (*51*) and potentially DEPS-1 (*52*) – two proteins with roles in heritable piRNA-induced silencing; and (3) loss of the germline Argonaute HRDE-1 results in upregulation of transcripts from a region that includes the *sdg-1* gene (*53*). Thus, one hypothesis suggested by the large and persistent change in *sdg-1* expression upon loss of SID-1 is that

extracellular dsRNA-based regulation of *sdg-1* protects it from heritable epigenetic change initiated by other mechanisms within the germline.

The proposed susceptibility of *sdg-1* expression to heritable epigenetic change is supported by four lines of evidence. One, simply mating animals that express SDG-1::mCherry with wild-type animals resulted in heritable changes along lineages that express *sdg-1::mCherryΔpi* mRNA or that express *sdg-1* mRNA (Fig. 4B, Fig. S13). Two, Cas9-mediated genome editing of genes required for dsRNA import or subsequent silencing (Fig. 4C), but not of unrelated genes (Fig. S14), resulted in some isolates that showed dramatically reduced or increased expression (Fig. 4C). While possible mechanisms mediating increased expression are unclear, decreased expression could be mediated by piRNAs that target *sdg-1* since expression in both isolates lacking DEPS-1, a protein required for piRNA-mediated silencing (*54-55*), showed increased expression (Fig. 4C). Three, isolating siblings led to lineages with distinct levels of *sdg-1* expression in some cases (compare sibling lineages in Fig. 4B and in Fig. S14). Four, many animals showed dramatic variation in SDG-1::mCherry expression between their two gonad arms (Fig. 4D). The two identical loci referred to as *sdg-1* are part of a ~40-kb duplicated region (Fig. S15), which could be a contributing feature for the observed stochasticity as suggested by RNA silencing of multi-copy genes (*41*).

While loss of SID-1 in otherwise wild-type animals led to a persistent increase in *sdg-1* mRNA in our earlier RNA-seq and RT-qPCR experiments (Fig. 3), loss of SID-1 in *sdg-1::mCherryΔpi* animals led to a decrease or increase in SDG-1::mCherry in separate lineages of newly generated *sid-1(-)* isolates (Fig. 4C, e.g., compare *sid-1(jam150)* and *sid-1(jam177)*), potentially because of differences in the levels of *sdg-1* expression before loss of SID-1. Once downregulated, reduced levels of SDG-1::mCherry persisted across generations after restoration

of dsRNA transport (Fig. 4E), just as the upregulation of untagged *sdg-1* mRNA also persisted (Fig. 3F, Fig. 3G).

Together, these results suggest that one or both *sdg-1* loci are subject to heritable changes upon loss of SID-1-mediated gene regulation and that the direction of change might depend upon the levels of *sdg-1* mRNA. Thus, one function of SID-1, and potentially dsRNA(s) that enter cells through SID-1, is to reduce stochastic initiation of heritable epigenetic changes in gene expression within the germline.

Discussion

We found that germline entry of dsRNA released from neurons upon oxidative damage and germline entry of ingested dsRNA occurs with spatiotemporal specificity. Such uptake of extracellular dsRNA from parental circulation and subsequent trafficking in progeny can occur through at least two routes that select for different forms of dsRNA. When the entry of all endogenous dsRNA into the cytosol is blocked, large increases or decreases in the expression of a germline gene can be observed in different animals that are genetically identical. These new expression states can persist for many generations despite restoration of dsRNA transport, suggesting a role for intercellular gene regulation by dsRNA in preventing heritable changes in gene expression.

Oxidative damage and the physiological conditions that favor secretion of dsRNA

The physiological conditions that promote secretion of dsRNA are not known. Our discovery that oxidative damage of neurons can enhance the secretion of dsRNA suggests that disruption of cell structures by oxidative damage (e.g., membrane integrity) or initiation of cellular processes that repair oxidative damage (e.g., through ejection of damaged

macromolecules (*56*)) also promote the release of dsRNA. Alternatively, damage-induced increase in the accumulation of dsRNA through indirect mechanisms could also explain the results observed. Pathologies of the central nervous system in humans, including cancer, stroke, multiple sclerosis, neurodegenerative disease, and brain injury, have been associated with extracellular RNAs detected in circulation (reviewed in (57)), although their origins and regulatory consequences, if any, remain unknown. The gene regulatory effects of neuronal dsRNA released upon oxidative damage of neurons provide convenient readouts that can be analyzed to understand neuronal damage and its consequences in animals.

Specificity in the intergenerational transport of extracellular dsRNA

The trafficking of extracellular dsRNA from parent to progeny has spatial specificity, as evidenced by more silencing within the proximal germline (Fig. 1), temporal specificity, as evidenced by the need for dsRNA beyond the fourth larval stage (Fig. 1) (*25-26*), and substrate specificity, as evidenced by the differential requirements for 50-bp dsRNA with 5'-OH versus a mix of longer dsRNAs with 5' triphosphates (Fig. 2). One possible explanation for these constraints could be that proteins mediating dsRNA transport differ in their availability during development and in their affinities for different substrates. For example, SID-1, which was not detected in the developing larval germline but was detected in the adult germline (Fig. 3), has an extracellular domain that binds dsRNA (*58*) and could prefer dsRNA molecules with 5' phosphates. Although the selectivity uncovered here could apply to all dsRNA delivered into the extracellular space of *C. elegans* from any source, the chemistry of the delivered dsRNA could be modified by as yet unidentified enzymes *in vivo* to overcome these requirements. Tracking labeled dsRNA with diverse chemistries from parental circulation to progeny could allow

correlation of differences observed in progeny silencing to differences in intergenerational trafficking.

SID-1-dependent defects in gene regulation

The germline is a major site of dsRNA import in *C. elegans* as evidenced by the expression of SID-1 in the germline (Fig. 3), heritable misregulation of germline genes in *sid-1(-)* animals (Fig. 3, Fig. 4), and accumulation of fluorescently-labeled dsRNA from the extracellular space in the germline (*25-26*). As a result, *sid-1(-)* animals could have a defect in the germline that is detectable only under conditions that promote dsRNA transport (e.g., oxidative damage). Multiple physiological defects in the germline and soma of *sid-1(-)* animals have been reported, but have not been widely reproduced, have only been characterized within single generations, and have not been attributed to any specific *sid-1*-dependent gene(s). These include defects in animals exiting the dauer stage (*59-60*), in animals exposed to pathogenic *P. aeruginosa* (*61-63*), in animals exposed to odor (*64*), and in intestinal cells that develop in the presence of a multi-copy transgene (*65*). RNA-seq experiments in this study suggest that genetic background-dependent changes can obscure genuine *sid-1*-dependent changes (Fig. S8, Fig. S9), raising caution in the interpretation of putative *sid-1*-dependent defects. Comparing *sid-1* mutants generated using genome editing with animals in which the mutated sequence has been reverted to wild-type sequence in the same genetic background could provide a firmer basis for the identification of *sid-1*-dependent processes.

Buffered RNA regulation in the germline as a guard against heritable epigenetic changes

A role for SID-1 in preventing heritable epigenetic changes in the expression of the endogenous gene *sdg-1* is unexpected in light of previous demonstration that the import of dsRNA into the germline through SID-1 can initiate heritable RNA silencing of a single-copy

transgene (*22*). This difference can be understood by considering that the regulatory context of a gene could dictate its response to dsRNA exposure. In support of this idea, targeting a few genes containing matching sequences with the same extracellular dsRNA revealed that while most genes recover from RNA silencing, some are susceptible to stable RNA silencing (*47*). Consistently, the expression of *sdg-1* is extraordinarily susceptible to heritable epigenetic change, precluding typical analysis of genetic requirements through mating to mutant backgrounds (Fig. 4B) and necessitating Cas9-mediated genome editing (Fig. 4C).

In general, genes expressed within the germline are likely regulated by positive feedback loops that continually produce factors for maintaining germline immortality and for preserving form and function across generations (*66-67*). Thus, germline genes could be particularly vulnerable to heritable epigenetic changes, where deviations in the expression levels of a gene that is regulated by or is part of such feedback loops have the potential to become permanent in descendants. Perturbations in *sdg-1* expression by multiple methods in this study suggest that *sdg-1* is part of a regulatory architecture that is susceptible to heritable epigenetic change. To buffer against such changes, levels of gene expression would need to be maintained within a particular range for a given regulatory context. We propose that expression of *sdg-1* is maintained by dsRNA imported through SID-1 and downstream small RNAs, and speculate that one role for extracellular RNAs that enter germ cells in other systems (e.g., tRNA fragments in mammals (*5-6, 8*)) could be to similarly buffer against heritable changes in gene expression.

Acknowledgements: We thank Mary Chey, Samiha Tasnim, and Daphne Knudsen for comments on the manuscript; the *Caenorhabditis elegans* Genetic Stock Center, the Seydoux laboratory (Johns Hopkins University) and the Hunter laboratory (Harvard University) for worm strains; Quentin Gaudry for help in creating our optogenetics apparatus; the Andrews laboratory for use of

a confocal microscope; Amy Beaven and the Imaging Core Facility for temporary use of a Leica TCS SP8 DLS microscope with HyVolution; Lanelle Edwards, Rex Ledesma, Carlos Machado, and Omega Bioservices for help with RNA sequencing and analysis. **Funding:** This work was supported by UMD CMNS Dean's Matching Award for "Training Program in Cell and Molecular Biology" T32GM080201 to N.S. and in part by National Institutes of Health Grants R01GM111457 and R01GM124356 to A.M.J. **Author contributions:** N.S. and A.M.J designed the research. N.S., A.L.Y., W.M.C., and A.S. performed all experiments, and collected and analyzed data. N.S. and A.M.J. prepared the manuscript with contributions from all authors. **Data and Materials availability:** All data and code are available in the manuscript or the supplementary materials. RNA-seq data has been deposited to Gene Expression Omnibus (GEO) with the accession number GSE185385.

References and Notes:

1. Q. Cai, L. Qiao, M. Wang, B. He, F. M. Lin, J. Palmquist, S. D. Huang, H. Jin, Plants send small RNAs in extracellular vesicles to fungal pathogen to silence virulence genes. *Science* **360**, 1126-1129 (2018).

2. J. Ashley, B. Cordy, D. Lucia, L. G. Fradkin, V. Budnik, T. Thomson, Retrovirus-like Gag protein Arc1 binds RNA and traffics across synaptic boutons. *Cell* **172**, 262-274 (2018).

3. E. D. Pastuzyn, C. E. Day, R. B. Kearns, M. Kyrke-Smith, A. V. Taibi, J. McCormick, N. Yoder, D. M. Belnap, S. Erlendsson, D. R. Morado, J. A. G. Briggs, C. Feschotte, J. D. Shephard, The neuronal gene *Arc* encodes a repurposed retrotransposon Gag protein that mediates intercellular RNA transfer. *Cell* **172**, 275-288 (2018).

4. T. Thomou, M. A. Mori, J. M. Dreyfuss, M. Konishi, M. Sakaguchi, C. Wolfrum, T. N. Rao, J. N. Winnay, R. Garcia-Martin, S. K. Grinspoon, P. Gorden, C. R. Kahn, Adipose-derived circulating miRNAs regulate gene expression in other tissues. *Nature* **542**, 450-455 (2017).

5. U. Sharma, C. C. Conine, J. M. Shea, A. Boskovic, A. G. Derr, X. Y. Bing, C. Belleannee, A. Kucukural, R. W. Serra, F. Sun, L. Song, B. R. Carone, E. P. Ricci, X. Z. Li, L. Fauquier, M. J. Moore, R. Sullivan, C. C. Mello, M. Garber, O. J. Rando, Biogenesis and function of tRNA fragments during sperm maturation and fertilization in mammals. *Science* **351(6271)**, 391-396 (2016).

6. Q. Chen, M. Yan, Z. Cao, X. Li, Y. Zhang, J. Shi, G.-H. Feng, H. Peng, X. Zhang, Y. Zhang, J. Qian, E. Duan, Q. Zhai, Q. Zhou, Sperm tsRNAs contribute to intergenerational inheritance of an acquired metabolic disorder. *Science* **351(6271)**, 397-400 (2016).

7. C. C. Conine, F. Sun, L. Song, J. A. Rivera-Pérez, O. J. Rando, Small RNAs gained during epididymal transit of sperm are essential for embryonic development in mice. *Dev. Cell* **46(4)**, 470-480.e3 (2018).

8. U. Sharma, F. Sun, C. C. Conine, B. Reichholf, S. Kukreja, V. A. Herzog, S. L. Ameres, O. J. Rando, Small RNAs are trafficked from the epididymis to developing mammalian sperm. *Dev. Cell* **46(4)**, 481-494.e6 (2018).

9. S. Das, Extracellular RNA Communication Consortium, K. M. Ansel, M. Bitzer, X. O. Breakefield, A. Charest, D. J. Galas, M. B. Gerstein, M. Gupta, A. Milosavljevic, M. T. McManus, T. Patel, R. L. Raffai, J. Rozowsky, M. E. Roth, J. A. Saugstad, K. Van Keuren-Jensen, A. M. Weaver, L. C. Laurent, The Extracellular RNA Communication Consortium: establishing foundational knowledge and technologies for extracellular RNA research. *Cell* **177**, 231-242 (2019).

10. R. L. Setten, J. J. Rossi, S. P. Han, The current state and future directions of RNAi-based therapeutics. *Nat. Rev. Drug Discov.* **18**, 421-446 (2019).

11. B. Hu, L. Zhong, Y. Weng, L. Peng, Y. Huang, Y. Zhao, X.-J. Liang, Therapeutic siRNA: state of the art. *Signal Transduct. Target Ther.* **5(1)**, 101 (2020).

12. A. Fire, S. Xu, M. K. Montgomery, S. A. Kostas, S. E. Driver, C. C. Mello, Potent and specific genetic interference by double-stranded RNA in *Caenorhabditis elegans*. *Nature* **391(6669)**, 806-811 (1998).

13. W. M. Winston, C. Molodowitch, C. P. Hunter, Systemic RNAi in *C. elegans* requires the putative transmembrane protein SID-1. *Science* **295**, 2456-2459 (2002).

14. E. H. Feinberg, C. P. Hunter, Transport of dsRNA into cells by the transmembrane protein SID-1. *Science* **301(5639)**, 1545-1547 (2003).

15. J. D. Shih, M. C. Fitzgerald, M. Sutherlin, C. P. Hunter, The SID-1 double-stranded RNA transporter is not selective for dsRNA length. *RNA* **15(3)**, 384-390 (2009).

16. Q. Chen, F. Zhang, L. Dong, H. Wu, J. Xu, H. Li, J. Wang, Z. Zhou, C. Liu, Y. Wang, Y. Liu, L. Lu, C. Wang, M. Liu, X. Chen, C. Wang, C. Zhang, D. Li, K. Zen, F. Wang, Q. Zhang, C.-Y. Zhang, SIDT1-dependent absorption in the stomach mediates host update of dietary and orally administered microRNAs. *Cell Res.* **31(3)**, 247-258 (2021).

17. T. A. Nguyen, B. R. C. Smith, K. D. Elgass, S. J. Creed, S. Cheung, M. D. Tate, G. T. Belz, I. P. Wicks, S. L. Masters, K. C. Pang, SIDT1 Localizes to Endolysosomes and Mediates Double-Stranded RNA Transport into the Cytoplasm. *J Immunol.* **202(12)**, 3483-3492 (2019).

18. T. A. Nguyen, B. R. C. Smith, M. D. Tate, G. T. Belz, M. H. Barrios, K. D. Elgass, A. S. Weisman, P. J. Baker, S. Preston, L. Whitehead, A. Garnham, R. J. Lundie, G. K. Smyth, M. Pellegrini, M. O'Keeffe, I. P. Wicks, S. L. Masters, C. P. Hunter, K. C. Pang, SIDT2 transports extracellular dsRNA into the cytoplasm for innate immune recognition. *Immunity* **47(3)**, 498-509.e6 (2017).

19. K. M. Méndez-Acevedo, V. J. Valdes, A. Asanov, L. Vaca, A novel family of mammalian transmembrane proteins involved in cholesterol transport. *Sci. Rep.* **7(1)**, 7450 (2017).

20. A. M. Jose, J. J. Smith, C. P. Hunter, Export of RNA silencing from *C. elegans* tissues does not require the RNA channel SID-1. *Proc. Natl. Acad. Sci.* **106**, 2283-2288 (2009).

21. S. Ravikumar, S. Devanapally, A. M. Jose, Gene silencing by double-stranded RNA from *C. elegans* neurons reveals functional mosaicism of RNA interference. *Nucleic Acids Res.* **47(19)**, 10059-10071 (2019).

22. S. Devanapally, S. Ravikumar, A. M. Jose, Double-stranded RNA made in *C. elegans* neurons can enter the germline and cause transgenerational gene silencing. *Proc. Natl. Acad. Sci.* **112**, 2133-2138 (2015).

23. L. Timmons, A. Fire, Specific interference by ingested dsRNA. *Nature* **395(6705)**, 854 (1998).

24. A. Grishok, H. Tabara, C. C. Mello, Genetic requirements for inheritance of RNAi in *C. elegans*. *Science* **287(5462)**, 2494-2497 (2000).

25. J. Marré, E. C. Traver, A. M. Jose, Extracellular RNA is transported from one generation to the next in *Caenorhabditis elegans*. *Proc. Natl. Acad. Sci.* **113**, 12496-12501 (2016).

26. E. Wang, C. P. Hunter, SID-1 functions in multiple roles to support parental RNAi in *Caenorhabditis elegans*. *Genetics* **207**, 547-557 (2017).

27. S. Xu, A. D. Chisholm, Highly efficient optogenetic cell ablation in *C. elegans* using membrane-targeted miniSOG. *Sci. Rep.* **6**, 21271 (2016).

28. S. Guang, A. F. Bochner, D. M. Pavelec, K. B. Burkhart, S. Harding, J. Lachowiec, S. Kennedy, An Argonaute transports siRNAs from the cytoplasm to the nucleus. *Science* **321**, 537-541 (2008).

29. J. P. T. Ouyang, W. Zhang, G. Seydoux, Two parallel sRNA amplification cycles contribute to RNAi inheritance in *C. elegans*. *bioRxiv*: 10.1101/2021.08.13.456232 (2021).

30. B. Grant, D. Hirsh, Receptor-mediated endocytosis in the *Caenorhabditis elegans* oocyte. *Mol. Biol. Cell* **10(12)**, 4311-4326 (1999).

31. Y. S. Choi, L. O. Edwards, A. DiBello, A. M. Jose, Removing bias against short sequences enables northern blotting to better complement RNA-seq for the study of small RNAs. *Nucleic Acids Res.* **45**, e87 (2017).

32. H. Tabara, E. Yigit, H. Siomi, C. C. Mello, The dsRNA binding protein RDE-4 interacts with RDE-1, DCR-1, and a DExH-box helicase to direct RNAi in *C. elegans*. *Cell* **109(7)**, 861-871 (2002).

33. N. Jain, L. R. Blauch, M. R. Szymanski, R. Das, S. K. Y. Tang, Y. W. Yin, A. Z. Fire, Transcription polymerase-catalyzed emergence of novel RNA replicons. *Science* **368(6487)**, eaay0688 (2020).

34. B. A. Buckley, K. B. Burkhart, S. G. Gu, G. Spracklin, A. Kershner, H. Fritz, J. Kimble, A. Fire, S. Kennedy, A nuclear Argonaute promotes multigenerational epigenetic inheritance and germline immortality. *Nature* **489**, 447-451 (2012).

35. W. J. Sharrock, Yolk proteins of *Caenorhabditis elegans*. *Dev. Biol.* **96(1)**, 182-188 (1983).

36. O. Bossinger, E. Schierenberg, The use of fluorescent marker dyes for studying intercellular communication in nematode embryos. *Int. J. Dev. Biol.* **40(1)**, 431-439 (1996).

37. W. M. Winston, M. Sutherlin, A. J. Wright, E. H. Feinberg, C. P. Hunter, *Caenorhabditis elegans* SID-2 is required for environmental RNA interference. *Proc. Natl. Acad. Sci.* **104**, 10565-10570 (2007).

38. D. L. McEwan, A. S. Weisman, C. P. Hunter, Uptake of extracellular double-stranded RNA by SID-2. *Mol. Cell* **47**, 746-754 (2012).

39. A. Hinas, A. J. Wright, C. P. Hunter, SID-5 is an endosome-associated protein required for efficient systemic RNAi in *C. elegans*. *Curr. Biol.* **22**, 1938-1943 (2012).

40. W. G. Kelly, S. Xu, M. K. Montgomery, A. Fire, Distinct requirements for somatic and germline expression of a generally expressed *Caenorhabditis elegans* gene. *Genetics* **146(1)**, 227-238 (1997).

41. H. H. Le, M. Looney, B. Strauss, M. Bloodgood, A. M. Jose, Tissue homogeneity requires inhibition of unequal gene silencing during development. *J. Cell Biol.* **14(3)**, 319-331 (2016).

42. J. Jumper, R. Evans, A. Pritzel, T. Green, M. Figurnov, O. Ronneberger, K. Tunyasuvunakool, R. Bates, A. Žídek, A. Potapenko, A. Bridgland, C. Meyer, S. A. A. Kohl, A. J. Ballard, A. Cowie, B. Romera-Paredes, S. Nikolov, R. Jain, J. Adler, T. Back, S. Petersen, D. Reiman, E. Clancy, M. Zielinski, M. Steinegger, M. Pacholska, T. Berghammer, S. Bodenstein, D. Silver, O. Vinyals, A. W. Senior, K. Kavukcuoglu, P. Kohli, D. Hassabis, Highly accurate protein structure prediction with AlphaFold. *Nature* **596(7873)**, 583-589 (2021).

43. L. A. Wurmthaler, M. Sack, K. Gense, J. S. Hartig, M. Gamerdinger, A tetracycline-dependent ribozyme switch allows conditional induction of gene expression in *Caenorhabditis elegans*. *Nat. Commun.* **10(1)**, 491 (2019).

44. J. P. T. Ouyang, A. Folkmann, L. Bernard, C.-Y. Lee, U. Seroussi, A. G. Charlesworth, J. M. Claycomb, G. Seydoux, P granules protect RNA interference genes from silencing by piRNAs. *Dev. Cell* **50(6)**, 716-728.e6 (2019).

45. A. E. Dodson, S. Kennedy, Germ granules coordinate RNA-based epigenetic inheritance pathways. *Dev. Cell* **50(6)**, 704-715.e4 (2019).

46. D. Zhang, S. Tu, M. Stubna, W.-S. Wu, W.-C. Huang, Z. Weng, H.-C. Lee, The piRNA targeting rules and the resistance to piRNA silencing in endogenous genes. *Science* **359(6375)**, 587-592 (2018).

47. S. Devanapally, P. Raman, M. Chey, S. Allgood, F. Ettefa, M. Diop, Y. Lin, Y. E. Cho, A. M. Jose, Mating can initiate stable RNA silencing that overcomes epigenetic recovery. *Nat. Commun.* **12(1)**, 4239 (2021).

48. P. G. Okkema, S. W. Harrison, V. Plunger, A. Aryana, A. Fire, Sequence requirements for myosin gene expression and regulation in *Caenorhabditis elegans*. *Genetics* **135(2)**, 385-404 (1993).

49. M. M. Crane, B. Sands, C. Battaglia, B. Johnson, S. Yun, M. Kaeberlein, R. Brent, A. Mendenhall, *In vivo* measurements reveal a single 5'-intron is sufficient to increase protein expression level in *Caenorhabditis elegans*. *Sci. Rep.* **9(1)**, 9192 (2019).

50. A. G. Charlesworth, U. Seroussi, N. J. Lehrbach, M. S. Renaud, A. E. Sundby, R. I. Molnar, R. X. Lao, A. R. Willis, J. R. Woock, M. J. Aber, A. J. Diao, A. W. Reinke, G. Ruvkun, J. M. Claycomb, Two isoforms of the essential *C. elegans* Argonaute CSR-1 differentially regulate sperm and oocyte fertility. *Nucleic Acids Res.*, gkab619 (2021).

51. M. Placentino, A. M. J. Domingues, J. Schreier, S. Dietz, S. Hellmann, B. F. de Albuquerque, F. Butter, R. F. Ketting, Intrinsically disordered protein PID-2 modulates Z granules and is required for heritable piRNA-induced silencing in the *Caenorhabditis elegans* embryo. *EMBO J.* **40(3)**, e105280 (2021).

52. I. F. Price, H. L. Hertz, B. Pastore, J. Wagner, W. Tang, Proximity labeling identifies LOTUS domain proteins that promote the formation of perinuclear germ granules in C. elegans *bioRxiv* 2021.07.27.453989 (2021); doi: https://doi.org/10.1101/2021.07.27.453989

53. N. Kalinava, J. Z. Ni, Z. Gajic, M. Kim, H. Ushakov, S. G. Gu, *C. elegans* heterochromatin factor SET-32 plays an essential role in transgenerational establishment of nuclear RNAi-mediated epigenetic silencing. *Cell Rep.* **25**, 2273-2284.e3 (2018).

54. C. A. Spike, J. Bader, V. Reinke, S. Strome, DEPS-1 promotes P-granule assembly and RNA interference in *C. elegans* germ cells. *Development* **135(5)**, 983-993 (2008).

55. K. M. Suen, F. Braukmann, R. Butler, D. Bensaddek, A. Akay, C.-C. Lin, D. Milonaitytė, N. Doshi, A. Sapetschnig, A. Lamond, J. E. Ladbury, E. A. Miska, DEPS-1 is required for piRNA-dependent silencing and PIWI condensate organisation in *Caenorhabditis elegans*. *Nat. Commun.* **11(1)**, 4242 (2020).

56. I. Melentijevic, M. L. Toth, M. L. Arnold, R. J. Guasp, G. Harinath, K. C. Nguyen, D. Taub, J. A. Parker, C. Neri, C. V. Gabel, D. H. Hall, M. Driscoll, *C. elegans* neurons jettison protein aggregates and mitochondria under neurotoxic stress. *Nature* **542(7641)**, 367-371 (2017).

57. K. Tielking, S. Fischer, K. T. Preissner, P. Vajkoczy, R. Xu, Extracellular RNA in central nervous system pathologies. *Front. Mol. Neurosci.* **12**, 254 (2019).

58. W. Li, K. S. Koutmou, D. J. Leahy, M. Li, Systemic RNA interference deficiency-1 (SID-1) extracellular domain selectively binds long double-stranded RNA and is required for RNA transport by SID-1. *J. Biol. Chem.* **290(31)**, 18904-18913 (2015).

59. M. C. Ow, K. Borziak, A. M. Nichitean, S. Dorus, S. E. Hall, Early experiences mediate distinct adult gene expression and reproductive programs in *Caenorhabditis elegans*. *PLoS Genet.* **14**, e1007219 (2018).

60. P. Kadekar, R. Roy, AMPK regulates germline stem cell quiescence and integrity through an endogenous small RNA pathway. *PLoS Biol*. **17**, e3000309 (2019).

61. M. F. Palominos, L. Verdugo, C. Gabaldon, B. Pollak, J. Ortiz-Severin, M. A. Varas, F. P. Chávez, A. Calixto, Transgenerational diapause as an avoidance strategy against bacterial pathogens in *Caenorhabditis elegans*. *mBio* **8**, pii: e01234-17 (2017).

62. R. S. Moore, R. Kaletsky, C. T. Murphy, Piwi/PRG-1 Argonaute and TGF-β mediate transgenerational learned pathogenic avoidance. *Cell* **177(7)**, 1827-1841 (2019).

63. R. Kaletsky, R. S. Moore, G. D. Vrla, L. R. Parsons, Z. Gitai, C. T. Murphy, *C. elegans* interprets bacterial non-coding RNAs to learn pathogenic avoidance. *Nature* **586(7829)**, 445-451 (2020).

64. R. Posner, I. A. Toker, O. Antonova, E. Star, S. Anava, E. Azmon, M. Hendricks, S. Bracha, H. Gingold, O. Rechavi, Neuronal small RNAs control behavior transgenerationally. *Cell* **177**, 1814-1826.e15 (2019).

65. H. Ohno, Z. Bao, Small RNAs couple embryonic developmental programs to gut microbes. *bioRxiv*: 10.1101/2020/11/13/381830 (2020).

66. A. M. Jose, Heritable epigenetic changes alter transgenerational waveforms maintained by cycling stores of information. *Bioessays* **42(7)**, e1900254 (2020).

67. M. Chey, A. M. Jose, Heritable epigenetic changes at single genes: challenges and opportunities in *Caenorhabditis elegans*. *Trends Genet*., in press (2021); doi: https://doi.org/10.1016/j.tig.2021.08.011

68. S. Brenner, The genetics of *Caenorhabditis elegans*. *Genetics* **77(1)**, 71-94 (1974).

69. C. C. Mello, J. M. Kramer, D. Stinchcomb, V. Ambros, Efficient gene transfer of *C. elegans*: extrachromosomal maintenance and integration of transforming sequences. *EMBO J*. **10(12)**, 3959-3970 (1991).

70. C. Frøkjær-Jensen, M. W. Davis, M. Ailion, E. M. Jorgensen, Improved Mos1-mediated transgenesis in *C. elegans*. *Nat. Methods* **9**, 117-118 (2012).

71. A. M. Jose, G. A. Garcia, C. P. Hunter, Two classes of silencing RNAs move between *C. elegans* tissues. *Nat. Struct. Mol. Biol*. **18(11)**, 1184-1188 (2011).

72. P. Raman, S. M. Zaghab, E. C. Traver, A. M. Jose, The double-stranded RNA binding protein RDE-4 can act cell autonomously during feeding RNAi in *C. elegans*. *Nucleic Acids Res*. **45(14)**, 8463-8473 (2017).

73. E. Kage-Nakadai, R. Imae, Y. Suehiro, S. Yoshina, S. Hori, S. Mitani, A conditional knockout toolkit for *Caenorhabditis elegans* based on the Cre/loxP recombination. *PLoS One* **9**, e114680 (2014).

74. J. A. Arribere, R. T. Bell, B. X. H. Fu, K. L. Artiles, P. S. Hartman, A. Z. Fire, Efficient marker-free recovery of custom genetic modifications with CRISPR/Cas9 in *Caenorhabditis elegans*. *Genetics* **198(3)**, 837-846 (2014).

75. A. Paix, A. Folkmann, D. Rasoloson, G. Seydoux, High efficiency, homology-directed genome editing in *Caenorhabditis elegans* using CRISPR-Cas9 ribonucleoprotein complexes. *Genetics* **201(1)**, 47-54 (2015).

76. G. A. Dokshin, K. S. Ghanta, K. M. Piscopo, C. C. Mello, Robust genome editing with short single-stranded and long, partially single-stranded DNA donors in *Caenorhabditis elegans*. *Genetics* **210(3)**, 781-787 (2018).

77. H. Tabara, M. Sarkissian, W. G. Kelly, J. Fleenor, A. Grishok, L. Timmons, A. Fire, C. C. Mello, The *rde-1* gene, RNA interference, and transposon silencing in *C. elegans*. *Cell* **99(2)**, 123-132 (1999).

78. J. Vicencio, C. Martínez-Fernández, X. Serrat, J. Cerón, Efficient generation of endogenous fluorescent reporters by nested CRISPR in *Caenorhabditis elegans*. *Genetics* **211(4)**, 1143-1154 (2019).

79. A. M. Jose, Y. A. Kim, S. Leal-Ekman, C. P. Hunter, Conserved tyrosine kinase promotes the import of silencing RNA into *Caenorhabditis elegans* cells. *Proc. Natl. Acad. Sci.* **109(36)**, 14520-14525 (2012).

80. A. D. Levy, J. Yang, J. M. Kramer, Molecular and genetic analyses of the *Caenorhabditis elegans dpy-2* and *dpy-10* collagen genes: a variety of molecular alterations affect organismal morphology. *Mol Biol Cell* **4(8)**, 803-817 (1993).

81. J. Schindelin, I. Arganda-Carreras, E. Frise, V. Kaynig, M. Longair, T. Pietzsch, S. Preibisch, C. Rueden, S. Saalfeld, B. Schmid, J.-Y. Tinevez, D. J. White, V. Hartenstein, K. Eliceiri, P. Tomancak, A. Cardona, Fiji: an open-source platform for biological-image analysis. *Nat. Methods* **9**, 676-682 (2012).

82. C. J. Harris, A. Molnar, S. Y. Müller, D. C. Baulcombe, FDF-PAGE: a powerful technique revealing previously undetected small RNAs sequestered by complementary transcripts. *Nucleic Acids Res.* **43**, 7590-7599 (2015).

83. M. Martin, Cutadapt removes adapter sequences from high-throughput sequencing reads. *EMBnet.journal* **17(1)**, 10-12 (2011).

84. R. Patro, G. Duggal, M. I. Love, R. A. Irizarry, C. Kingsford, Salmon provides fast and bias-aware quantification of transcript expression. *Nat. Methods* **14**, 417-419 (2017).

85. C. Soneson, M. I. Love, M. D. Robinson, Differential analyses for RNA-seq: transcript-level estimates improve gene-level inferences. *F1000Research* **4**, doi: 10.12688/f1000research.7563.1 (2015).

86. M. D. Robinson, A. Oshlack, A scaling normalization method for differential expression analysis of RNA-seq data. *Genome Biol*. **11(3)**, R25 (2010).

87. C. W. Law, Y. Chen, W. Shi, G. K. Smyth, voom: precision weights unlock linear model analysis tools for RNA-seq read counts. *Genome Biol*. **15**, R29 (2014).

88. K. J. Reed, J. M. Svendsen, K. C. Brown, B. E. Montgomery, T. N. Marks, T. Vijayasarathy, D. M. Parker, E. O. Nishimura, D. L. Updike, T. A. Montgomery, Widespread roles for piRNAs and WAGO-class siRNAs in shaping the germline transcriptome of *Caenorhabditis elegans*. *Nucleic Acids Res*. **48(4)**, 1811-1827 (2020).

89. D. Kim, J. M. Paggi, C. Park, C. Bennett, S. L. Salzberg, Graph-based genome alignment and genotyping with HISAT2 and HISAT-genotype. *Nat. Biotechnol*. **37**, 907-915 (2019).

90. H. Li, B. Handsaker, A. Wysoker, T. Fennell, J. Ruan, N. Homer, G. Marth, G. Abecasis, R. Durbin, 1000 Genome Project Data Processing Subgroup, The Sequence Alignment/Map format and SAMtools. *Bioinformatics* **25(16)**, 2078-2079 (2009).

91. F. Madeira, Y. M. Park, J. Lee, N. Buso, T. Gur, N. Madhusoodanan, P. Basutkar, A. R. N. Tivey, S. C. Potter, R. D. Finn, R. Lopez, The EMBL-EBI search and sequence analysis tools APIs in 2019. *Nucleic Acids Res*. **47(W1)**, W636-W641 (2019).

92. N. J. Bowen, J. F. McDonald, Genomic analysis of *Caenorhabditis elegans* reveals ancient families of retroviral-like elements. *Genome Res* **9(10)**, 924-935 (1999).

Figures and Legends:

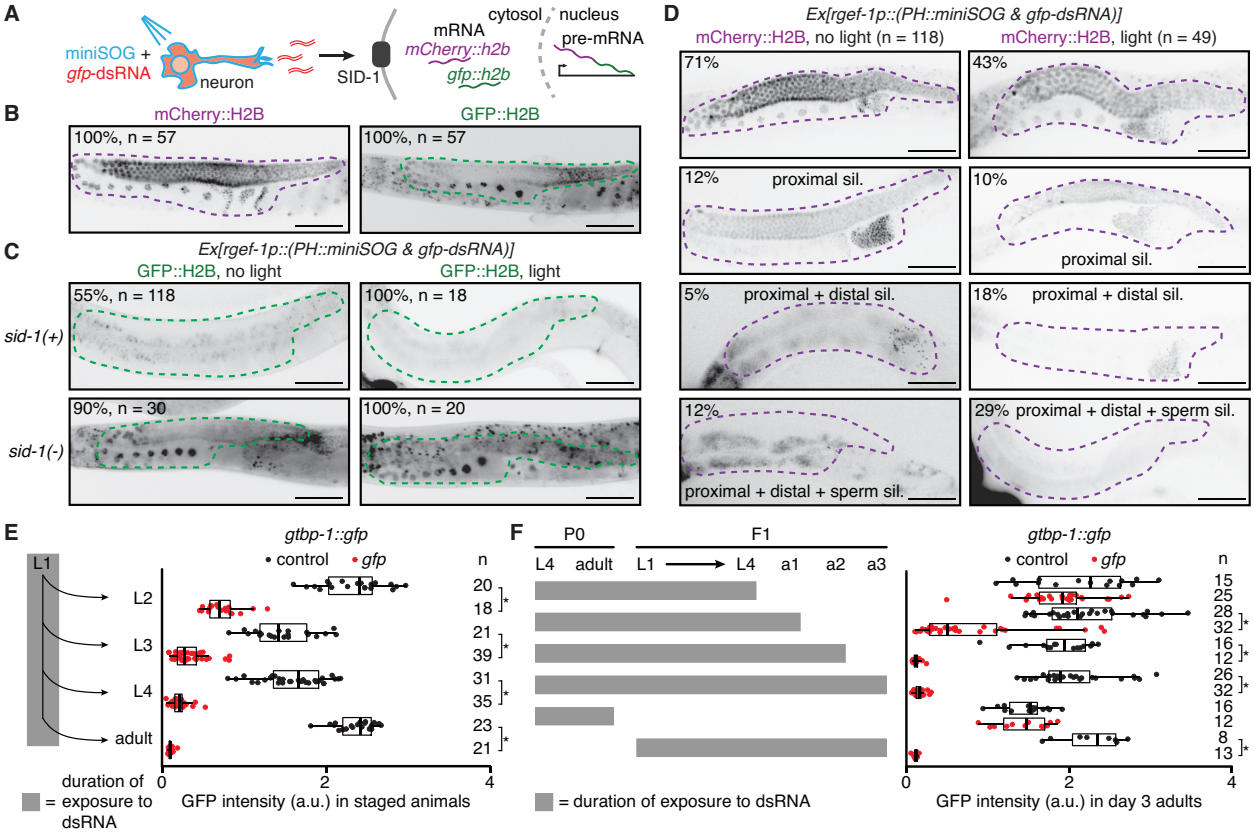

Fig. 1. Timed delivery of neuronal or ingested dsRNA suggests spatiotemporal differences in germline entry. (**A**) Schematic illustrating exposure of animals expressing a singlet oxygen generator (miniSOG) and *gfp*-dsRNA in neurons to blue light and subsequent release of dsRNA. Such extracellular dsRNA can enter the germline through the dsRNA importer SID-1 and silence *gfp::h2b* mRNA from a two-gene operon that expresses *mCherry::h2b* and *gfp::h2b* as part of a single pre-mRNA. (**B**, **C**, and **D**) Images of single gonad arms in adult animals with the two-gene operon (*mex-5p::mCherry::h2b::gfp::h2b*) showing fluorescence (black) of mCherry::H2B (magenta outline) or of GFP::H2B (green outline). Punctate autofluorescence from the intestine can also be seen. Numbers of animals assayed (n) and percentages of adult animals with the depicted expression patterns are indicated. Scale bars, 50 μm. (B) mCherry::H2B fluorescence is seen throughout the germline (*left*) and GFP::H2B fluorescence is seen in the oocytes and in the

distal gonad (*right*). (C) GFP::H2B fluorescence in *sid-1(+)* and *sid-1(-)* animals expressing membrane-localized miniSOG (*PH::miniSOG*) and *gfp*-dsRNA driven by a neuronal promoter (*rgef-1p*) from a multi-copy transgene (*Ex*, *jamEx214*) without (*left*) or with (*right*) exposure to blue light at 48 hours post L4-stage of parent. (D) mCherry::H2B fluorescence in *sid-1(+)* animals with the transgene *Ex*. Silencing of mCherry is enhanced in the distal gonad (third row) and sperm (fourth row) after exposing animals to blue light at 48 hours and 54 hours post L4-stage of parent. Also see Supplementary Fig. S1 and Supplementary Fig. S2. (**E**) Silencing in the germline after continuous exposure of *gtbp-1::gfp* animals to bacteria expressing dsRNA starting at the L1 stage, and imaging of separate cohorts at each subsequent stage. (*left*) Schematic of assay. (*right*) GFP intensity (a.u.) in *gtbp-1::gfp* animals at indicated stages quantified in germ cells (larvae) or eggs *in utero* (adults) after exposure to control (black) or *gfp*-dsRNA (red). The numbers of animals scored at each stage (n) are depicted. (**F**) Schematic depicting duration of exposure for different cohorts of P0 and F1 animals to bacteria expressing dsRNA (*left*) and quantification of GFP intensity (a.u.) as in (E) in F1 animals on the third day of adulthood (*right*). The numbers of adult day 3 F1 animals scored (n) are depicted. Asterisks in (E) and (F) indicate $P < 0.05$ with Bonferroni correction using Mann-Whitney U test for two-sided comparisons between animals exposed to control or *gfp*-dsRNA. Also see Supplementary Fig. S3.

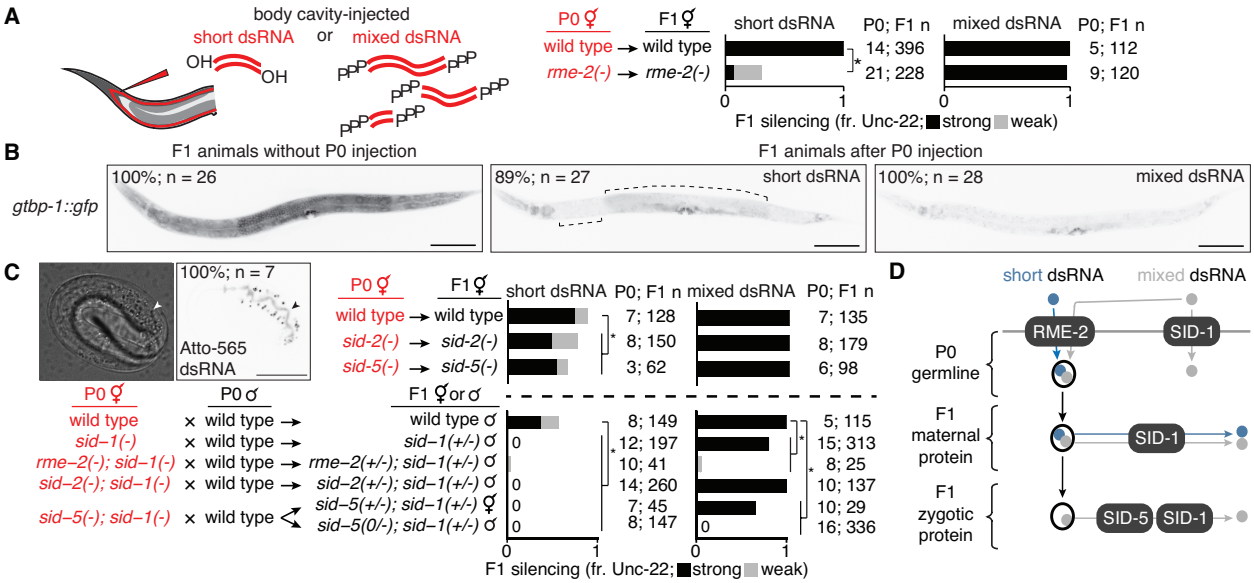

Fig. 2. Transport of dsRNA from parental circulation to progeny occurs through two routes with distinct substrate selectivity. (**A**) Hermaphrodite animals of indicated genotypes (in red) were injected in the body cavity with 50-bp *unc-22*-dsRNA synthesized with a 5'-OH (short dsRNA, left bars) or *unc-22*-dsRNA with a 5'-triphosphate transcribed from a ~1.1 kb template (mixed dsRNA, right bars). Hermaphrodite self-progeny of injected animals were scored for *unc-22* silencing (fr. Unc-22: strong, black; weak, grey). Numbers of injected parents and scored progeny (P0; F1 n) are indicated. Also see Supplementary Fig. S2 and Supplementary Fig. S4. (**B**) Fluorescence images of progeny from animals with a *gfp* tag of the ubiquitously expressed gene *gtbp-1* (*gtbp-1::gfp*) that were not injected (*left*), injected with 50-bp *gfp*-dsRNA (short dsRNA injection, *middle*), or injected with dsRNA transcribed from a ~730-bp template (mixed dsRNA injection, *right*). Complete silencing is not observed in neurons or in the developing vulva; brackets indicate additional regions with dim GFP fluorescence. Numbers of animals assayed (n) and percentages of L4-staged animals with the depicted expression patterns are indicated. Scale bar, 100 μm. Also see Supplementary Fig. S5. (**C**) Requirements for intergenerational transport of extracellular dsRNA. (*top left*) Differential Interference Contrast

(DIC) and fluorescence images of a developing embryo from an animal injected in the body cavity with 50-bp dsRNA of the same sequence as in (B) and labeled at the 5' end of the antisense strand with Atto-565. Accumulation within the intestinal lumen (arrowhead), number of embryos imaged (n), and percentage of embryos with depicted pattern of fluorescence are indicated. Scale bar, 20 μm. (*top right* and *bottom*) Hermaphrodite animals of the indicated genotypes were injected with short dsRNA (left bars) or mixed dsRNA (right bars) and self-progeny (*top right*) or cross progeny after mating with wild-type males (*bottom*) were analyzed as in (A). Cases of no observable silencing are indicated with '0'. (**D**) Schematic summarizing requirements for transport of dsRNA from parental circulation to developing progeny. Asterisks indicate $P < 0.05$ with Bonferroni correction using χ^2 test.

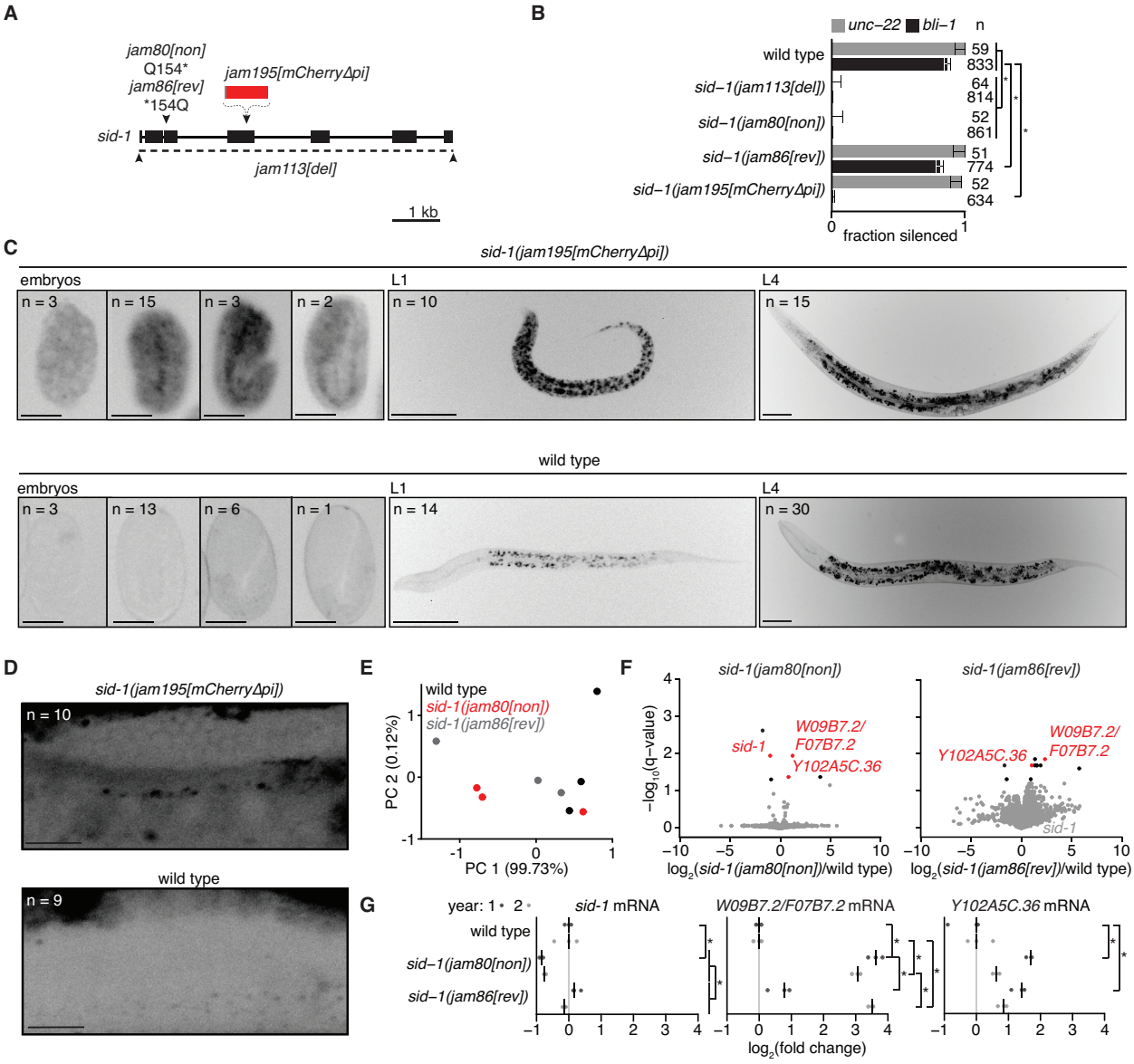

Fig. 3. Ancestral loss of the dsRNA importer SID-1 results in the accumulation of mRNAs of two germline genes in wild-type descendants. (**A**) Schematic of modifications at the *sid-1* gene generated using Cas9-mediated genome editing. Deletion of the entire coding sequence (*jam113[del]*), a nonsense mutation (*jam80[non]*), its reversion to wild-type sequence (*jam86[rev]*), and insertion of *mCherry* sequence that lacks piRNA binding sites (*46-47*) (*jam195[mCherryΔpi]*) are depicted. (**B**) Fractions of animals of the indicated genotypes that show silencing in response to *unc-22*-dsRNA (grey) or *bli-1*-dsRNA (black) are plotted. Tagging

SID-1 with mCherry (*sid-1(jam195[mCherryΔpi])*) likely results in a partially functional SID-1::mCherry fusion protein because *unc-22* silencing is robust but *bli-1* silencing is very weak (only 6 of 634 animals showed the Bli-1 defect). Numbers of animals scored (n), significant differences using two-tailed test with Wilson's estimates for single proportions (asterisks, $P < 0.05$ with Bonferroni correction) and 95% CI (error bars) are indicated. (**C** and **D**) Representative images showing fluorescence from SID-1::mCherry (black) in (C) developing embryos (*left*), L1-stage (*middle*), L4-stage (*right*) or (D) adult gonad arms of *sid-1(jam195[mCherryΔpi])* animals (*top*) compared to no detectable fluorescence in wild-type animals of the same stages (*bottom*). Numbers of (C) embryos of each stage, L1 animals, L4 animals, and (D) adult gonad arms imaged (n) are depicted and 100% of animals exhibited the depicted expression patterns. For animals imaged in (D), the distal germline was obstructed by the intestine in 1/10 *sid-1(jam195[mCherryΔpi])* and 5/9 wild-type animals. Scale bar for embryos in (C) and adult gonad arms in (D), 20 μm; scale bar for larvae in (C), 50 μm. Also see Supplementary Fig. S6. (**E**) Principal components explaining the variance between wild type (black), *sid-1(jam80[non])* (red), and *sid-1(jam86[rev])* (grey) polyA+ RNA samples. Almost all of the variance between samples is explained by PC 1. (**F**) Volcano plots of changes in the abundance of polyA+ RNA in *sid-1(jam80[non])* (*left*) and *sid-1(jam86[rev])* (*right*) animals compared with wild-type animals (black, $q < 0.05$; red, $q < 0.05$ and with change in the same direction in *sid-1(jam80[non])* and *sid-1(jam113[del])*; see Supplementary Fig. S9). While *sid-1* transcript levels in *sid-1(jam86[rev])* are comparable to that in wild type (grey), *W09B7.2/F07B7.2* and *Y102A5C.36* transcript levels remain elevated in *sid-1(jam86[rev])* (red). (**G**) Levels of spliced *sid-1*, *W09B7.2/F07B7.2* and *Y102A5C.36* transcripts measured using RT-qPCR. The median of three technical replicates is plotted for each of three biological replicates (bar indicates median)

assayed one year apart (year 1, dark grey; year 2, light grey). Asterisks indicate $P < 0.05$ with Bonferroni correction using two-tailed Student's t-test.

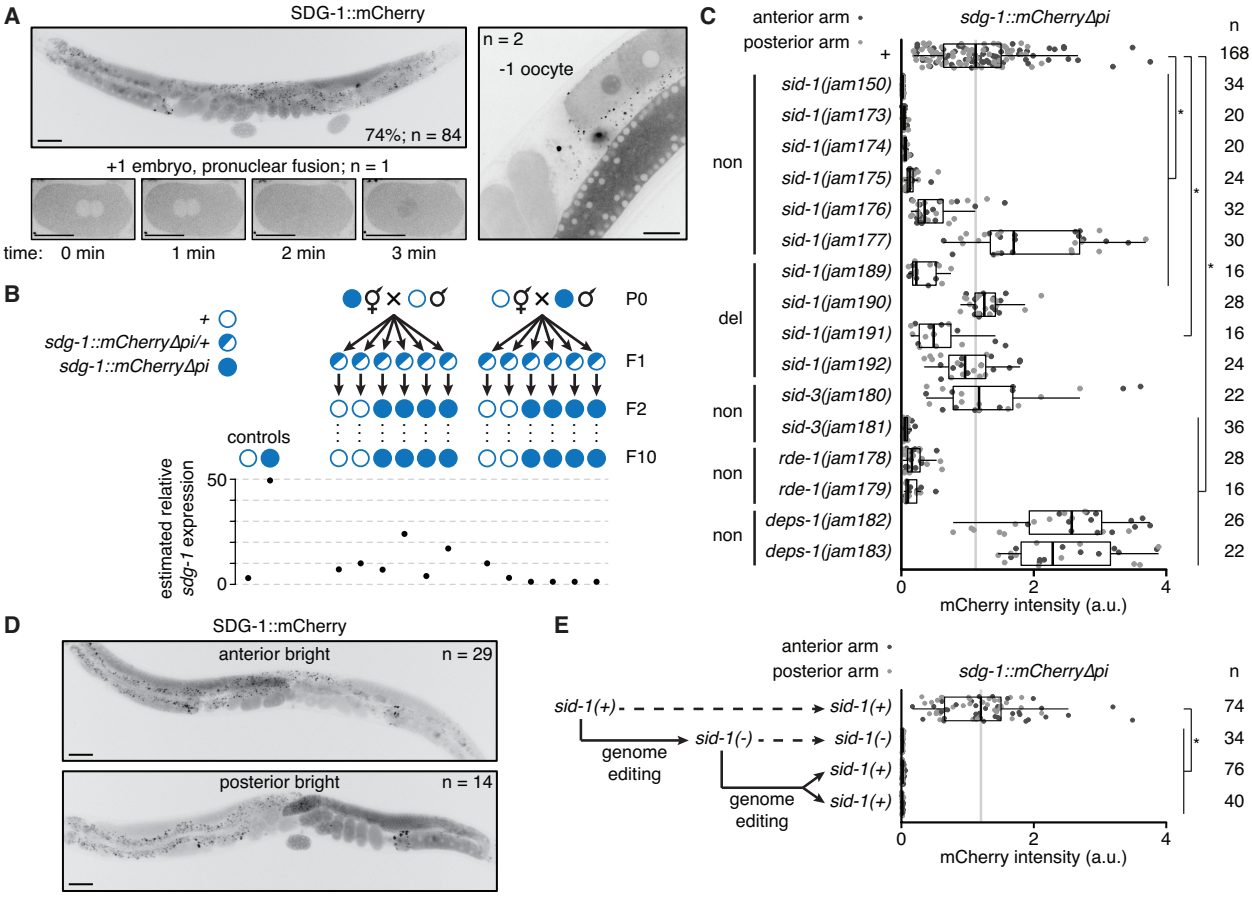

Fig. 4. A SID-1-dependent gene is prone to stochastic changes in gene expression that can become heritable. (**A**) Fluorescence images of SDG-1::mCherry in adult animals. Numbers of animals assayed (n) and percentages of adult animals with the depicted expression patterns (*top left*) are indicated. Punctate fluorescence in the intestine likely represents autofluorescence. Scale bars, 50 μm (*top left*) or 20 μm (*right* and *bottom left*). (*top left*) Cytoplasmic fluorescence is detectable throughout the germline and in embryos. (*right*) Nuclear localization of SDG-1::mCherry in the -1 oocyte was detected in confocal imaging of two animals. (*bottom left*) An embryo undergoing pronuclear fusion after fertilization showed dynamic nuclear localization before the first cell division (time in minutes). (**B**) Lineages and estimated relative *sdg-1* expression 10 generations after mating wild-type (open circle) males and *sdg-1::mCherryΔpi* (filled circle) hermaphrodites and vice versa and isolating *sdg-1(+)* or *sdg-1::mCherry* animals

from F1 heterozygotes (half-filled circle). Expression of *sdg-1* in the F10 generation was measured by RT-qPCR of *sdg-1* mRNA purified from pooled wild-type animals of mixed stages or by quantification of SDG-1::mCherry fluorescence in gonad arms of adult *sdg-1::mCherryΔpi* animals. Relative levels of *sdg-1* mRNA and SDG-1::mCherry fluorescence intensity were converted to units of estimated relative *sdg-1* expression (see Materials and methods) for comparison. See Supplementary Fig. S13 for raw data. (**C**) Fluorescence intensity measurements (arbitrary units, a.u.) quantified as in (B) (anterior gonad arm, light grey; posterior gonad arm, dark grey) in adult animals with *sdg-1::mCherryΔpi* (+) and additionally with mutations in single genes that regulate dsRNA import (*sid-1* or *sid-3*) or RNA silencing (*rde-1* or *deps-1*) are shown. Nonsense mutations (non) or deletions (del) introduced by genome editing and numbers of gonad arms (n) quantified for each isolate are indicated. Asterisks indicate $P < 0.05$ with Bonferroni correction using Mann-Whitney U test for two-sided comparisons between animals with *sdg-1::mCherryΔpi* (+) and animals with additional mutations. (**D**) Representative images showing asymmetric fluorescence of SDG-1::mCherry (black) with bright anterior (*top*) or bright posterior (*bottom*) gonad arms. Animals with at least one gonad arm brighter than the dimmest wild-type gonad arm in (C) and with >2-fold difference in fluorescence between both gonad arms were selected as having asymmetric fluorescence (anterior bright (n = 29): wild type (+) – 17/84, *sid-1(-)* – 5/122, *sid-3(-)* – 1/29, *rde-1(-)* – 2/22, *deps-1(-)* – 4/24, and posterior bright (n = 14): wild type (+) – 5/84, *sid-1(-)* – 6/122, *rde-1(-)* – 2/22, *deps-1(-)* – 1/24). Mutations in genes required for dsRNA import or subsequent silencing resulted in fewer animals with asymmetric fluorescence between gonad arms (a combined proportion of 21/197 for *sid-1*, *sid-3*, *rde-1* and *deps-1* mutants versus 22/84 for wild type, $P = 0.0009$ using two-tailed test with Wilson's estimates for single proportions). Punctate fluorescence in the intestine likely

represents autofluorescence. Scale bar, 50 μm. (**E**) Animals with *sdg-1::mCherryΔpi* that show altered fluorescence upon loss of *sid-1* remain changed despite reversion of *sid-1* nonsense mutation to wild-type sequence. Quantification of SDG-1::mCherry in adult gonad arms as in (B). Also see Supplementary Fig. S12 and S14.

Supplementary Materials for

Intercellular transport of RNA can limit heritable epigenetic changes

Nathan Shugarts et al.

Corresponding author: Antony Jose, amjose@umd.edu

The PDF file includes:

Materials and methods
Figs S1 to S15
Tables S1 and S2

Other supplementary materials include the following:

Movies S1 to S3
Supplementary file 1 (code for RNA-seq analysis)

Materials and Methods

Strains and oligonucleotides used

All strains (listed in Supplemental Table S1) were cultured on Nematode Growth Medium (NGM) plates seeded with 100 µl of OP50 *E. coli* at 20ºC and strains made through mating were generated using standard methods (*68*). Oligonucleotides used are in Supplemental Table S2 (for genotyping *sid-1(qt9)*: P1-P2, *ttTi5605*: P3-P5, *eri-1(mg366)*: P6-P7, *sid-1(tm2700)*: P8-P10, *hrde-1(tm1200)*: P11-P13, and *nrde-3(tm1116)*: P14-P16). Strains made through mating existing mutant strains and genotyping using the above primers are listed below.

To create *gtbp-1::gfp* animals with *hrde-1(tm1200)* in the background: AMJ577 (*22*) was crossed with JH3197 males to create AMJ1220 and one other independent isolate.

To create *gtbp-1::gfp* animals with *nrde-3(tm1116)* in the background: JH3197 was crossed with WM156 males to create AMJ1383.

Transgenesis

Animals were transformed with plasmids and/or PCR products using microinjection (*69*) to generate extrachromosomal arrays or single-copy transgenes. All plasmids were purified from bacterial culture using QIAprep Spin Miniprep Kit (Qiagen) and all PCR products were generated with Phusion® High-Fidelity DNA Polymerase (New England BioLabs) and purified using NucleoSpin Gel and PCR Clean-up Kit (Macherey-Nagel).

To express *sid-1::DsRed* in the muscle from an integrated array: pAJ53a (*myo-3p::sid-1::DsRed::unc-54 3'UTR*, made by AMJ while in Hunter Lab, Harvard University) was generated by amplifying part of *sid-1* cDNA from pHC355 (*20*) with primers P27 and P18, *DsRed* and *unc-54 3'UTR* from pHC183 (*13*) with primers P17 and P30, fusing the fragments using PCR with primers P30 and P31, and then cloning the fusion product into the pHC355 vector backbone using the restriction enzymes NruI and EagI. pAJ53a (40 ng/µl) was then injected into HC196 and animals expressing DsRed were isolated. AMJ3 was isolated as a spontaneous integrant. AMJ3 males were then crossed with AMJ308 hermaphrodites to generate AMJ327.

To express *sid-1::DsRed* in the germline from a single-copy transgene: The *mex-5* promoter was amplified from pJA252 (Addgene #21512) using the primers P19 and P20. The *sid-1* gene was amplified from N2 genomic DNA using the primers P21 and P22. The *DsRed* gene was amplified from pAJ53a (*myo-3p::sid-1(+)::DsRed::unc-54 3'UTR*; made by AMJ and Tessa Kaplan while in Hunter Lab, Harvard University) using the primers P23 and P24. The *sid-1* 3'UTR was amplified using the primers P25 and P26. Using NEBuilder® HiFi DNA Assembly (New England BioLabs), these four amplicons were placed into pCFJ151 (Addgene #19330) digested with AflII (New England BioLabs) and treated with CIP (New England BioLabs) to generate pJM10. pJM10 (50 ng/µl) and the coinjection markers pCFJ601 (50 ng/µl), pMA122 (10 ng/µl), pGH8 (10 ng/µl), pCFJ90 (2.5 ng/µl), and pCFJ104 (5 ng/µl) (plasmids described in (*70*)) were injected into the germline of adult EG4322 animals. One transgenic line was isolated as described previously (*70*) and crossed with HC196 males to generate AMJ576. The integration of *mex-5p::sid-1(+)::DsRed::sid-1 3'UTR* in AMJ576 was verified by genotyping with primers P3-P5 and Sanger sequencing of the insertion.

To express *sid-1::gfp* in the muscle from an extrachromosomal array: pTK2 (*myo-3p::sid-1::gfp*, made by AMJ and Tessa Kaplan while in Hunter Lab, Harvard University) was

constructed by amplifying part of *sid-1* cDNA from pHC355 (*20*) with primers P27 and P28, *gfp* and *unc-54 3'UTR* from pPD95.75 (Addgene #1494) using primers P29 and P30, and then fusing the fragments using PCR with primers P30 and P31 and cloning the product into the pHC355 vector backbone using the restriction enzymes NruI and EagI. pTK2 (10 ng/µl) was injected into HC196 and animals expressing GFP were isolated as AMJ706.

To express *PH::miniSOG* in neurons from an extrachromosomal array: pNMS03 (*rgef-1p::PH::miniSOG::unc-54 3'UTR*) was generated by amplifying the vector backbone of pHC337 excluding the *gfp*-dsRNA hairpin sequence using primers P35 and P36, and assembling it with *PH::miniSOG(Q103L)* amplified from pCZGY2851 (gift from Andrew Chisholm) with primers P33 and P34 using NEBuilder® HiFi DNA Assembly (New England BioLabs). pNMS03 (40 ng/µl) was injected into N2 animals with pHC448 (*myo-2p::DsRed2::unc-54 3'UTR*; 40 ng/µl (*71*)) as a coinjection marker to create AMJ837 and two other isolates.

pNMS03 (40 ng/µl) was also injected into N2 animals with PCR products forming *rgef-1p::DsRed* (40 ng/µl) generated previously (*71*) as a coinjection marker to create AMJ936 and two other isolates.

To express *PH::miniSOG* in neurons from a single-copy transgene: pNMS05 (*rgef-1p::PH::miniSOG::unc-54 3'UTR* with *ttTi5605* homology arms and *Cbr-unc-119(+)*) was generated by amplifying the transgene *rgef-1p::PH::miniSOG::unc-54 3'UTR* from pNMS03 with primers P37 and P38 containing AvrII restriction sites and cloning the fragment into pCFJ151 after AvrII (New England BioLabs) digestion. pNMS05 (50 ng/µl) and the coinjection markers pCFJ601 (50 ng/µl), pMA122 (10 ng/µl), pGH8 (10 ng/µl), pCFJ90 (2.5 ng/µl), and pCFJ104 (5 ng/µl) (plasmids described in (*70*)) were injected into the germline of adult EG4322 animals. One transgenic line was isolated as described previously (*70*) and designated as AMJ1019. The integration of *rgef-1p::PH::miniSOG::unc-54 3'UTR* in AMJ1019 was verified by genotyping with primers P3-P5 and Sanger sequencing of the insertion.

To express *PH::miniSOG* with *bli-1*-dsRNA in neurons from an extrachromosomal array: pNMS03 (40 ng/µl) was injected with *rgef-1p::bli-1-sense* (40 ng/µl) and *rgef-1p::bli-1-antisense* (40 ng/µl) PCR products generated previously (*72*) into GR1373 animals with pHC448 (*myo-2p::DsRed2::unc-54 3'UTR*) as a coinjection marker (40 ng/µl) to create AMJ1007 and one other independent isolate. AMJ1007 was crossed with HC731 males to create AMJ1108 and two other isolates. AMJ1108 was crossed with HC196 males to create AMJ1114 and one other isolate. AMJ1007 was crossed with N2 males to create AMJ1123 and one other isolate. AMJ1123 males were crossed with 3X outcrossed FX02700 (designated as AMJ1153) to create AMJ1151 and two other isolates. AMJ1151 was crossed with GR1373 males to create AMJ1173 and two other isolates.

To express *PH::miniSOG* with *gfp*-dsRNA in neurons from an extrachromosomal array: pNMS03 (40 ng/µl) and pHC337 (*rgef-1p::gfp-dsRNA::unc-54 3'UTR*; 40 ng/µl) were injected into AMJ819 (*47*) with pHC448 (*myo-2p::DsRed2::unc-54 3'UTR*; 40 ng/µl) as a coinjection marker to create AMJ1009 and one other independent isolate. AMJ1009 was crossed with N2 males to create AMJ1134. AMJ1159 was crossed with AMJ1134 males to create AMJ1312 and two other isolates.

All other transgenes were generated previously (*ccIs4251* (*12*); *oxSi487* (*70*); *tmIs1005* (*73*); *jamEx140* (*22*); *qtEx136* (*21*)).

Cas9-mediated genome editing

Genome editing was performed by injecting nuclear-localized Cas9 (PNA Bio) preincubated at 37ºC for 10 min with either a single guide RNA (sgRNA) generated by *in vitro* transcription (SP6 RNA Polymerase, New England BioLabs) or hybridized crRNA/tracrRNA (Integrated DNA Technologies), as well as an oligonucleotide or PCR-amplified homology repair template, into the *C. elegans* distal gonad. Screening for plates with successfully edited F1 animals was performed using either *dpy-10* co-CRISPR (*74-75*) or the pRF4 plasmid used as a co-injection marker (*76*). All plasmids were purified from bacterial culture using QIAprep Spin Miniprep Kit (Qiagen) and all PCR products were generated with Phusion® High-Fidelity DNA Polymerase (New England BioLabs) and purified using NucleoSpin Gel and PCR Clean-up Kit (Macherey-Nagel). Alleles generated by genome editing are schematized in Fig. 3A (*sid-1*), Supplementary Fig. S2 (*deps-1*, *sid-2*, *rme-2*, *sid-1*, *rde-1*, *sid-5*, and *sid-3*), Supplementary Fig. S4B (*rme*-2), Supplementary Fig. S6A (*sid-1*), Supplementary Fig. S12A (*W09B7.2*/*F07B7.2* (*sdg-1*)), and oligonucleotides used are in Supplemental Table S2.

To delete the *rme-2* coding sequence: Two sgRNAs targeting the start and end of the *rme-2* coding sequence were *in vitro* transcribed from a SP6 transcription template amplified from pDD162 (Addgene #47549) using primers P42 (start sgRNA) or P43 (end sgRNA) as forward primers and P40 as a universal reverse primer. An sgRNA targeting *dpy-10* for co-CRISPR was also *in vitro* transcribed using a similar template amplified from pDD162 with primers P39 and P40. All sgRNAs were purified using organic extraction, were precipitated using ethanol, and resuspended in water prior to injection. Injection into HC196 with all sgRNAs, Cas9 and the homology repair templates for *rme-2* (P44) and *dpy-10* (P41), and screening for edited animals were performed as described above. Genotyping for *rme-2(del)* was performed using a triplex PCR with primers P45-P47 to isolate AMJ1120 and one other isolate and the *rme-2* deletion was verified using Sanger sequencing. AMJ1120 was crossed with N2 males to isolate AMJ1131.

To delete the *sid-1* coding sequence: Injection of crRNAs targeting the start (P59) and end (P52) of the *sid-1* coding sequence (Integrated DNA Technologies), tracrRNA, Cas9, a *sid-1(del)* homology repair template (P60) and pRF4 into N2 and AMJ1372, and subsequent screening were performed as described above. Genotyping for *sid-1(del)* was performed using triplex PCR with primers P9, P54 and P55 to isolate AMJ1324 and one other independent isolate from N2 and AMJ1479-AMJ1482 from AMJ1372. The *sid-1* deletion was verified by Sanger sequencing in all isolates. AMJ1324 was crossed with AMJ1131 males to create AMJ1366.

To delete the *sid-2* coding sequence: Injection of crRNAs targeting the start (P71) and end (P72) of the *sid-2* coding sequence (Integrated DNA Technologies), tracrRNA, Cas9, a *sid-2(del)* homology repair template (P73) and pRF4 into N2, and subsequent screening were performed as described above. Genotyping for *sid-2(del)* was performed using triplex PCR with primers P74-P76 to isolate AMJ1368 and one other independent isolate. The *sid-2* deletion was verified by Sanger sequencing in both isolates. AMJ1368 was crossed with AMJ1324 males to create AMJ1380.

To delete the *sid-5* coding sequence: Injection of crRNAs targeting the start (P61) and end (P62) of the *sid-5* coding sequence (Integrated DNA Technologies), tracrRNA, Cas9, a *sid-5(del)* homology repair template (P63) and pRF4 into N2, and subsequent screening were performed as described above. Genotyping for *sid-5(del)* was performed using duplex PCR with primers P64 and P65 to isolate AMJ1332 and three other independent isolates. The *sid-5* deletion was verified by Sanger sequencing in all four isolates. AMJ1332 was crossed with AMJ1324 males to create AMJ1367.

To introduce a nonsense mutation into *sid-1* coding sequence: An sgRNA was designed to introduce a nonsense mutation mimicking the *qt9* allele (*13*) into *sid-1*. This sgRNA was *in vitro* transcribed from a SP6 transcription template amplified from pDD162 (Addgene #47549) using primers P48 and P40. An sgRNA targeting *dpy-10* for co-CRISPR was also *in vitro* transcribed using a similar template amplified from pDD162 with primers P39 and P40. Both sgRNAs were purified using organic extraction and were ethanol precipitated prior to injection. Injection into N2 with both sgRNAs, Cas9 and the homology repair templates for *sid-1(non)* (P49) and *dpy-10* (P41), and screening for edited animals were performed as described above. Genotyping for *sid-1(non)* was performed using a duplex PCR with primers P1 and P2 followed by restriction digestion with HpyCH4V to isolate AMJ1159. The nonsense mutation was confirmed using Sanger sequencing. AMJ1159 males were crossed with AMJ581 (*22*) to create AMJ1504 and two other independent isolates.

Injection of a crRNA with the same target sequence (P88) (Integrated DNA Technologies) as the sgRNA described above, tracrRNA, Cas9, a *sid-1(non)* homology repair template (P49) and pRF4 into N2 and AMJ1372 and subsequent screening were performed as described above. Genotyping for *sid-1(non)* was performed using duplex PCR with primers P1 and P2 followed by restriction digestion with HpyCH4V to isolate AMJ1399 from N2, and AMJ1389 and AMJ1442-AMJ1446 from AMJ1372. The nonsense mutation was verified using Sanger sequencing in all isolates.

To revert the mutation in *sid-1(non)* animals: An sgRNA was designed to revert the nonsense mutation described above back to wild-type *sid-1* sequence. The sgRNA was *in vitro* transcribed from a SP6 transcription template amplified from pDD162 (Addgene #47549) using primers P50 and P40. An sgRNA targeting *dpy-10* for co-CRISPR was also *in vitro* transcribed using a similar template amplified from pDD162 with primers P39 and P40. Both sgRNAs were purified using organic extraction and were ethanol precipitated prior to injection. Injection into AMJ1159 with both sgRNAs, Cas9 and the homology repair templates for *sid-1(rev)* (P51) and *dpy-10* (P41) and screening for edited animals were performed as described above. Genotyping for *sid-1(rev)* was performed using duplex PCR with primers P1 and P2 followed by restriction digestion with HpyCH4V to isolate AMJ1217 and two other independent isolates. The revertant was verified using Sanger sequencing in all isolates.

Injection of a crRNA with the same target sequence (P93) (Integrated DNA Technologies) as the sgRNA described above, tracrRNA, Cas9, a *sid-1(rev)* homology repair template (P51) and pRF4 into AMJ1389 and AMJ1399, and subsequent screening were performed as described above. Genotyping for *sid-1(rev)* was performed using duplex PCR with primers P1 and P2 followed by restriction digestion with HpyCH4V to isolate AMJ1412 and AMJ1413 from AMJ1389, and AMJ1405-AMJ1410 from AMJ1399. The revertant was verified using Sanger sequencing in all isolates.

To tag *W09B7.2/F07B7.2* with *mCherry*: Injection of a crRNA with the target sequence listed as P80 (Integrated DNA Technologies), tracrRNA, Cas9, an *mCherry* sequence lacking piRNA binding sites amplified from pSD6 (*47*) as a homology repair template with homology arms to the C-terminus of *W09B7.2/F07B7.2* using primers P81 and P82 and pRF4 into N2, and subsequent screening were performed as described above. Genotyping for identical tags of *W09B7.2::mCherryΔpi/F07B7.2::mCherryΔpi* was performed using triplex PCR with primers P79, P83 and P84 to isolate AMJ1372 (tagging of both loci indicated by agarose gel stained with ethidium bromide in Supplementary Fig. S12B). The *mCherryΔpi* insertion was verified by Sanger sequencing. AMJ1372 hermaphrodites and males generated by heatshock were mated

with N2 males and hermaphrodites, respectively, to examine expression in cross progeny and homozygosed wild-type and *W09B7.2/F07B7.2(jam137[mCherryΔpi]*) animals across generations in six independent F1 lineages from each cross. See Fig. 4B and Supplementary Fig. S13 for associated data.

To introduce a nonsense mutation into *rde-1* coding sequence: Injection of a crRNA with the target sequence listed as P94 (Integrated DNA Technologies), tracrRNA, Cas9, a *rde-1(non)* homology repair template (P95) mimicking *rde-1(ne300)* (*77*), and pRF4 into AMJ1372 and subsequent screening were performed as described above. Genotyping for *rde-1(non)* was performed using duplex PCR with primers P96 and P97 and restriction digestion with NlaIII to isolate AMJ1447 and AMJ1448. The nonsense mutation was verified by Sanger sequencing for all isolates.

To tag *sid-1* with *wrmScarlet* at the 3' end: Injection of a crRNA with the target sequence listed as P52 (Integrated DNA Technologies), tracrRNA, Cas9, a *sid-1::wrmScarlet13* homology repair template with the beginning (1) and end (3) but not the middle (2) of the coding sequence (P53) (*78*), and pRF4 into N2 and subsequent screening were performed as described above. Genotyping for *wrmScarlet13* was performed using duplex PCR with primers P54 and P55 to isolate AMJ1280. The *wrmScarlet13* insertion was verified by Sanger sequencing. Subsequent injections were performed into AMJ1280 with a *wrmScarlet13* specific crRNA with the target sequence listed as P56 (Integrated DNA Technologies), a complete *wrmScarlet* coding sequence amplified from pSEM89 (made in Boulin Lab – gift from Kevin O'Connell) with primers P57 and P58 and the same components as described previously. After similar screening, genotyping for full *wrmScarlet* insertion was performed using duplex PCR with primers P54 and P55 to isolate AMJ1282 and one other independent isolate. The full *wrmScarlet* insertion was verified by Sanger sequencing. AMJ1282 was crossed with AMJ577 males to create AMJ1365.

To tag *rme-2* with *wrmScarlet* at the 3' end: Injection of a crRNA with the target sequence listed as P67 (Integrated DNA Technologies), tracrRNA, Cas9, a *rme-2::wrmScarlet13* homology repair template with the beginning (1) and end (3) but not the middle (2) of the coding sequence (P69) (*78*), and pRF4 into N2 and subsequent screening were performed as described above. Genotyping for *wrmScarlet13* was performed using duplex PCR with primers P70 and P47 to isolate AMJ1281. The *wrmScarlet13* insertion was verified by Sanger sequencing. Subsequent injections were performed into AMJ1281 with a *wrmScarlet13* specific crRNA with the target sequence listed as P77 (Integrated DNA Technologies), a complete *wrmScarlet* coding sequence amplified from pSEM89 (made in Boulin Lab – gift from Kevin O'Connell) with primers P57 and P58 and the same components as described previously. After similar screening, genotyping for full *wrmScarlet* insertion was performed using duplex PCR with primers P54 and P55 to isolate AMJ1284 and two other independent isolates. The full *wrmScarlet* insertion was verified by Sanger sequencing.

To tag *sid-1* internally with *mCherry*: Injection of a crRNA with the target sequence listed as P110 (Integrated DNA Technologies), tracrRNA, Cas9, an *mCherry* lacking piRNA binding sites amplified from pSD6 (*47*) as a homology repair template with homology arms to the exon 4 of *sid-1* with primers P111 and P112, and pRF4 into N2 and subsequent screening were performed as described above. Genotyping for *mCherryΔpi* was performed using triplex PCR with primers P113, P114 and P79 to isolate AMJ1438 and one other isolate from the same lineage. The *mCherryΔpi* insertion was verified by Sanger sequencing. Subsequent injections were performed into AMJ1438 with a crRNA targeting the 5'-end of *mCherryΔpi* (P115) (Integrated DNA Technologies), a homology repair template containing a 45-nt linker sequence

(P116) and the same components as described previously. After similar screening, genotyping for the linker insertion was performed using duplex PCR with primers P113 and P79 to isolate AMJ1485 and two other independent isolates. Insertion of the linker was verified by Sanger sequencing in all three isolates.

To introduce a nonsense mutation into *sid-3* coding sequence: Injection of a crRNA with the target sequence listed as P66 (Integrated DNA Technologies), tracrRNA, Cas9, a *sid-3(non)* homology repair template (P85) mimicking *sid-3(qt31)* (*79*) and pRF4 into AMJ1372 and subsequent screening were performed as described above. Genotyping for *sid-3(non)* was performed using duplex PCR with primers P86 and P87, and restriction digestion with StyI to isolate AMJ1449 and AMJ1450. The nonsense mutation was verified by Sanger sequencing for both isolates.

To introduce a nonsense mutation into *deps-1* coding sequence: Injection of a crRNA with the target sequence listed as P68 (Integrated DNA Technologies), tracrRNA, Cas9, a *deps-1(non)* homology repair template (P137) mimicking *deps-1(bn124)* (*54*) and pRF4 into AMJ1372 and subsequent screening were performed as described above. Genotyping for *deps-1(non)* was performed using allele specific PCR with primers P138 and P139 amplifying the wild-type sequence and primers P140 and P141 amplifying the mutant allele to isolate AMJ1451 and AMJ1452. The nonsense mutation was verified by Sanger sequencing for both isolates.

To insert the tetracycline K4 aptazyme into the 3'UTR of *sid-1*: Injection of a crRNA with the target sequence listed as P52 (Integrated DNA Technologies), tracrRNA, Cas9, a *sid-1::tetracycline-K4-aptazyme* homology repair template (P78) and pRF4 into N2 and subsequent screening were performed as described above. Genotyping for insertion of the aptazyme sequence was performed using duplex PCR with primers P54 and P55 to isolate AMJ1323. The aptazyme insertion was verified by Sanger sequencing. AMJ1323 was crossed with AMJ477 (*21*) males to create AMJ1330, AMJ471 (*22*) males to create AMJ1350, and AMJ1323 males were crossed with JH3197 to create AMJ1355.

To insert the tetracycline K4 aptazyme into the 3'UTR of *gtbp-1(ax2053[gtbp-1::gfp])*: Injection of a crRNA with the target sequence listed as P89 (Integrated DNA Technologies), tracrRNA, Cas9, a *gtbp-1::gfp::tetracycline-K4-aptazyme* homology repair template (P90) and pRF4 into JH3197 and subsequent screening were performed as described above. Genotyping for insertion of the aptazyme sequence was performed using duplex PCR with primers P91 and P92 to isolate AMJ1542. The aptazyme insertion was verified by Sanger sequencing.

To introduce a missense mutation into *dpy-10* coding sequence: Injection of crRNA with the target sequence listed as P142 (Integrated DNA Technologies), tracrRNA, Cas9, and a *dpy-10(mis)* homology repair template (P41) mimicking *dpy-10(cn64)* (*80*) in AMJ1372 was performed as described above and heterozygous F1 animals were screened for by passaging "rolling" animals. Animals that appeared wild-type and those that appeared Dpy (homozygous *dpy-10(-)*) were isolated from three independently edited F1 animals. See Supplementary Fig. S14 for associated data.

Light-induced damage of neurons

Optimizing duration of light exposure: 20-30 animals expressing PH::miniSOG in neurons (multi copy, AMJ837; single copy, AMJ1019) were placed on an unseeded NGM plate and exposed to blue light (470 nm wavelength) at a distance of approximately 7.5 cm from an LED (Cree Xlamp XP-E2 Color High Power LED Star – Single 1 UP, LED supply) producing light at a power of ~2 mW/mm^2 flashing at a frequency of 2 Hz for different durations of time.

Animals were then scored for movement defects immediately after light exposure, OP50 was seeded onto the plate, and animals were scored again 24 h post light exposure (Supplementary Fig. S1A). Wild-type animals were exposed to blue light for the same durations as control. Representative widefield images of unparalyzed (wild type) and paralyzed (coiled, AMJ837) animals were taken using a Nikon AZ100 microscope and Photometrics Cool SNAP HQ^2 camera (Supplementary Fig. S1B, *top*). Confocal images of animals expressing PH::miniSOG and DsRed in neurons (AMJ936) with and without 30 minutes of blue light exposure were taken using a Leica TCS SP8 DLS microscope with HyVolution using a 40X oil objective lens. DsRed was excited using a 638 nm laser and fluorescence was collected through a 598 nm emission filter (Supplementary Fig. S1B, *bottom*). Images were adjusted for display using Fiji (NIH) (*81*).

Silencing by *bli-1*-dsRNA: Five L4 animals with an extrachromosomal array expressing PH::miniSOG and *bli-1*-dsRNA in neurons were placed on seeded NGM plates and allowed to lay progeny for 24 h. P0 animals were then removed and F1 progeny were exposed to blue light as described above for 60 min at different time points after initial P0 L4 animals were passaged. 96 h post light exposure F1 progeny with the array were scored for *bli-1* silencing (presence of blisters) in gravid adults (Supplementary Fig. S1C, *top*, Supplementary Fig. S1D, Supplementary Fig. S1E).

Silencing by *gfp*-dsRNA: L4 animals with the *mex-5p::mCherry::h2b::gfp::h2b* transgene (*oxSi487*) (Fig. 1B) were mated with L4 male animals with an extrachromosomal array expressing PH::miniSOG and *gfp*-dsRNA in neurons (Fig. 1A). After 36 h of mating and laying progeny, P0 animals were removed from plates and F1 progeny were exposed to blue light as described above for 60 min at different time points after initial P0 L4 animals were mated. 96 h after mating, F1 cross progeny hermaphrodites with the array were imaged as adults (Supplementary Fig. S1C, *bottom*) under a coverslip in 10 µl of 3 mM levamisole on a 2% agar pad using a Nikon AZ100 microscope and Photometrics Cool SNAP HQ^2 camera. A C-HGFI Intensilight Hg Illuminator was used to excite GFP (filter cube: 450 to 490 nm excitation, 495 dichroic, and 500 to 550 nm emission) and mCherry (filter cube: 530 to 560 nm excitation, 570 dichroic, and 590 to 650 nm emission). Animals were scored as bright if fluorescence was easily detectable without adjusting levels, dim if fluorescence could be observed after level was adjusted to saturation, and not detectable if fluorescence was still not observed after level adjustments (Supplementary Fig. S1F). Representative images were adjusted in Adobe Photoshop to identical levels for presentation (Fig. 1B, Fig. 1C, Fig. 1D).

Sensitive northern blotting

RNA was *in vitro* transcribed from a PCR amplicon using T7 RNA Polymerase (New England BioLabs) (Supplementary Fig. S4F) or expressed in HT115 *E. coli* after IPTG induction during exponential growth (Supplementary Fig. S4D, Supplementary Fig. S4E) and extracted using TRIzol (Fisher Scientific). RNA was then separated by size using fully denaturing formaldehyde polyacrylamide gel electrophoresis (FDF-PAGE (*82*)) wherein 10 µg RNA samples were heated with formaldehyde to disrupt dsRNA duplexes and run on a 4% denaturing polyacrylamide gel next to 1-kb and 100-bp DNA ladders for size comparison. After migration, the ladder lanes were stained with ethidium bromide and imaged, and the RNA lanes were transferred to a positively charged nitrocellulose membrane using a Trans-Blot® Turbo™ Transfer System (Bio-Rad) and crosslinked using 120 mJ/cm^2 UV radiation. Blots were then exposed to 2.5 pmol of 40-nt HPLC purified DNA oligonucleotides conjugated to digoxigenin (DIG) using the DIG Oligonucleotide Tailing Kit (Roche) hybridized to the nitrocellulose

membrane at 60°C overnight (42°C for 2 h for 5S rRNA) in ULTRAhyb™ buffer (Invitrogen™) to probe the sense or antisense strands of *unc-22* (Supplementary Fig. S4D, Supplementary Fig. S4F) or *gfp*-dsRNA (Supplementary Fig. S4E) at different positions (adapted from (*31*)). After hybridization, the membrane was washed and blocked using the DIG Wash and Block Buffer Set (Roche), incubated with Anti-DIG-AP, Fab fragments (Roche) and developed with CSPD (Roche) at 37°C for 15 min. Chemiluminescence from the AP/CSPD reaction was imaged using a LAS-3000 (Fujifilm) or iBright™ CL1000 (Invitrogen™) imager. Overexposed blots were compared to ethidium bromide-stained ladders after imaging to visualize fragment size. Blots were stripped using two washes with 5% SDS (Sigma Aldrich) and two washes with 2X SSC (Sigma Aldrich) and the hybridization, blocking and development procedures were repeated for each probe (5S RNA probe: P118; *unc-22* probes: P119-P124; *gfp* probes: P125-P130).

Injection of dsRNA

Injection of synthetic dsRNA: RNA oligonucleotides were purchased from IDT and resuspended in IDT Duplex Buffer (*unc-22*: P131 and P132; *gfp*: P133 and P134; fluorescently-labeled *gfp*: P135 and P136). 1 µg each of HPLC purified 50-nt sense and antisense oligonucleotides was diluted to 100-350 ng/µl with IDT Duplex Buffer at a final volume of 10 µl. Alternatively, *unc-22* single-stranded RNA was treated with polynucleotide kinase and annealed in equal proportion at a final concentration of ~97 ng/µl of *unc-22*-dsRNA in IDT Duplex Buffer (Supplementary Fig. S4G, Supplementary Fig. S4H). This mixture was heated to 95ºC for 1 min and cooled at a rate of 1ºC/min to a final temperature of 25ºC. The mix was centrifuged at 16500 x g for 20-30 min and loaded into a microinjection needle. Young adult animals were injected 24 h after the L4 stage in the body cavity just beyond the bend of the posterior gonad arm (*25*). Injected animals were recovered with M9 buffer and isolated onto NGM plates and allowed to lay progeny. In cases where animals were mated with N2 males post injection, two adult N2 males were placed on each plate with an injected hermaphrodite.

Injection of *in vitro* transcribed dsRNA: Templates for transcription were amplified from RNAi vectors using one common primer specific to the T7 promoter sequence (P117). PCR products were purified using column purification (Macherey-Nagel, ref. 740609.50) and subsequently used for transcription by T7 RNA Polymerase (New England BioLabs). Many transcription reactions were pooled and purified using one column to produce concentrated RNA samples. Annealing, centrifugation, and injection into the body cavity of animals staged as L4s (injected between pharynx and anterior intestine) or young adults were performed as described for synthetic dsRNA with identical concentrations unless otherwise indicated in figure legends. In cases where animals were mated with N2 males post injection, two adult N2 males were placed on each plate with an injected hermaphrodite.

Scoring of gene silencing: For scoring silencing by *unc-22* dsRNA, 10-30 L4 animals were passaged into 10 µl of 3 mM levamisole and scored for twitching, observed as rapid movement of the head and/or tail (as in (*25*)), 3-4 days after injection for progeny of *rme-2(+)* parents and 4-5 days after injection for progeny of *rme-2(-)* parents with no appreciable difference between days in which animals were scored post injection. Weak and strong twitching were scored as in Supplemental Movies S1-S3 of (*25*). Numbers of silenced animals and total animals scored were summed across all days of scoring and experimental replicates.

When scoring silencing of *gfp*, animals were either scored by eye in comparison to animals injected with duplex buffer only (i.e. buffer; Supplementary Fig. S3B) or were mounted in 10 µl of 3 mM levamisole on a 2% agar pad and imaged under a coverslip as P0 adults (2 days

post injection) or F1 L4s (3 days post P0 injection) using a Nikon AZ100 microscope and Photometrics Cool SNAP HQ^2 camera. A C-HGFI Intensilight Hg Illuminator was used to excite GFP (filter cube: 450 to 490 nm excitation, 495 dichroic, and 500 to 550 nm emission). Representative images for *gfp* expression in F1 animals after P0 injection were adjusted to identical levels in Adobe Photoshop for presentation (Fig. 2B). See "Imaging and quantification of reporters using widefield microscopy" for other methods of scoring *gfp* expression after imaging.

Imaging of fluorescently labeled dsRNA: Embryos were imaged 22 hours post P0 injection with labeled dsRNA. Laid embryos were picked off plates and placed into 5 µl of 3 mM levamisole on a coverslip let sit for at least 5 minutes before placing on a 2% agarose pad on a slide. Embryos were imaged using the Eclipse Ti Spinning Disk Confocal (Nikon) with the 60X objective lens. Atto 565 was excited using a 561 nm laser and fluorescence was collected through a 415-475 nm and 580-650 nm emission filter. Images were adjusted for display using Fiji (NIH (*81*)).

Feeding RNAi

P0 and F1 feeding: *E. coli* (HT115) expressing dsRNA was cultured in LB media with 100 µg/µl carbenicillin overnight at 250 rpm. 100 µl of cultured bacteria was then seeded onto RNAi plates and incubated at room temperature for approximately 24 h. L4 animals were passaged onto seeded RNAi plates and progeny were scored for silencing by bacteria expressing dsRNA targeting *unc-22* (twitching in levamisole), *bli-1* (blisters), *pos-1* (dead eggs) or expressing L4440 as an empty vector control.

P0 only feeding: RNAi bacteria were cultured and seeded as described above. L4-stage or young adult-stage (24 h post L4) animals were passaged onto seeded RNAi plates and cultured at 20ºC for approximately 24 h. Animals were then picked into 1 ml of M9 buffer and washed four times to remove any residual bacteria (as in (*25*)). After washing, animals were resuspended in 200 µl of remaining M9 buffer and placed onto a seeded NGM plate. 1 h later, animals were isolated onto single NGM plates and their progeny were scored for silencing as described above.

F1 only feeding: L4-staged animals were passed onto RNAi plates seeded with 10 µl of *E. coli* (OP50). Animals were allowed to develop into adults and lay eggs over 24 h and then removed from plates. Plates were then seeded with 100 µl of *E. coli* (HT115) expressing the L4440 empty vector control or *gfp*-dsRNA cultured in LB media with 100 µg/µl carbenicillin for 24 h. Progeny were imaged throughout development or as adults 3 days after being staged as L4 animals (day 3 adults).

Tetracycline-induced expression

For animals cultured with OP50 *E. coli*: 81.6 µl of a 500 µM solution of tetracycline in water was added to NGM plates previously seeded with OP50 *E. coli* (at least two days earlier) to create 4 mL plates with 10 µM tetracycline (concentration based on (*43*)). Volumes of 166.7 µl and 444.4 µl of tetracycline solution were used to create plates with final concentrations of 20 µM or 50 µM, respectively (see Supplementary Fig. S7D). Control plates were also made by adding the same amount of water to seeded NGM plates without tetracycline. Tetracycline plates and control plates were incubated at room temperature out of direct light overnight to allow any remaining liquid to dry. Animals were passaged to tetracycline or water plates with or without previous injection of 10 µM tetracycline or water into adult gonads. Progeny expressing neuronal *unc-22* or *gfp*-dsRNA were scored for silencing on the first day of adulthood. In the case of

silencing of *gtbp-1::gfp* by neuronal *gfp*-dsRNA, animals with the array expressing *gfp*-dsRNA were passaged as L4s onto new tetracycline or water plates to be imaged as day 1 adults. The brood size of animals cultured on OP50 with 10 μM tetracycline or water was scored by staging single L4 animals on NGM plates with 10 μM tetracycline or water and moving animals every 24 h to new 10 μM tetracycline or water plates. Progeny laid on each of the four days were counted after growing to adulthood, continuously cultured under either condition.

For animals cultured on HT115 *E. coli* expressing dsRNA: Bacteria expressing *bli-1*-dsRNA, *gfp*-dsRNA, *pos-1*-dsRNA or L4440 control vector were cultured overnight to a maximum time of 24 hours (for *gfp*-dsRNA and L4440 only) and 100 μl of bacteria was seeded onto RNAi plates. Plates were incubated for 1-2 days at room temperature to allow for growth and drying of bacteria. 10 μM tetracycline or water was added to newly seeded plates as described above. After drying of tetracycline and water, P0 animals were added to plates and F1 animals were scored for silencing by *bli-1*-dsRNA or *gfp*-dsRNA as adults in the next generation. Silencing by *pos-1*-dsRNA was scored by measuring the brood of three L4 animals staged on a single RNAi plate with *pos-1*-dsRNA and 10 μM tetracycline or water. Brood size over four days was measured after moving all P0 animals every 24 h to new 10 μM tetracycline or water plates and scoring adult progeny cultured under either condition.

In all experiments, animals expressing *unc-22*-dsRNA in neurons were exposed to the same tetracycline and water solutions used and scored for *unc-22* silencing as adults as a control for effectiveness of tetracycline (see summary of data in Supplementary Fig. S7B).

Imaging and quantification of reporters using widefield microscopy

All animals and embryos expressing fluorescent reporters were imaged in 10 μl of 3 mM levamisole on a 2% agar pad using a Nikon AZ100 microscope and Photometrics Cool SNAP HQ^2 camera. A C-HGFI Intensilight Hg Illuminator was used to excite mCherry (filter cube: 530 to 560 nm excitation, 570 nm dichroic, and 590 to 650 nm emission), GFP or other autofluorescent molecules in the green channel (filter cube: 450 to 490 nm excitation, 495 nm dichroic, and 500 to 550 nm emission) and autofluorescent molecules in the blue channel (filter cube: 325 to 375 nm excitation, 400 nm dichroic, 435 to 485 nm emission). Intensity of GFP and mCherry were quantified in Fiji (NIH) (*81*) using the methods described below. Representative images were adjusted in Fiji (NIH) (*81*) and/or Adobe Photoshop to identical levels for presentation (Fig. 3C, Fig. 3D, Fig. 4A (*top left*), Fig. 4D, Supplementary Fig. S6E, Supplementary Fig. S6F, and Supplementary Fig. S6G).

For GTBP-1::GFP quantification post injection: Somatic *gfp* expression was quantified between the pharynx and anterior gonad arm by drawing a circle or ventral to dorsal line within the boundaries of the animal (Supplementary Fig. S5A) on a brightfield image, creating a mask, imposing that mask onto the GFP channel image and measuring average intensity or intensity along the line, respectively. To measure background fluorescence, the same circle or a new circle was used to measure average intensity outside of the animal. Germline GFP expression was quantified by freely selecting part of the distal or proximal region of the anterior or posterior gonad arm (Supplementary Fig. S5A) excluding the intestine to avoid intestinal autofluorescence. Selection was performed using a brightfield image, a mask was created and imposed onto the GFP channel image and average intensity was measured. To measure background fluorescence, the same selection boundary was moved outside of the animal and average background intensity was measured. To plot average GFP intensity measured by a circle or free selection, average background intensity was subtracted from GFP intensity for each

image and plotted with a box plot (Supplementary Fig. S5C). To plot GFP intensity along the ventral to dorsal axis in the anterior soma, the average intensity in each tenth of the axis was calculated for each animal and plotted with a shaded region representing 95% confidence intervals (Supplementary Fig. S5B, *top*). To calculate differences in intensity between the interior and exterior of animals, the average intensity of the 0.4-0.6 region of the axis was divided by the average intensity of the 0.1 and 0.9 points of the axis. These values were calculated and plotted for each animal with a box plot (Supplementary Fig. S5B, *bottom*). All plotting was done using custom R scripts.

For GTBP-1::GFP quantification post feeding: Animals fed L4440 or *gfp*-dsRNA for different durations of the P0 and/or F1 generation were scored for germline silencing at different stages during the F1 generation (Fig. 1E, Fig. 1F, Supplementary Fig. S3A). GFP intensity (a.u.) was measured by free selection of germ cells but avoiding intestinal cells at each stage, selecting a region around the primordial vulva in L2 animals, in one of two extending gonad arms in L3 and L4 animals, and of eggs *in utero* in gravid adults. To measure background fluorescence, the same selection or a new selection was used to measure average intensity outside of the animal. To plot average GFP intensity measured by free selection, average background intensity was subtracted from GFP intensity for each image and shown as a box plot (Fig. 1E, Fig. 1F, Supplementary Fig. S3A). All plotting was done using custom R scripts.

For adjustment of fluorescence images of *sid-1::mCherryΔpi* animals for comparison to images of wild-type animals: Representative images of *sid-1(jam195[linker::mCherryΔpi])* and wild type animals at different stages were adjusted to the same maximum and minimum displayed values of intensity using Fiji (NIH) (*81*) to highlight each region of interest below saturation (Fig. 3C, Fig. 3D, Supplementary Fig. S6E, Supplementary Fig. S6F, Supplementary Fig. S6G).

For SDG-1::mCherry quantification: Germline mCherry intensity was quantified by freely selecting part of the distal or proximal region of the anterior or posterior gonad arm excluding the intestine to avoid quantifying intestinal autofluorescence. Selection was performed using a brightfield image, a mask was created and imposed onto the mCherry channel image and average intensity was measured. To measure background fluorescence, the same selection boundary was moved outside of the measured gonad arm and average background intensity was measured. To plot average mCherry intensity, average background intensity was subtracted from mCherry intensity for each gonad arm and shown as a box plot using custom R scripts (Fig. 4C, Fig. 4E, Supplementary Fig. S12C, Supplementary Fig. S13, Supplementary Fig. S14). In Fig. 4B, SDG-1::mCherry intensity measurements, adjusted by subtracting background intensity and intensity measurements made in a wild-type animal lacking mCherry, were normalized to RT-qPCR measurements by multiplying each median intensity value by a conversion factor. This conversion factor was calculated by dividing the median SDG-1::mCherry intensity in AMJ1372 animals by the median relative *sdg-1* mRNA level in AMJ1372 RNA samples. All estimated relative *sdg-1* expression values were then normalized to those of wild-type animals by dividing all values by the wild-type value.

Imaging and quantification of reporters using confocal microscopy

For *sid-1* reporters expressed from multi-copy transgenes: L4 animals expressing *myo-3p::sid-1 cDNA::DsRed* and *myo-3p::sid-1::gfp* were placed in 10 µl of 3 mM levamisole and imaged using the Eclipse Ti Spinning Disk Confocal (Nikon) with the 100X objective lens. DsRed was excited using a 561 nm laser and fluorescence was collected through a 415-475 nm

and 580-650 nm emission filter. GFP was excited using a 488 nm laser and fluorescence was collected through a 500-550 nm emission filter. Images were adjusted in Fiji (NIH (*81*)) and Adobe Photoshop to identical levels for presentation (Supplementary Fig. S6B).

For the endogenous gene tag *W09B7.2/F07B7.2::mCherryΔpi*: Adult animals were placed in 10 µl of 3 mM levamisole and imaged using the Eclipse Ti Spinning Disk Confocal (Nikon) with the 60X objective lens. mCherry was excited using a 561 nm laser and fluorescence was collected through a 415-475 nm and 580-650 nm emission filter. Images and movies were adjusted in Fiji (NIH) (*81*) and Adobe Photoshop to identical levels for presentation (Fig. 4A, *right* and *bottom left*, Supplementary Movies S1-S3).

RNA sequencing, principal component analysis and differential expression analysis

For analysis of previously generated *sid-1(-)* alleles: Mixed-stage animals were washed from 10 plates in biological duplicate 5 days after passaging L4-stage animals. Total RNA was extracted from pellets using TRIzol (Fisher Scientific). PolyA+ RNAs were purified and converted to DNA libraries by the University of Maryland Genomics Core using the Illumina TruSeq Library Preparation Kit. FASTQ files were processed using the command "`cutadapt -j 0 -a AGATCGGAAGAGCACACGTCTGAACTCCAGTCA -m 20 -q 20 -o cutread.gz fasta1.gz`" (*83*). Reads were assigned transcript IDs and counted using the command "`salmon quant -i celegans.index -l A -r cutread.gz -p 8 –validateMappings -o quant_file`" (*84*). For conversion of transcript IDs to gene IDs, a table of matching transcript and gene IDs was generated from a GTF file using the command "`grep "^[^#]" Caenorhabditis_elegans.WBcel235.###.gtf | awk '{if($3 == "transcript"){print}}' | awk '{print $12,$14}' | tr -d '";' > transcript_id_gene_id.tsv`". Conversion was then made using this table with tximport (*85*) in R, whereafter only genes with more than 0.1 counts per million for at least 2 samples were used in subsequent analyses with pairs of sample types (*sid-1(qt9[non])* vs. wild type and *sid-1(tm2700[del]); tmIs1005[sid-1(+)* vs. *sid-1(tm2700[del])*). After normalizing samples using the trimmed mean of M-values method (*86*), principal component analysis was performed in R by comparing samples based on the 500 genes with the largest standard deviations in their $\log_2$-fold change between each set of samples (Supplementary Fig. S8A). Differential expression analysis was performed using limma(voom) (*87*) in R (sample R script in Supplementary File 1). Volcano plots of differential expression for all genes compared were plotted using custom R scripts with genes having an adjusted *p*-value threshold (*q*-value) less than 0.05 in black and those greater than 0.05 in grey (Supplementary Fig. S8B).

For analysis of newly generated *sid-1(-)* alleles: Total RNA >200 nt was extracted using RNAzol (Sigma-Aldrich) from 200 µl pellets of mixed-stage animals collected from 6 non-starved but crowded plates in biological triplicate for each strain. PolyA+ RNAs were purified and converted to DNA libraries using the Illumina TruSeq Stranded mRNA Library Preparation Kit. Library quality was assayed using TapeStation (Agilent) and libraries were sequenced using a HiSeq X10 (Illumina) by Omega Bioservices. FASTQ files were processed using the command "`cutadapt -j 0 -a AGATCGGAAGAGCACACGTCTGAACTCCAGTCA -A AGATCGGAAGAGCGTCGTGTAGGGAAAGAGTGT -m 20 -q 20 -o cutread1.gz –p cutread2.gz read1.gz read2.gz`" (*83*). Reads were assigned transcript IDs and counted using the command "`salmon quant -i celegans.index -l A -1 cutread1.gz -2 cutread2.gz -p 8 –validateMappings -o quant_files`" (*84*). For conversion of transcript IDs to gene IDs, a table of matching transcript and gene IDs

was generated from a GTF file using the command "`grep "^[^#]" Caenorhabditis_elegans.WBcel235.###.gtf | awk '{if($3 == "transcript"){print}}' | awk '{print $12,$14}' | tr -d '";' > transcript_id_gene_id.tsv`". Conversion was then made using this table with tximport (*85*) in R, whereafter only genes with more than 0.1 counts per million for at least 3 samples were used in subsequent analyses. After normalizing samples using the trimmed mean of M-values method (*86*), principal component analysis was performed in R by comparing samples based on the 500 genes with the largest standard deviations in their $\log_2$-fold change between each set of samples (Fig. 3E, Supplementary Fig. S9A). Differential expression analysis was performed using limma(voom) (*87*) in R (sample R script in Supplementary File 1). Volcano plots of differential expression for all genes compared were plotted using custom R scripts with genes having an adjusted *p*-value threshold (*q*-value) less than 0.05 in black and those greater than 0.05 in grey (Fig. 3F, Supplementary Fig. S9B). Genes that were similarly misregulated in Fig. 3F and Supplementary Fig. S9B are in red.

For analysis of data from (*88*): FASTQ files were processed using the command "`cutadapt -j 0 -a AGATCGGAAGAGCACACGTCTGAACTCCAGTCA -m 20 -q 20 -o cutread.gz fasta1.gz`" (*83*). Reads were assigned transcript IDs and counted using the command "`salmon quant -i celegans.index -l A -r cutread.gz -p 8 –validateMappings -o quant_file`" (*84*). For conversion of transcript IDs to gene IDs, a table of matching transcript and gene IDs was generated from a GTF file using the command "`grep "^[^#]" Caenorhabditis_elegans.WBcel235.###.gtf | awk '{if($3 == "transcript"){print}}' | awk '{print $12,$14}' | tr -d '";' > transcript_id_gene_id.tsv`". Conversion was then made using this table with tximport (*85*) in R. After normalizing samples using the trimmed mean of M-values method (*86*), differential expression analysis was performed using limma(voom) (*87*) in R (sample R script in Supplementary File 1). Volcano plots of differential expression for all genes compared were created using custom R scripts with *sid-1*, *W09B7.2/F07B7.2* and *Y102A5C.36* in red and all other genes in grey (Supplementary Fig. S10).

Genome mapping and visualization of sequencing reads for sid-1-dependent genes

After RNA sequencing samples were processed as described above, reads were mapped to the *C. elegans* genome using the command "`hisat2 -p 8 -x Celegans98index -1 cutread1.gz -2 cutread2.gz -S sam1`" (*89*). The SAM file outputs were then converted to BAM files using the command "`samtools view -b sam1 | samtools sort -> bam1.bam`" and BAM index files were created for visualization using "`samtools index bam1.bam`" (*90*). Reads for the *sid-1* and *F14F9.5* locus, *W09B7.2/F07B7.2* locus, and *Y102A5C.36* locus were plotted using custom R scripts and axes were normalized for each sample based on its total mapped reads, calculated using the command "`samtools view -c -F 4 bam1.bam`" (Supplementary Fig. S9D).

Reverse transcription and quantitative PCR

Total RNA was extracted using TRIzol (Fisher Scientific) from 200 µl pellets of mixed-stage animals collected from 3-6 nonstarved but crowded plates in biological triplicate for each strain. The aqueous phase was then washed with an equal amount of chloroform and precipitated overnight on ice with 100 µl of 3 M sodium acetate, 1 ml of 100% ethanol and 10 µg glycogen (Invitrogen). RNA pellets were washed twice with 70% ethanol and resuspended in 22 µl

nuclease free water. RNA samples were then DNase-treated in DNase buffer (10 mM Tris-HCl pH 8.5, 2.5 mM MgCl, 0.5 mM $CaCl_2$) with 0.5 U DNase I (New England BioLabs) at 37°C for 60 minutes followed by heat inactivation at 75°C for 10 minutes. RNA concentration was measured and 1 µg of total RNA was used as input for reverse transcription using 50 U SuperScript III Reverse Transcriptase (Invitrogen) (+RT) or no reverse transcriptase as a negative control (-RT) (RT primers: *tbb-2* (P98), *sid-1* (P101), *W09B7.2/F07B7.2* (P104), *Y102A5C.36* (P107)). For qPCR, each +RT biological replicate was assayed in technical triplicate for each gene target, along with a single -RT sample for each corresponding biological replicate and a no template control (NTC) using 2 µl cDNA and the LightCycler® 480 SYBR Green I Master kit (Roche). Ct values were measured with the Bio-Rad C1000 CFX96 Real-Time System and Bio-Rad CFX Software (qPCR primers: *tbb-2* (P99 and P100), *sid-1* (P102 and P103), *W09B7.2/F07B7.2* (P105 and P106), *Y102A5C.36* (P108 and P109)). To calculate relative change in mRNA abundance compared to wild type, we calculated $\log_2(2^{(-(\text{gene Ct} - \text{tbb-2 Ct}))})$ using the median of technical replicates for the biological triplicates of each genotype. Ct values were only used if they were lower than corresponding -RT and NTC Ct values. The median value of wild-type biological replicates was then subtracted from the value for each sample to plot calculated values with respect to wild-type levels (Fig. 3G, Supplementary Fig. S9C, Supplementary Fig. S12D, Supplementary Fig. 13).

BLAST searches and protein alignment

BLAST (NCBI) searches were performed using the W09B7.2/F07B7.2 (SDG-1) amino acid sequence with default parameters and any homologs identified were aligned to SDG-1 using Clustal Omega (*91*) with default parameters. Alignments produced are shown in Supplementary Fig. S15 with residues shared by two proteins (grey highlight) or all three proteins (black highlight) indicated.

Annotation of the Cer9 retrotransposon containing W09B7.2/F07B7.2

The *Cer9* retrotransposon containing *W09B7.2/F07B7.2* (*sdg-1*) was annotated using sequence features from UCSC Genome Browser and amino acid sequences obtained from (*92*). The 5' and 3' LTR sequences were identified using RepeatMasker and were confirmed to have TC and GA dinucleotides at the beginning and end of each sequence, respectively (*92*). Amino acid sequences from (*92*) corresponding to *gag* and *pol* (PR: protease, RT: reverse transcriptase, RH: RNaseH, IN: integrase) elements of *Cer9* were used in tblastn (NCBI) searches to determine their positions in the *Cer9* retrotransposon sequence that also contains *sdg-1*.

Rationale for inferences

Prior models and assumptions: All dsRNA are trafficked similarly. Entry of dsRNA into the germline can initiate transgenerational RNA silencing of some but not all genes. No SID-1-dependent genes are known, suggesting that SID-1 could be used solely in response to viral infection by analogy with roles of other members of RNA interference pathways.

Evidence supporting key conclusions: Temporal selectivity of dsRNA transport was probed using three approaches for delivery of dsRNA (damage-induced release from neurons, ingestion, and injection). Spatial selectivity was inferred based on differences in the frequency of patterns of silencing within the germline. Substrate selectivity of dsRNA transport pathways was probed using genetic mutants and dsRNA of different lengths and 5' chemistry. Diversity of dsRNAs made in bacteria and upon *in vitro* transcription was visualized using Northern blotting.

Analysis of *sid-1* mutants and a revertant was used for better control of genetic background, aiding in the identification of ***s****id-1*-**d**ependent **g**enes (*sdg*). Separate measurement of *sdg-1* expression in descendants of independently-edited isolates, along different lineages after perturbations, and in different gonads within single animals demonstrated stochasticity in gene expression and revealed establishment of different heritable epigenetic states.

Supplementary Figures

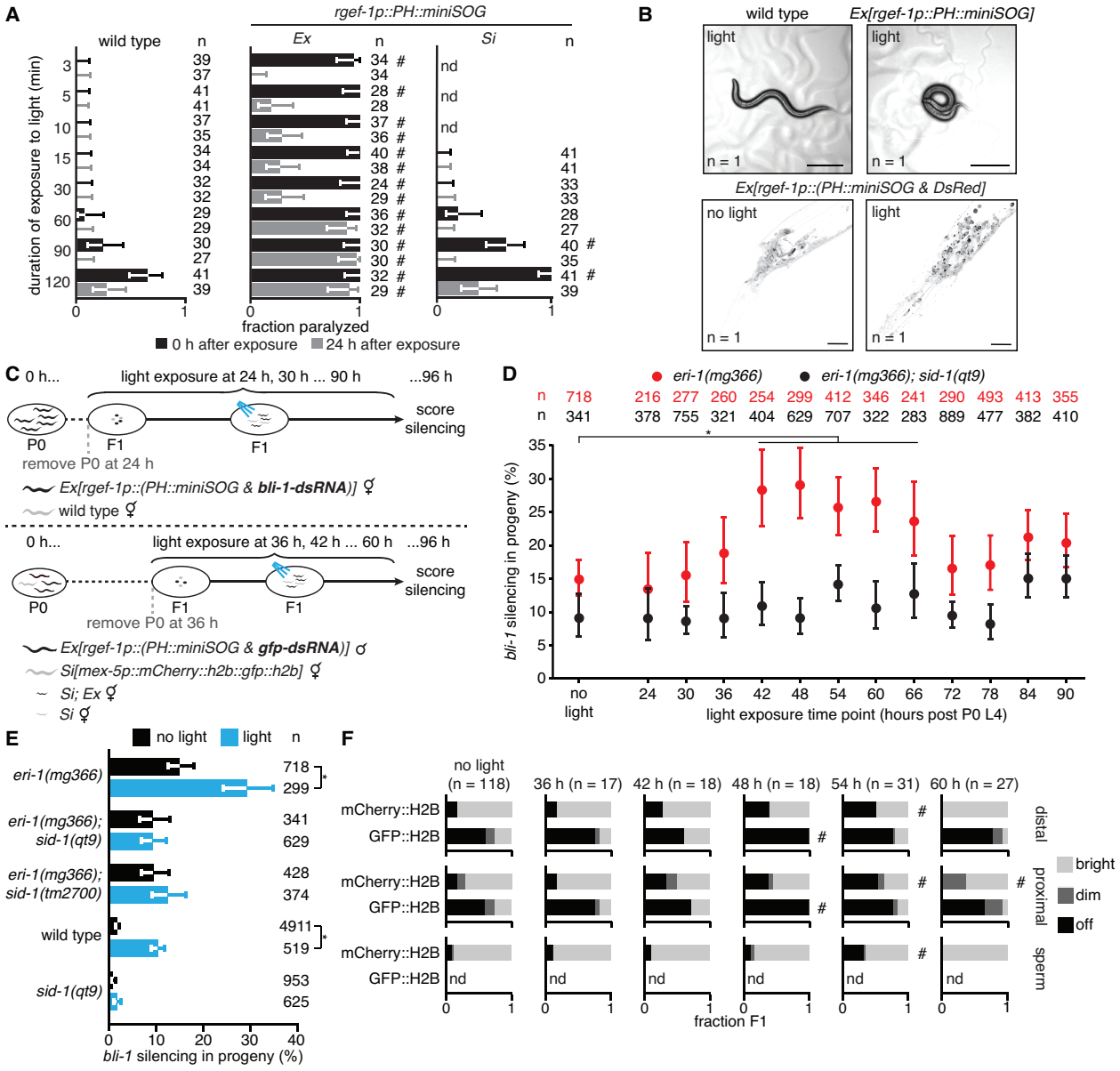

Fig. S1. Oxidative damage of neurons that express dsRNA can enhance silencing by neuronal dsRNA in the soma and germline. (**A**) Wild-type animals (*left*) and animals expressing membrane-tethered mini singlet oxygen generator protein (*PH::miniSOG)* from an extrachromosomal array (*Ex*, *middle*) or a single-copy transgene (*Si*, *right*) under a pan-neuronal promoter (*rgef-1p*) were exposed to blue light for different durations (minutes) and animals were scored for paralysis immediately after exposure (0 h, black) and 24 hours later (24 h, grey). (**B**) Functional and anatomical evidence for oxidative damage in neurons. (*top*) Widefield images of animals without (*left*) and with (*right*) *Ex[rgef-1p::PH::miniSOG]* after 5 minutes of blue light exposure. Animals paralyzed in (A) often appear coiled (*right*). Scale bar, 100 µm. (*bottom*) Confocal fluorescence images of neurons in the head region of animals with *Ex[rgef-1p::(PH::miniSOG & DsRed)]* without (*left*) and with (*right*) 30 minutes of blue light exposure

showing light-induced changes (black, DsRed fluorescence). Scale bar, 20 μm. (**C**) Schematic of assay for measuring the impact of oxidative damage in neurons at different times during development on silencing by neuronal dsRNA. For measuring silencing in the hypodermis (*top*) or germline (*bottom*), cohorts of animals with *Ex[rgef-1p::(PH::miniSOG & bli-1-dsRNA)]* (*top*), or *Ex[rgef-1p::(PH::miniSOG & gfp-dsRNA)]* obtained by mating males with the array and hermaphrodites with *Si[mex-5p::mCherry::h2b::gfp::h2b]* (*bottom*) were exposed to blue light as indicated and scored for *bli-1* silencing (*top*) or imaged (*bottom*) as stage-matched adults (at ~96 hours after the fourth larval stage of parent animals). (**D**) Percentages of *eri-1(mg366)* (red) or *eri-1(mg366); sid-1(qt9)* (black) animals silenced when assayed as described in (C, *top*). Silencing in the absence of exposure to blue light (no light) was also measured for comparison. (**E**) Percentages of stage-matched animals of the indicated genetic backgrounds with *Ex[rgef-1p::(PH::miniSOG & bli-1-dsRNA)]* that show *bli-1* silencing without (black) or with (blue) a 1-hour exposure to blue light 48 hours after the fourth larval stage of parent animals. The 48 hr time point from (D) is replotted to facilitate comparison. (**F**) Fractions of animals exhibiting bright (light grey), dim (dark grey) or not detectable (black) mCherry::H2B or GFP::H2B fluorescence in the distal gonad (*top*), proximal gonad (*middle*) or sperm (*bottom*) when assayed as described in (C, *bottom*). Silencing in the absence of exposure to blue light (no light) was used as the reference. Numbers of animals scored (n), measurements that were not done (nd), significant differences using two-tailed Wilson's estimates for single proportion (asterisks in A, D, E) or χ^2 test (hashes in F) ($P < 0.05$ with Bonferroni correction), and error bars (95% CI) are indicated.

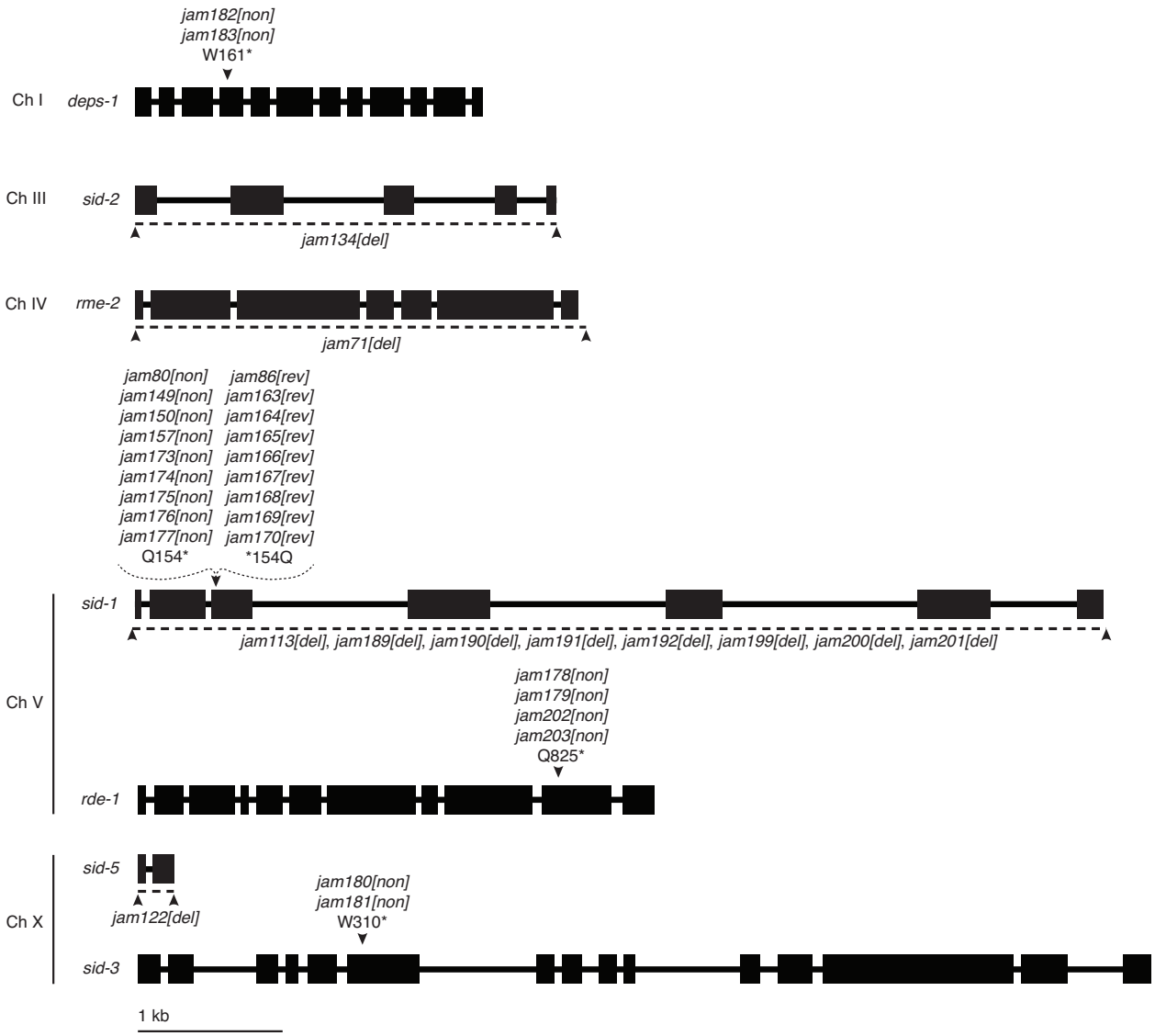

Fig. S2. Schematics depicting mutations generated in this study. Structures (boxes, exons; lines, introns) and chromosomal locations of genes with mutations generated using Cas9-mediated genome editing. Nonsense mutations (e.g., *jam182[non]*) with associated amino acid changes (e.g., W161* for tryptophan at position 161 to stop) are indicated with black arrowheads and deletions of coding regions (e.g., *jam134[del]*) are indicated with a dashed line (deleted region) and flanking black arrowheads. Scale bar, 1 kb.

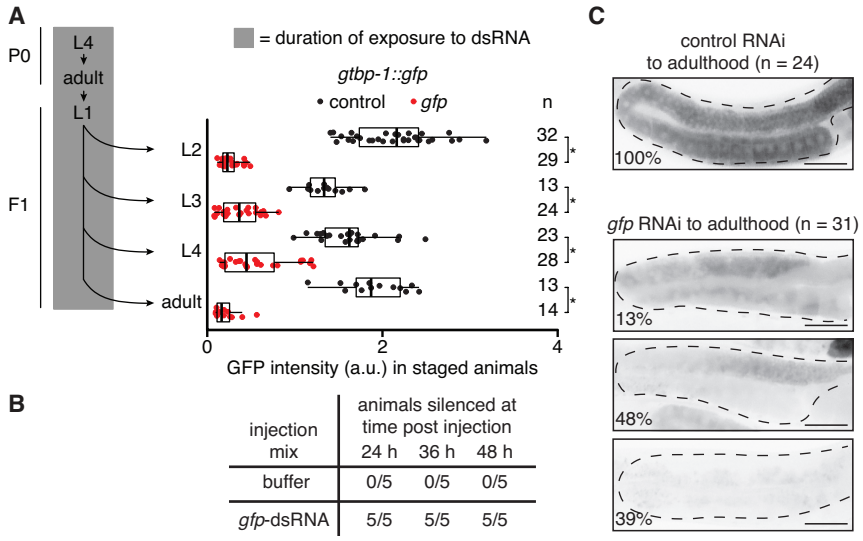

Fig. S3. Spatiotemporal specificity in germline silencing by ingested dsRNA. (**A**) (*left*) Schematic depicting continuous exposure of *gtbp-1::gfp* P0 animals, starting at the L4 stage, and their F1 progeny to bacteria expressing dsRNA, followed by subsequent imaging of animals at the indicated stages. (*right*) Quantification of representative GTBP-1::GFP intensity (arbitrary units, a.u.) in germ cells (larvae) or embryos *in utero* (adults) of F1 animals at indicated stages after P0 and F1 exposure to control (dark grey) or *gfp*-dsRNA (red). Numbers of animals scored at each stage (n) are indicated. Asterisks indicate $P < 0.05$ with Bonferroni correction using Mann-Whitney U test for two-sided comparisons between animals exposed to L4440 or *gfp*-dsRNA. (**B**) Silencing of *gtbp-1::gfp* in animals injected with duplex buffer (buffer) or *in vitro* transcribed *gfp*-dsRNA in duplex buffer during the first day of adulthood and scored for silencing 24, 36 and 48 h post injection. The numbers of animals out of 5 injected with each injection mix that exhibited silencing of both gonad arms are indicated for each time point. Animals injected with buffer never exhibited silencing in either gonad arm. (**C**) Representative fluorescence images of GTBP-1::GFP (black) in the germlines (dashed outline) of day 3 *gtbp-1::gfp* adult animals after P0 and F1 ingestion of *gfp*-dsRNA up to the first day of adulthood. Numbers of animals imaged (n) and the percentages of animals exhibiting the depicted expression patterns are shown. Scale bars, 50 μm.

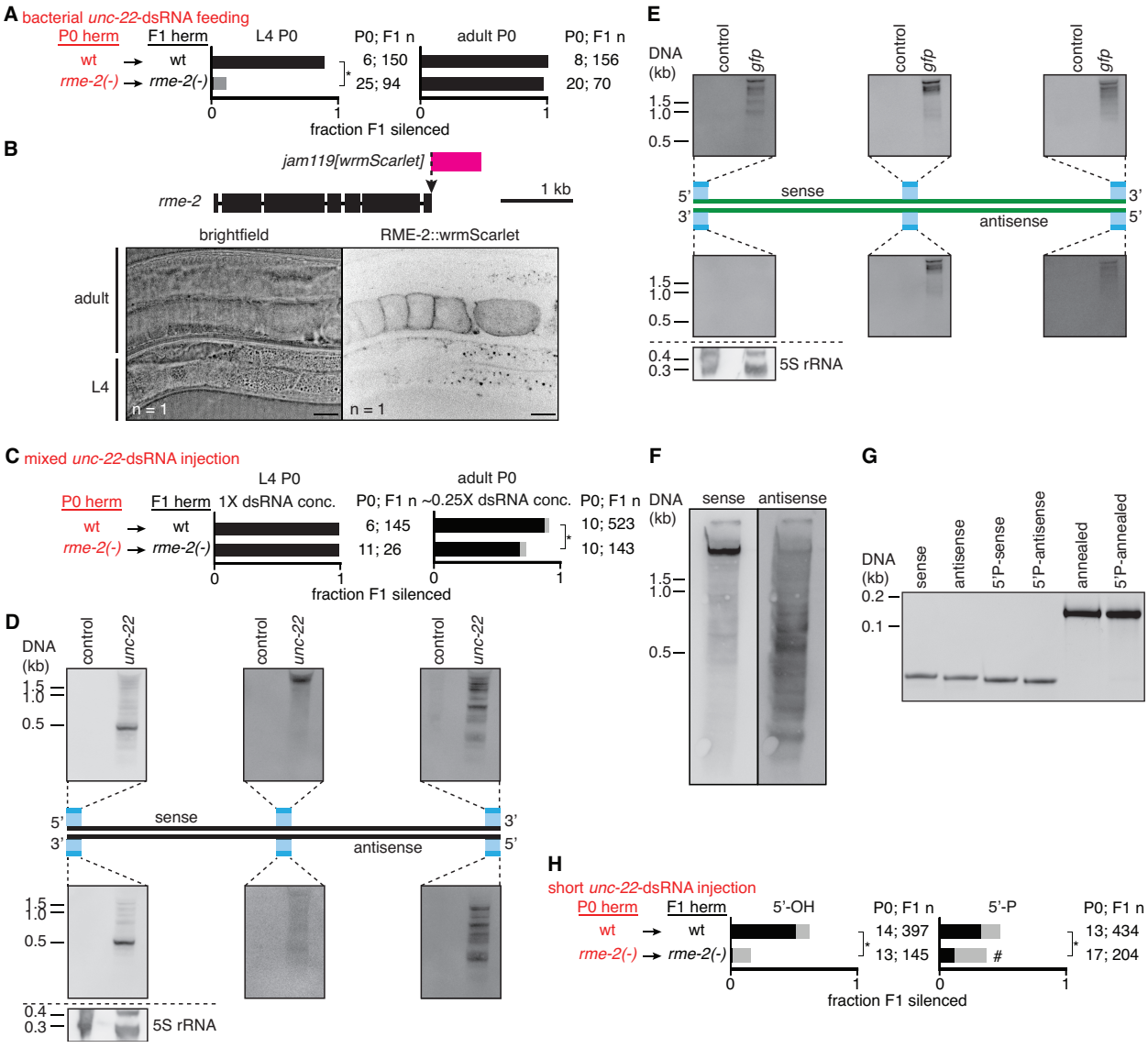

Fig. S4. Requirement of RME-2 for silencing in progeny by parental dsRNA depends on source, concentration, length, and 5' modification of dsRNA. (**A**) Hermaphrodite animals of the L4 stage (left bars) or young adult stage (24 hour post L4, right bars) of the indicated genotypes were fed *unc-22*-dsRNA expressed in bacteria for 24 hours (red font). Hermaphrodite self-progeny of fed animals were scored for *unc-22* silencing (strong, black; weak, grey). Numbers of injected P0 parents and scored F1 progeny (P0; F1 n) are as indicated. Previously generated *rme-2(-)* animals were used in this assay (DH1390). (**B**) Expression of RME-2. (*top*) Schematic showing insertion of *wrmScarlet* (*rme-2(jam119[wrmScarlet])*) at the *rme-2* locus. (*bottom*) Brightfield and fluorescence images of a *rme-2(jam119[wrmScarlet])* L4-stage and adult animal (only confocal image taken, n = 1). Scale bars, 20 μm. (**C**) Hermaphrodite animals of indicated genotypes were exposed to *unc-22*-dsRNA (red font) and unexposed F1 progeny animals were scored as in (A). (*left*), L4-staged hermaphrodites were injected with transcribed *unc-22*-dsRNA in the body cavity at the same concentration as in Fig. 2A (1X). (*right*), Young adult-staged hermaphrodites were injected with transcribed *unc-22*-dsRNA at ~0.25X of concentration in Fig. 2A. Newly generated *rme-2(-)* animals were used in this assay (AMJ1131).

(**D** and **E**) Northern blots of bacterial *unc-22*-dsRNA (*unc-22*, D) or *gfp*-dsRNA (*gfp*, E) separated alongside empty vector control RNA using fully-denaturing formaldehyde polyacrylamide gel electrophoresis (FDF-PAGE (*82*)). 40-nt digoxigenin (DIG)-labeled oligonucleotides (in blue) were used to probe the 5' end, middle and 3' end of the sense (*top*) and antisense (*bottom*) strands of the *unc-22* (D) and *gfp* (E) sequences present in the bacterial vectors. A 1-kb DNA ladder was used as a size reference and 5S rRNA was probed as a control for equal loading of total RNA. (**F**) Northern blot of *unc-22*-dsRNA transcribed from a ~1.1 kb template, separated using FDF-PAGE as in (D) and (E), and probed using 40-nt DIG-labeled oligonucleotides complementary to the sense (*left*) or antisense (*right*) strands of the *unc-22* gene. (**G**) Polyacrylamide gel stained with ethidium bromide showing 50-nt single-stranded (sense, antisense, 5'P-sense, 5'P-antisense) and 50-bp double-stranded *unc-22*-RNA (annealed, 5'P-annealed). A 100-bp DNA ladder was run alongside for rough size estimation. 5'-phosphate (5'P) was added using a polynucleotide kinase. (**H**) Young adult-staged hermaphrodites were injected with short *unc-22*-dsRNA with 5'-OH (left bars) or with 5'-phosphate added using a polynucleotide kinase (right bars) and self-progeny were scored as in (A). Newly generated *rme-2(-)* animals were used in this assay (AMJ1131). Comparisons with $P < 0.05$ after Bonferroni correction using χ^2 test between genotypes within conditions (asterisks in (A, C and H)) or between conditions in *rme-2(-)* animals (hash in (H)) are indicated.

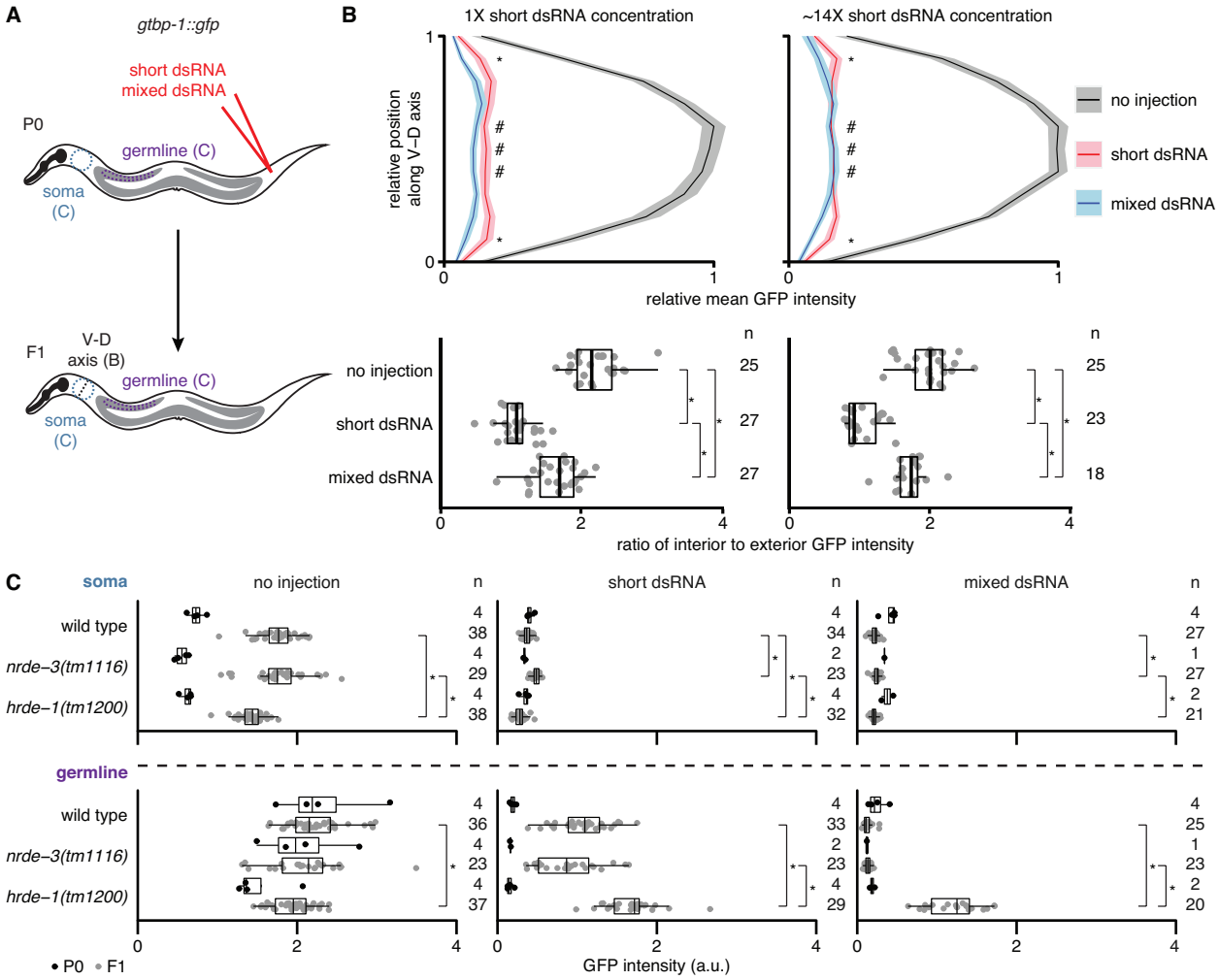

Fig. S5. Extent of silencing in progeny by short or mixed dsRNA injected into parental circulation varies between tissues, but has similar nuclear Argonaute requirements. GTBP-1::GFP fluorescence from the ubiquitously expressed gene *gtbp-1::gfp* in the F1 progeny of uninjected P0 animals (no injection) or of P0 animals injected into the body cavity with synthetic 50-bp *gfp*-dsRNA (short dsRNA) or *gfp*-dsRNA transcribed from a ~730-bp DNA template (mixed dsRNA) was analyzed. (**A**) Schematic illustrating injection site (red) and scoring scheme. For the soma, a region between the pharynx and anterior gonad arm within a circle (blue, data in (C)) or along a ventral to dorsal (V-D) axis (black, data in (B)) was quantified. For the germline, a gonadal region that excluded the intestine (purple, data in (C)) was quantified. (**B**) Quantification of F1 progeny after injection of two different concentrations of short dsRNA (1X, 350 ng/µl, *left*; ~14X, 4977 ng/µl, *right*) into the body cavity of P0 animals. (*top*) The relative mean intensity profile of fluorescence along the V-D axis for progeny of uninjected animals (black), animals injected with short dsRNA (red), or animals injected with mixed dsRNA (blue). Shaded bands indicate 95% CI. (*bottom*) Ratios of mean intensities within interior points (hashes in *top*) to those of the exterior points (asterisks in *top*) are depicted for each imaged animal. (**C**) Quantification of P0 (black) and F1 (grey) wild-type, *nrde-3(tm1116)* or *hrde-1(tm1200)* animals. Regions within the soma and the germline were quantified as indicated in (A). The numbers of P0 and F1 animals quantified (P0; F1 n) are indicated. For each genotype, F1

progeny after no injection, short dsRNA injection, or mixed dsRNA injection into P0 animals showed significantly different fluorescence values from each other ($P < 0.05$ after Bonferroni correction using Mann-Whitney U test for two-sided comparisons). Similarly significant differences between treatments across genotypes are indicated (asterisks).

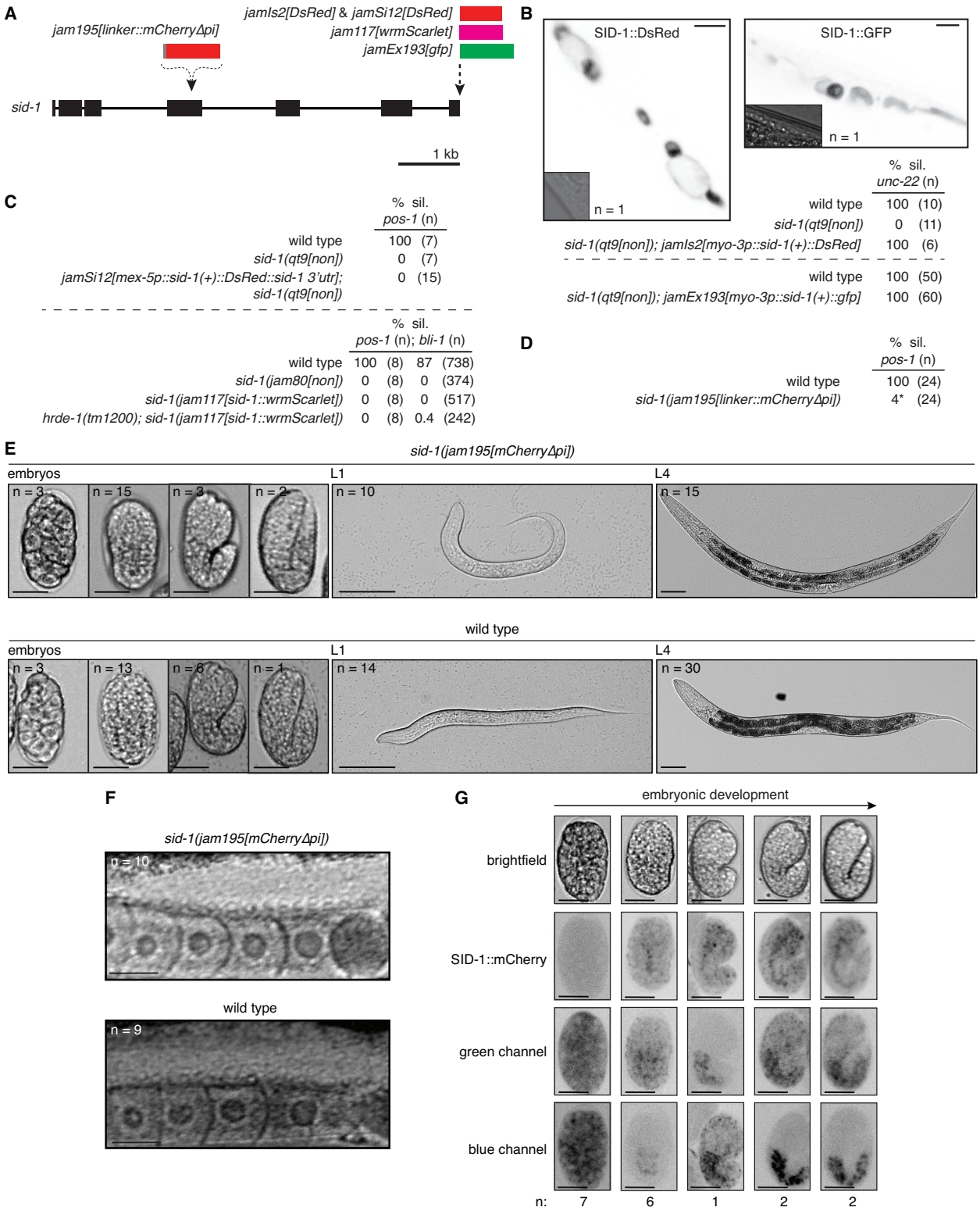

Fig. S6. An internally tagged and partially functional SID-1 fusion protein shows dynamic changes in SID-1 expression across development. (A) Schematic of transgenic *sid-1* reporters or modifications at the *sid-1* gene generated using Cas9-mediated genome editing. An integrated

sid-1::DsRed array (*jamIs2[DsRed]*), a single-copy *sid-1::DsRed* transgene inserted using Mos-mediated single copy insertion (*70*) (*jamSi12[DsRed]*), insertion of *wrmScarlet* at the *sid-1* (*jam117[wrmScarlet]*) locus, an extrachromosomal array of *sid-1::gfp* (*jamEx193[gfp]*), and an insertion of *mCherry* sequence that lacks piRNA binding sites (*46-47*) along with a linker at the *sid-1* locus (*jam195[linker::mCherryΔpi]*) are depicted. (**B**) C-terminal SID-1 fusion proteins expressed from multicopy transgenes apparently rescue function and show intracellular localization. (*top*) Fluorescence images of SID-1::GFP (*left*) and SID-1::DsRed (*right*) fusion proteins expressed from multicopy arrays in the muscle (*Pmyo-3*). Insets, brightfield images; scale bars, 5 μm. (*bottom*) Percentages of *unc-22* silencing (% sil.) upon ingestion of bacterial *unc-22*-dsRNA in *sid-1(qt9[non])* animals with and without these transgenes. Numbers of animals scored (n) are indicated. (**C**) C-terminal SID-1 fusion proteins expressed from a single copy transgene or the endogenous *sid-1* locus appear non-functional. (*top*) Percentage of *pos-1* silencing after ingestion of bacterial *pos-1*-dsRNA in *sid-1(qt9[non])* animals with or without a single-copy transgene designed to express SID-1::DsRed in the germline (*jamSi12[mex-5p::sid-1(+)::DsRed::sid-1 3'utr]*). (*bottom*) Percentages of *pos-1* (*left*) or *bli-1* (*right*) silencing after ingestion of bacterial *pos-1* or *bli-1*-dsRNA in animals with the endogenous *sid-1* gene tagged at the 3'end with *wrmScarlet* sequence (*sid-1(jam117[sid-1::wrmScarlet])*) with or without the secondary Argonaute HRDE-1. Numbers of animals scored (n) are indicated. Wild-type and *sid-1(-)* animals (*sid-1(qt9[non])*, *top*; *sid-1(jam80[non])*, *bottom*) were used as controls. When expressed in single copy, animals expected to have C-terminal fusions of SID-1 (SID-1::DsRed and SID-1::wrmScarlet) remained RNAi defective, suggesting that the SID-1 fusion proteins are either not expressed because of silencing at the *sid-1* locus or that the tagging disrupts SID-1 protein function or stability. Consistent with loss of protein function and/or stability upon C-terminal tagging, RNAi was not restored upon loss of HRDE-1 (*hrde-1(tm1200)*), which is expected to disrupt silencing (if any), and an internal tag of SID-1 showed substantial function (Fig. 3B). Given the diversity of gene products that can be made from multicopy transgenes (*41*), we reason that the apparent functionality of C-terminal fusions of SID-1 expressed from multicopy arrays in (B) reflects the activity of variants that could be untagged. Therefore, the observed subcellular localization in (B) cannot be attributed to functional SID-1. (**D**) Percentage of *pos-1* silencing after ingestion of bacterial *pos-1*-dsRNA in wild-type and *sid-1(jam195[linker::mCherryΔpi])* animals. Numbers of animals scored (n) are indicated. Asterisk indicates weak silencing in one animal (partially viable F1 brood). (**E** and **F**) Representative brightfield images of *sid-1(jam195[linker::mCherryΔpi])* (*top*) and wild-type (*bottom*) animals corresponding to mCherry images in Fig. 3C and Fig. 3D. Images of (E) embryos (*left*), L1 animals (*middle*), L4 animals (*right*), and (F) adult gonad arms are shown. Numbers of images for each stage (n) are depicted. For adult gonad arms imaged in (F), only the proximal germline was visible in 1/10 *sid-1(jam195[mCherryΔpi])* and 5/9 wild-type animals. Scale bars for embryos (E) and adult gonad arms (F), 20 μm. Scale bars for larvae (E), 50 μm. (**G**) Representative brightfield (*first row*), SID-1::mCherry (*second row*), green channel (*third row*) and blue channel (*fourth row*) images of *sid-1(jam195[linker::mCherryΔpi])* embryos throughout embryogenesis. Green and blue channel images are depicted to highlight potential sources of autofluorescence, if any, in the mCherry channel. The numbers of embryos represented (n) are depicted (*bottom*) and 100% of embryos exhibited the represented patterns. Scale bar, 20 μm.

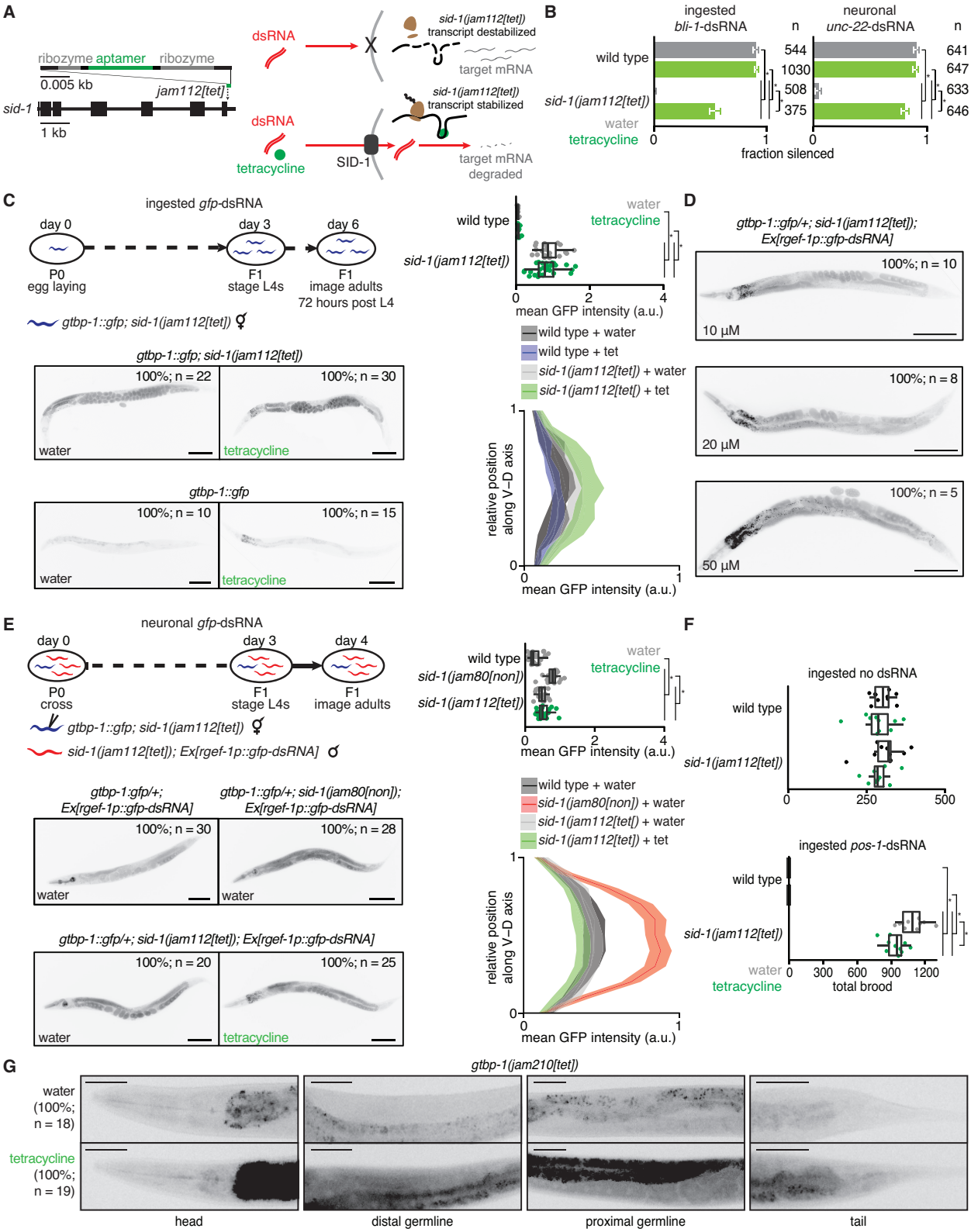

Fig. S7. Tetracycline-induced functional rescue of *sid-1* expression is evident in somatic tissues but not within the germline. (**A**) Schematic illustrating a cell expressing *sid-1* transcript

with a tetracycline aptazyme (*43*) inserted into the *sid-1* 3'UTR (*left*) in the presence (*bottom right*) or absence (*top right*) of tetracycline. Tetracycline stabilizes *sid-1* transcripts by inhibiting ribozyme-based cleavage in the 3'UTR and thereby allows for the expression of SID-1 protein and dsRNA import. (**B)** Fraction of wild-type or *sid-1(jam112[tet])* animals silenced after ingestion of *bli-1*-dsRNA (*left*) or expression of neuronal *unc-22*-dsRNA (*right*) in the presence of water (grey bars) or 10 μM tetracycline (green bars). Numbers of animals scored for silencing (n) are depicted. (**C**) The extent of *gfp* silencing in *gtbp-1::gfp; sid-1(jam112[tet])* day 3 adult animals after ingestion of *gfp*-dsRNA in the presence of water or 10 μM tetracycline. A schematic illustrating the experimental design (*top left*), representative images of animals from each condition with numbers of animals imaged (n) and percentages of animals represented (*bottom left*), and quantification of representative germline (*top right*) and somatic (*bottom right*) GTBP-1::GFP intensity (a.u.) are depicted. Mean germline GFP intensity was measured in representative regions of the posterior germline and somatic GFP intensity was measured along a dorsal to ventral axis in the tail region (shaded region represents 95% CI) to avoid increased autofluorescence in the intestines of animals exposed to tetracycline. Scale bars, 100 μm. (**D**) Representative images of *gtbp-1::gfp; sid-1[jam112[tet])* F1 day 1 adult animals after P0 and F1 ingestion of *gfp*-dsRNA until day 1 of F1 adulthood in the presence of different concentrations of tetracycline (10 μM, 20 μM, 50 μM). Higher concentrations of tetracycline did not enhance silencing in *gtbp-1::gfp; sid-1(jam112[tet])* animals. Scale bars, 100 μm. (**E**) The extent of *gfp* silencing in cross progeny of *gtbp-1::gfp; sid-1(jam112[tet])* hermaphrodites injected with water or 10 μM tetracycline and *sid-1(jam112[tet]); Ex[rgef-1p::gfp-dsRNA]* males in the presence of water or 10 μM tetracycline. A schematic illustrating the experimental design including injection of *gtbp-1::gfp; sid-1(jam112[tet])* hermaphrodites with water or 10 μM tetracycline (*top left*), representative images of animals with the *Ex[rgef-1p::gfp-dsRNA]* array from each condition with numbers of animals imaged (n) and percentages of animals represented (*bottom left*), and quantification of representative germline (*top right*) and somatic (*bottom right*) GFP intensity (a.u.) as in (C) are depicted. Scale bars, 100 μm. (**F**) Total brood of wild-type or *sid-1(jam112[tet])* animals after culturing on OP50 *E. coli* or *pos-1*-dsRNA bacteria in the presence of water or 10 μM tetracycline. Silencing by *pos-1*-dsRNA typically results in inviable embryos (wild type, *bottom*), but culturing *sid-1(jam112[tet])* with 10 μM tetracycline and *pos-1*-dsRNA only resulted in a minor decrease in brood size (*sid-1(jam112[tet]*), *bottom*). This decrease was not observed when *sid-1(jam112[tet])* animals were cultured on 10 μM tetracycline plates in the absence of *pos-1*-dsRNA (*top*, brood of 1 worm unlike that of 3 worms in *bottom*). (**G**) Representative fluorescence images of GTBP-1::GFP (black) in the heads, distal germlines, proximal germlines, and tails of *gtbp-1::gfp* animals with a tetracycline-aptazyme sequence inserted into the *gtbp-1::gfp* 3'UTR (*gtbp-1(jam210[tet])*) after culturing with water or 10 μM tetracycline. The numbers of animals imaged (n) and the percentages of animals with the represented expression patterns are depicted. An increase in GTBP-1::GFP intensity was observed in the soma and germline, but increased fluorescence in the intestine cannot be distinguished from increased autofluorescence caused by culturing with 10 μM tetracycline. Scale bars, 50 μm.

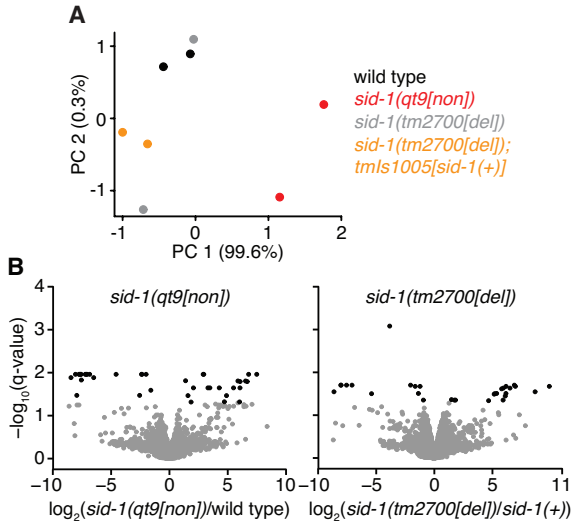

C

sid-1(qt9[non])		*sid-1(tm2700[del])*	
srw-85	*H19N07.3*	*vps-45*	*F36D1.13*
Y102A5C.6	*col-2*	*F10D2.8*	*F26H11.8*
npl-4.1	*col-84*	*Y69A2AR.51*	*Y82E9BR.10*
F32A7.8	*grl-19*	*Y69A2AR.24*	*T08B2.4*
Y102A5C.5	*R02F11.11*	*Y53F4B.40*	*F40H7.12*
Y111B2A.2	*C23H5.11*	*Y44A6D.1*	*T26H5.11*
Y59A8B.t5	*Y39F10C.1*	*Y7A5A.5*	*nduo-4*
ZK673.12	*col-36*	*nspd-11*	*Y68A4A.13*
C10C6.13	*Y102A5C.36*	*ZK637.18*	*snb-5*
K12H6.10	*K02E2.10*	*T28A11.2*	*Y53F4B.46*
Y119C1B.11	*F58G1.8*	*C34E11.7*	
Y105C5A.26	*ZC204.14*	*F54F2.6*	
Y38E10A.33	*Y57G11C.38*	*T05C7.6*	
fipr-19	*hsp-16.1*	*F28H6.7*	
Y46E12A.5	*col-43*	*M163.21*	
T03E6.10	*ZK381.62*	*C08E8.6*	
T24D8.6	*K09C4.9*	*his-58*	
C29A12.22	*col-40*	*clec-52*	
C35B1.3	*T03D3.5*	*T28A11.25*	
T02D1.7		*F55C9.11*	

Fig. S8. Two RNA sequencing experiments using previously generated *sid-1(-)* alleles do not reveal any *sid-1*-dependent genes in common. (**A**) Principal components explaining the variance between wild type (black), *sid-1(qt9[non])* (red), *sid-1(tm2700[del])* (grey) and *sid-1(tm2700[del]); tmIs1005[sid-1(+)]* (orange) animals. (**B**) Volcano plots of changes in the abundance of polyA+ RNA in *sid-1(qt9[non])* vs. wild-type animals (*left*) and *sid-1(tm2700[del])* vs. *sid-1(tm2700[del]); tmIs1005[sid-1(+)]* animals (*right*) (black, $q < 0.05$; grey, $q > 0.05$). (**C**) Lists of genes with $q < 0.05$ (black in (B)) for both comparisons in (B). No genes appeared in both lists of significantly misregulated polyA+ transcripts.

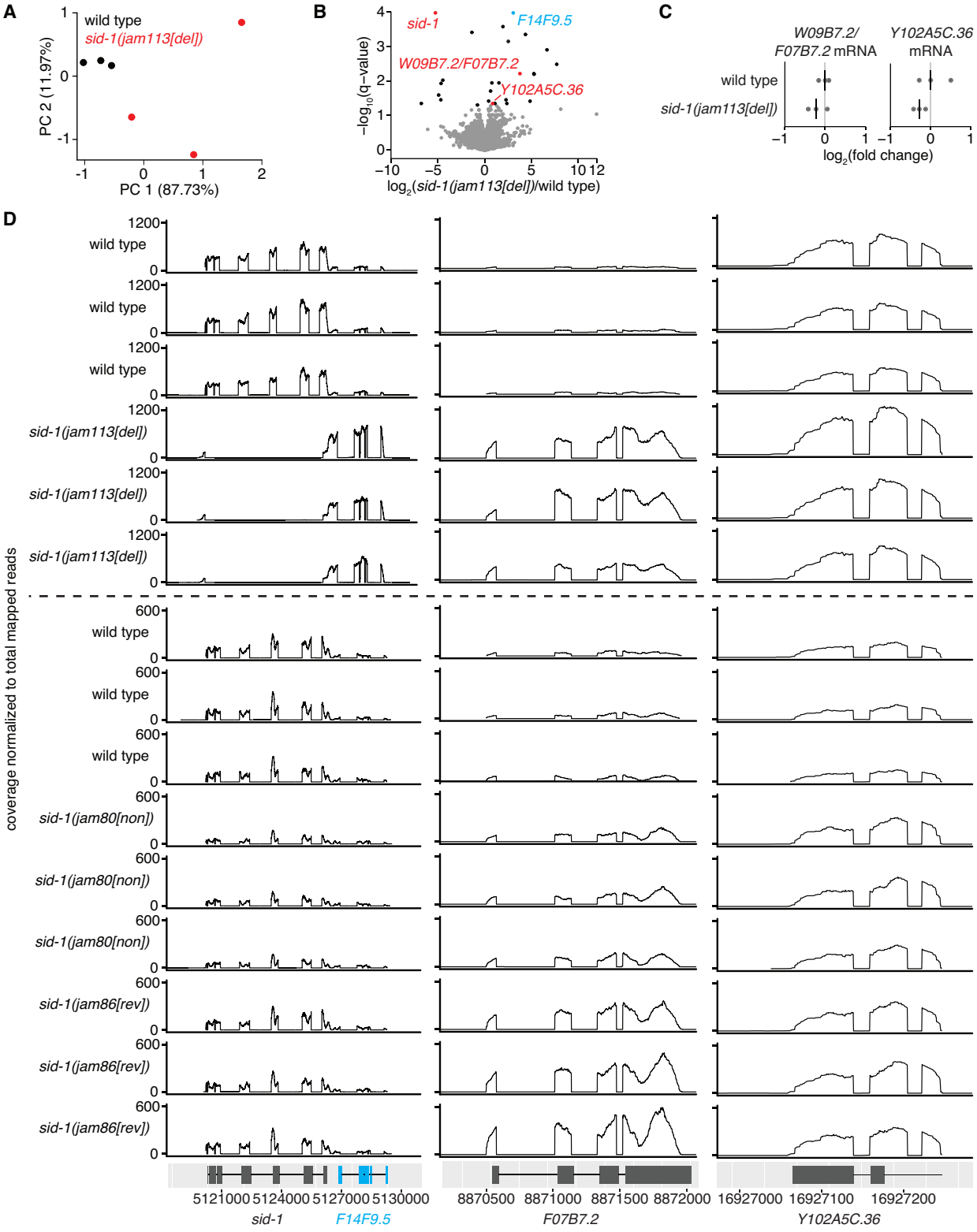

Fig. S9. Selective disruption of *sid-1* followed by restoration to wild type reveals two *sid-1*-dependent transcripts that show heritable change. (**A**) Principal components explaining the variance between wild type (black) and *sid-1(jam113[del])* (red) animals. (**B**) Volcano plots of

changes in the abundance of polyA+ RNA in *sid-1(jam113[del])* animals compared with wild-type animals (black, $q < 0.05$; red, $q < 0.05$ and with change in the same direction in *sid-1(jam80[non])*; see Fig. 3F, *left*) (**C**) Levels of spliced *sid-1* transcripts in the indicated genotypes measured using RT-qPCR. The median (line) of three technical replicates is plotted for each of three biological replicates. Asterisks indicate $P < 0.05$ with Bonferroni correction using two-tailed Student's t-test. (**D**) Read coverage at *sid-1* and *F14F9.5* (*left*), *W09B7.2/F07B7.2* (represented by *F07B7.2* locus, *middle*) and *Y102A5C.36* (*right*) of polyA+ RNA in wild-type and *sid-1(jam113[del])* animals (experiment #1, *top*), and in wild-type, *sid-1(jam80[non])*, and *sid-1(jam86[rev])* animals (experiment #2, *bottom*) normalized to total mapped reads per sample. Deletion of *sid-1* coding sequence caused accumulation of transcripts from *F14F9.5* (blue), requiring point mutation (*jam80[non]*) for selective disruption of *sid-1* (see Fig. 3).

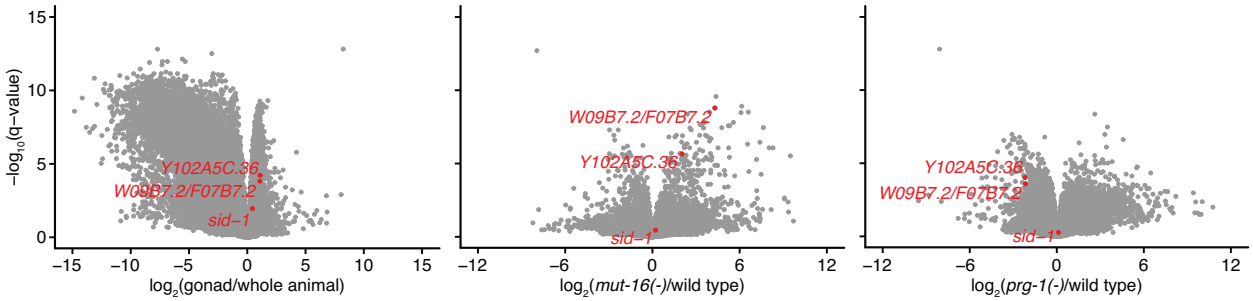

Fig. S10. *sid-1*-dependent transcripts are enriched in the germline and in *mut-16(-)* animals, but depleted in *prg-1(-)* animals. Volcano plots of changes in the abundance of RNA in wild-type gonads vs. whole animals (*left*), *mut-16(-)* vs. wild-type animals (*middle*), and *prg-1(-)* vs. wild-type animals (*right*) using data from (*88*). *W09B7.2/F07B7.2*, *Y102A5C.36* and *sid-1* transcripts are highlighted (red).

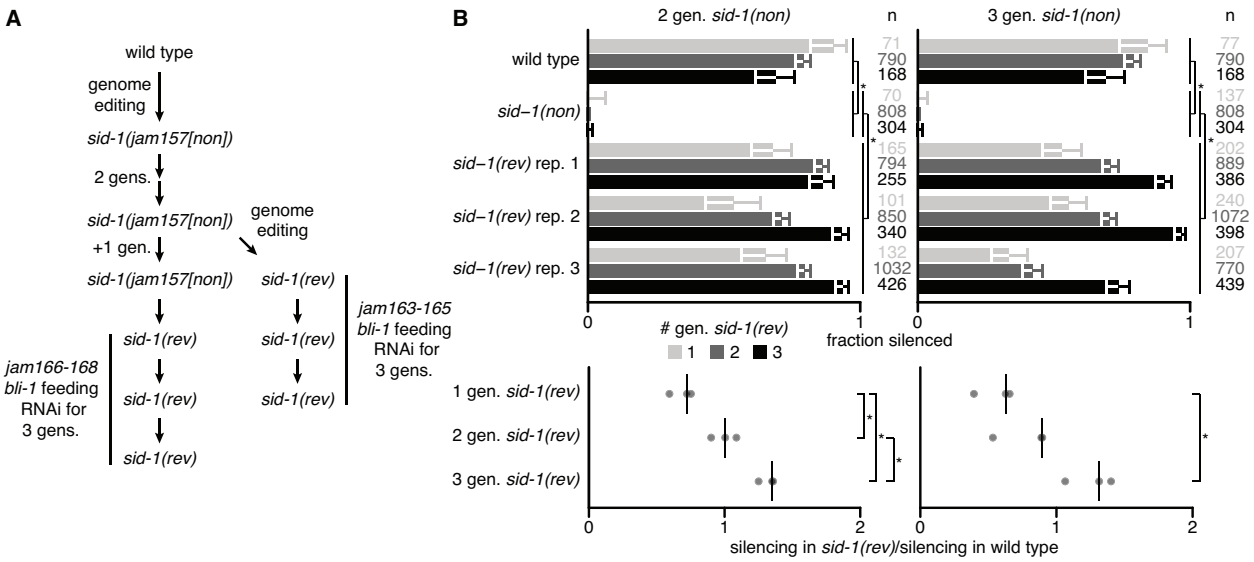

Fig. S11. Reversion of *sid-1(-)* to wild type results in delayed recovery of efficient RNA silencing in descendants. (**A**) Schematic illustrating mutation of *sid-1* (*sid-1(jam157[non])*) and subsequent reversions (*sid-1(rev)*) after two (2 gens., *jam163-165*) or three (+1 gen., *jam166-168*) generations using genome editing, and measurement of silencing by ingested dsRNA (feeding RNAi) at the indicated generations after reversion. (**B**) Silencing of *bli-1* in animals generated as described in (A). (*top*) Wild-type (positive control) and *sid-1(non)* (negative control) animals were fed *bli-1*-dsRNA at the same time as three *sid-1(rev)* replicates (rep. 1, rep. 2, rep. 3) within a cohort (2 gen. *sid-1(non)* or 3 gen. *sid-1(non)*) one (light grey), two (dark grey) or three (black) generations after reversion. Numbers of animals scored (n in corresponding colors) and 95% CI (error bars) are depicted. (*bottom*) Ratio of silencing in *sid-1(rev)* animals to that in wild-type animals for each replicate, generation, and cohort in (B, *top*) (replicates – circles indicate ratio and bar indicates median; generations – 1, 2 or 3 gen. *sid-1(rev)*; cohort – 2 gen. or 3 gen. *sid-1(non)*). Asterisks indicate $P < 0.05$ with Bonferroni correction using two-tailed Student's t-test.

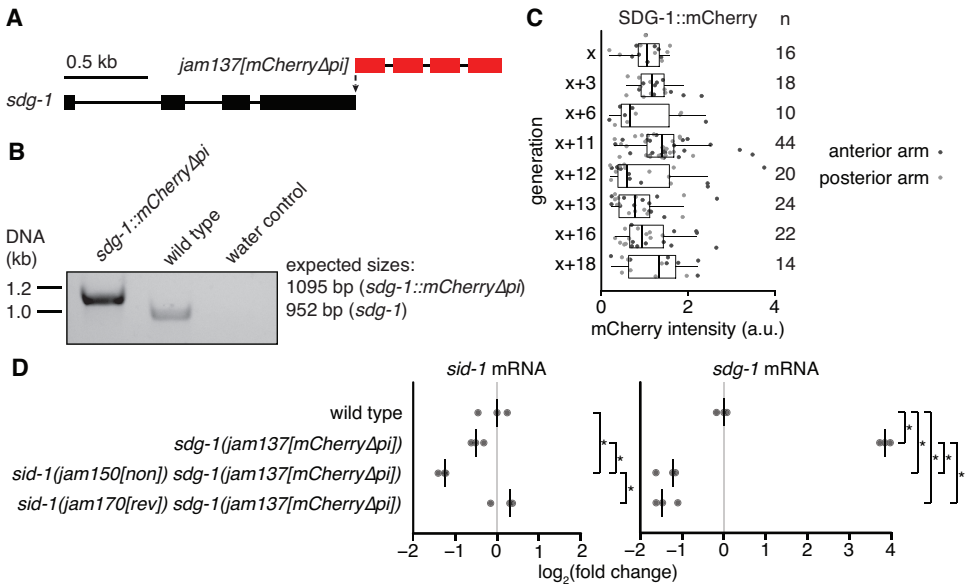

Fig. S12. SDG-1::mCherry fluorescence is variable across generations with loss of expression in *sid-1(non)* that fails to recover in *sid-1(rev)*. (**A**) Schematic depicting insertion of *mCherry* sequence that lacks piRNA binding sites (*46-47*) at the 3' end of *sdg-1*(*jam137[mCherryΔpi]*). (**B**) Genotyping gel showing insertion of *mCherryΔpi* sequences at both loci of *sdg-1* (1095 bp). Absence of bands corresponding to wild-type *W09B7.2*/*F07B7.2* DNA (952 bp) in *sdg-1(jam137[mCherryΔpi])* suggests that both *W09B7.2* and *F07B7.2* were tagged with *mCherryΔpi*. (**C**) Quantification of SDG-1::mCherry fluorescence intensity in adult gonad arms (anterior arm, dark grey; posterior arm, light grey) of *sdg-1(jam137[mCherryΔpi])* animals starting in one generation (x) and continuing in successive generations indicated. Numbers of gonad arms quantified (n) is indicated. Expression in one generation was not significantly different when compared to that in the previous tested generation using Mann-Whitney U test for two-sided comparisons and Bonferroni correction. (**D**) Levels of spliced *sid-1* and *sdg-1* transcripts in wild-type animals and *sdg-1(jam137[mCherryΔpi])* animals with a wild-type (+), *sid-1(jam150[non])* or *sid-1(jam169[rev])* background measured using RT-qPCR. The median of three technical replicates is plotted for each of three biological replicates (bar indicates median). Asterisks indicate $P < 0.05$ with Bonferroni correction using two-tailed Student's t-test.

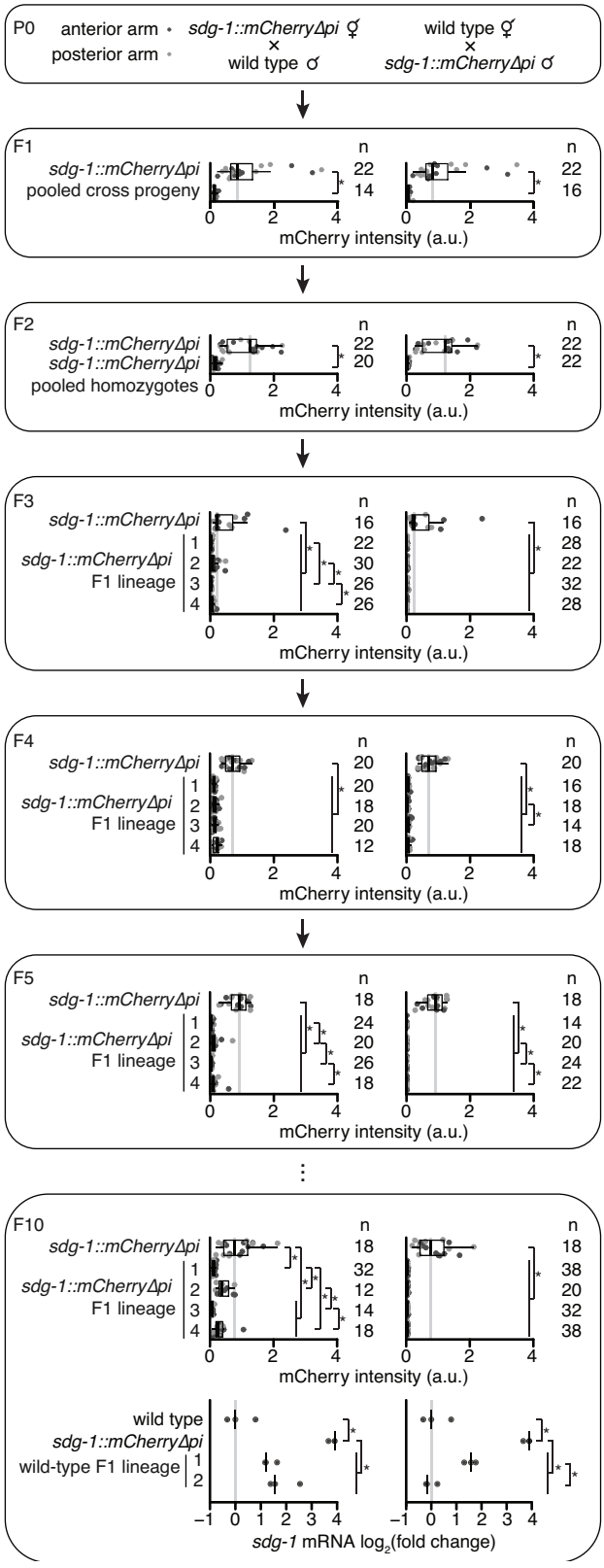

Fig. S13. Mating and isolation of siblings can initiate lineages with distinct heritable changes in *sdg-1* expression. (P0 to F10, *top*) Quantification of SDG-1::mCherry fluorescence

intensity (a.u.) in adult gonad arms (anterior arm, dark grey; posterior arm, light grey) across generations after mating hermaphrodite and male *sdg-1(jam137[mCherryΔpi])* animals with male and hermaphrodite wild-type animals, respectively. The generations assayed and numbers of gonad arms quantified (n) are indicated. In F1 and F2, fluorescence intensity values of animals with lineages that were not propagated to F10 but were heterozygous or homozygous *sdg-1(jam137[mCherryΔpi])*, respectively, were pooled with values of animals with lineages that were propagated to F10. In F3 to F10 (*top*), animals from four different F1 lineages were scored. Fluorescence intensity of animals descending from the self-progeny of P0 *sdg-1(jam137[mCherryΔpi])* animals was measured in each generation and is depicted, with the same data plotted for each mating direction for comparison. Asterisk indicates $P < 0.05$ with Bonferroni correction using Mann-Whitney U test for two-sided comparisons. (F10, *bottom*) Levels of spliced *sdg-1* mRNA transcripts in wild-type animals, *sdg-1(jam137[mCherryΔpi])* animals or two lineages of wild-type F10 progeny from each cross direction, measured using RT-qPCR. The median of three technical replicates is plotted for each of three biological replicates (bar indicates median). Asterisks indicate $P < 0.05$ with Bonferroni correction using two-tailed Student's t-test.

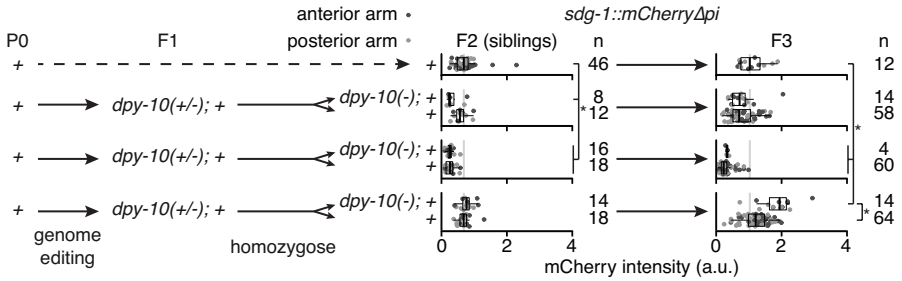

Fig. S14. Animals expressing SDG-1::mCherry with a Cas9-mediated mutation in a marker gene and their unmutated siblings have comparable expression. (*left*) Schematic illustrating mutation of *dpy-10* in three P0 lineages of *sdg-1(jam137[mCherryΔpi]* animals and subsequent segregation of the *dpy-10* mutation. (*right*) Both *dpy-10(-)* and *dpy-10(+)* F2 and F3 animals from each of the three P0 lineages were imaged and SDG-1::mCherry intensity was quantified (a.u.) in adult gonad arms (anterior arm, dark grey; posterior arm, light grey). Minor differences in SDG-1::mCherry expression were observed between mutants and nonmutants in some cases, as well as between lineages. The numbers of gonad arms quantified (n) are depicted. Asterisks indicates $P < 0.05$ with Bonferroni correction using Mann-Whitney U test for two-sided comparisons.

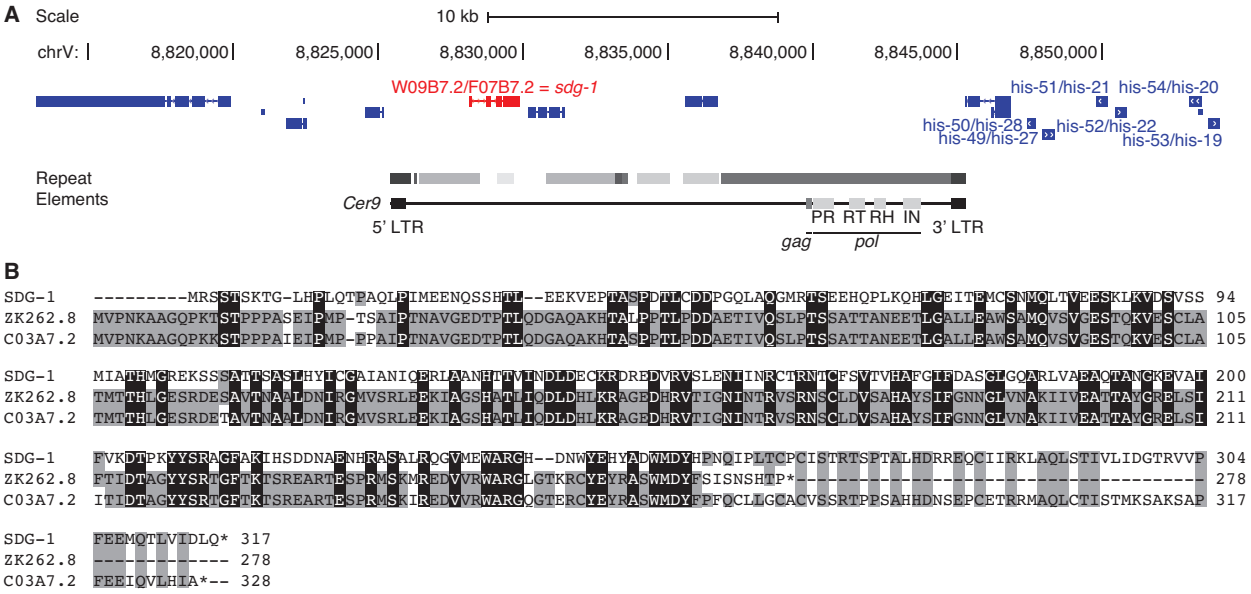

Fig. S15. The *sid-1*-dependent gene *sdg-1* represents two identical loci (*W09B7.2/F07B7.2*) within copies of the *Cer9* retrotransposon and has two paralogs. (**A**) Schematic adapted from UCSC Genome Browser depicting *W09B7.2/F07B7.2* (red) located within a repeated ~40-kb locus on chromosome V (8813207-8896495 depicted; duplicate locus at 8855302-8896495) that includes many histone genes (dark blue; duplicate genes also depicted). *W09B7.2/F07B7.2* are located within full-length *Cer9* retrotransposons with repeated regions in grey (darker color indicates fewer repeat element-associated mismatches/insertions/deletions). Loci encoding *gag* and *pol* elements (PR: protease, RT: reverse transcriptase, RH: RNaseH, IN: integrase) within *Cer9* are depicted. (**B**) Alignment of the SDG-1 protein sequence encoded by *W09B7.2/F07B7.2* to the paralogs ZK262.8 and C03A7.2 with conserved residues between two (grey) or three (black) proteins highlighted.

Table S1. Strains used.

Strains	Genotype
AMJ3	*sid-1(qt9) V; jamIs2[myo-3p::sid-1::gfp]*
AMJ308	*ccIs4251[myo-3p::gfp::lacZ::nls & myo-3p::mito-gfp & dpy-20(+)] I; sid-1(qt9) V*
AMJ327	*ccIs4251[myo-3p::gfp::lacZ::nls & myo-3p::mito-gfp & dpy-20(+)] I; sid-1(qt9) V; jamIs2[myo-3p::sid-1 cDNA::DsRed]*
AMJ471	*jamEx140[rgef-1p::gfp-dsRNA & myo-2p::DsRed]*
AMJ477	*qtEx136[rgef-1p::unc-22-dsRNA & rgef-1p::DsRed]*
AMJ576	*jamSi12[mex-5p::sid-1::DsRed::sid-1 3'UTR]; unc-119(ed3) III; sid-1(qt9) V*
AMJ577	*hrde-1(tm1200[4X outcrossed]) III*
AMJ581	*oxSi487[mex-5p::mCherry::h2b::gfp::h2b & Cbr-unc-119(+)] dpy-2(e8) II; unc-119(ed3) III*
AMJ706	*sid-1(qt9) V; jamEx193[myo-3p::sid-1::gfp]*
AMJ819	*eri-1(mg366) gtbp-1(ax2053[gtbp-1::gfp]) IV*
AMJ837	*jamEx209[rgef-1p::PH::miniSOG & myo-2p::DsRed]*
AMJ936	*jamEx210[rgef-1p::PH::miniSOG & rgef-1p::DsRed]*
AMJ1007	*eri-1(mg366) IV; jamEx213[rgef-1p::PH::miniSOG & rgef-1p::bli-1-dsRNA & myo-2p::DsRed]*
AMJ1009	*eri-1(mg366) gtbp-1(ax2053[gtbp-1::gfp]) IV; jamEx214[rgef-1p::PH::miniSOG & rgef-1p::gfp-dsRNA & myo-2p::DsRed]*
AMJ1019	*jamSi36[rgef-1p::PH::miniSOG & Cbr-unc-119(+)] II; unc-119(ed3) III*
AMJ1108	*eri-1(mg366) IV; sid-1(qt9) V; jamEx213[rgef-1p::PH::miniSOG & rgef-1p::bli-1-dsRNA & myo-2p::DsRed]*
AMJ1114	*sid-1(qt9) V; jamEx213[rgef-1p::PH::miniSOG & rgef-1p::bli-1-dsRNA & myo-2p::DsRed]*
AMJ1120	*rme-2(jam71[deletion]) IV; sid-1(qt9) V*
AMJ1123	*jamEx213[rgef-1p::PH::miniSOG & rgef-1p::bli-1-dsRNA & myo-2p::DsRed]*
AMJ1131	*rme-2(jam71[deletion]) IV*
AMJ1134	*jamEx214[rgef-1p::PH::miniSOG & rgef-1p::gfp-dsRNA & myo-2p::DsRed]*
AMJ1151	*sid-1(tm2700) V; jamEx213[rgef-1p::PH::miniSOG & rgef-1p::bli-1-dsRNA & myo-2p::DsRed]*
AMJ1153	*sid-1(tm2700)[3X outcrossed] V*
AMJ1159	*sid-1(jam80[nonsense]) V*
AMJ1173	*eri-1(mg366) IV; sid-1(tm2700) V; jamEx213[rgef-1p::PH::miniSOG & rgef-1p::bli-1-dsRNA & myo-2p::DsRed]*
AMJ1217	*sid-1(jam86[revertant]) V*
AMJ1220	*hrde-1(tm1200) III; gtbp-1(ax2053[gtbp-1::gfp]) IV*
AMJ1280	*sid-1(jam115[sid-1::wrmScarlet13]) V*
AMJ1281	*rme-2(jam116[rme-2::wrmScarlet13]) IV*
AMJ1282	*sid-1(jam117[sid-1::wrmScarlet]) V*

AMJ1284	*rme-2(jam119[rme-2::wrmScarlet]) IV*
AMJ1312	*sid-1(jam80[nonsense]) V; jamEx214[rgef-1p::PH::miniSOG & rgef-1p::gfp-dsRNA & myo-2p::DsRed]*
AMJ1323	*sid-1(jam112[sid-1::tetracycline-K4-aptazyme::3'UTR]) V*
AMJ1324	*sid-1(jam113[deletion]) V*
AMJ1330	*sid-1(jam112[sid-1::tetracycline-K4-aptazyme::3'UTR]) V; qtEx136[rgef-1p::unc-22-dsRNA & rgef-1p::DsRed]*
AMJ1332	*sid-5(jam122[deletion]) X*
AMJ1350	*sid-1(jam112[sid-1::tetracycline-K4-aptazyme::3'UTR]) V; jamEx140[rgef-1p::gfp-dsRNA & myo-2p::DsRed]*
AMJ1355	*gtbp-1(ax2053[gtbp-1::gfp]) IV; sid-1(jam112[sid-1::tetracycline-K4-aptazyme::3'UTR]) V*
AMJ1365	*hrde-1(tm1200) III; sid-1(jam117[sid-1::wrmScarlet]) V*
AMJ1366	*rme-2(jam71[deletion]) IV; sid-1(jam113[deletion]) V*
AMJ1367	*sid-1(jam113[deletion]) V; sid-5(jam122[deletion]) X*
AMJ1368	*sid-2(jam134[deletion]) III*
AMJ1372	*W09B7.2/F07B7.2(jam137[W09B7.2/F07B7.2::mCherryΔpi]) V*
AMJ1380	*sid-2(jam134[deletion]) III; sid-1(jam113[deletion]) V*
AMJ1383	*gtbp-1(ax2053[gtbp-1::gfp]) IV; nrde-3(tm1116) X*
AMJ1389	*sid-1(jam150[nonsense]) W09B7.2/F07B7.2(jam137[W09B7.2/F07B7.2::mCherryΔpi]) V*
AMJ1399	*sid-1(jam157[nonsense]) V*
AMJ1405	*sid-1(jam163[revertant]) V*
AMJ1406	*sid-1(jam164[revertant]) V*
AMJ1407	*sid-1(jam165[revertant]) V*
AMJ1408	*sid-1(jam166[revertant]) V*
AMJ1409	*sid-1(jam167[revertant]) V*
AMJ1410	*sid-1(jam168[revertant]) V*
AMJ1412	*sid-1(jam170[revertant]) W09B7.2/F07B7.2(jam137[W09B7.2/F07B7.2::mCherryΔpi]) V*
AMJ1413	*sid-1(jam171[revertant]) W09B7.2/F07B7.2(jam137[W09B7.2/F07B7.2::mCherryΔpi]) V*
AMJ1438	*sid-1(jam172[sid-1 N-term::mCherryΔpi::sid-1 C-term]) V*
AMJ1442	*sid-1(jam173[nonsense]) W09B7.2/F07B7.2(jam137[W09B7.2/F07B7.2::mCherryΔpi]) V*
AMJ1443	*sid-1(jam174[nonsense]) W09B7.2/F07B7.2(jam137[W09B7.2/F07B7.2::mCherryΔpi]) V*
AMJ1444	*sid-1(jam175[nonsense]) W09B7.2/F07B7.2(jam137[W09B7.2/F07B7.2::mCherryΔpi]) V*
AMJ1445	*sid-1(jam176[nonsense]) W09B7.2/F07B7.2(jam137[W09B7.2/F07B7.2::mCherryΔpi]) V*
AMJ1446	*sid-1(jam177[nonsense]) W09B7.2/F07B7.2(jam137[W09B7.2/F07B7.2::mCherryΔpi]) V*
AMJ1447	*W09B7.2/F07B7.2(jam137[W09B7.2/F07B7.2::mCherryΔpi]) rde-1(jam178[nonsense]) V*

AMJ1448	*W09B7.2/F07B7.2(jam137[W09B7.2/F07B7.2::mCherryΔpi]) rde-1(jam179[nonsense]) V*
AMJ1449	*W09B7.2/F07B7.2(jam137[W09B7.2/F07B7.2::mCherryΔpi]) V; sid-3(jam180[nonsense]) X*
AMJ1450	*W09B7.2/F07B7.2(jam137[W09B7.2/F07B7.2::mCherryΔpi]) V; sid-3(jam181[nonsense]) X*
AMJ1451	*deps-1(jam182[nonsense]) I; W09B7.2/F07B7.2(jam137[W09B7.2/F07B7.2::mCherryΔpi]) V*
AMJ1452	*deps-1(jam183[nonsense]) I; W09B7.2/F07B7.2(jam137[W09B7.2/F07B7.2::mCherryΔpi]) V*
AMJ1479	*sid-1(jam189[deletion]) W09B7.2/F07B7.2(jam137[W09B7.2/F07B7.2::mCherryΔpi]) V*
AMJ1480	*sid-1(jam190[deletion]) W09B7.2/F07B7.2(jam137[W09B7.2/F07B7.2::mCherryΔpi]) V*
AMJ1481	*sid-1(jam191[deletion]) W09B7.2/F07B7.2(jam137[W09B7.2/F07B7.2::mCherryΔpi]) V*
AMJ1482	*sid-1(jam192[deletion]) W09B7.2/F07B7.2(jam137[W09B7.2/F07B7.2::mCherryΔpi]) V*
AMJ1485	*sid-1(jam195[sid-1 N-term::linker::mCherryΔpi::sid-1 C-term]) V*
AMJ1504	*oxSi487[mex-5p::mCherry::h2b::gfp::h2b & Cbr-unc-119(+)] dpy-2(e8) II; unc-119(ed3) III; sid-1(jam80[nonsense]) V*
AMJ1542	*gtbp-1(jam210[gtbp-1::gfp::tetracycline-K4-aptazyme::3'UTR]) IV*
DH1390	*rme-2(b1008) IV*
EG4322	*ttTi5605 II; unc-119(ed9) III*
EG6787	*oxSi487[mex-5p::mCherry::h2b::gfp::h2b & Cbr-unc-119(+)] II; unc-119(ed3) III*
FX02700	*sid-1(tm2700) V*
FX15992	*sid-1(tm2700) V; tmIs1005[sid-1(+) & vps-45 mini]*
GR1373	*eri-1(mg366) IV*
HC196	*sid-1(qt9) V*
HC731	*eri-1(mg366) IV; sid-1(qt9) V*
JH3197	*gtbp-1(ax2053[gtbp-1::gfp]) IV*
N2	wild type

Table S2. Oligonucleotides used.

Name	Sequence
P1	caccttcgccaattatcacctc
P2	cgtcagcttctgattcgacaac
P3	ataaggagttccacgcccag
P4	ctagtgagtcgtattataagtg
P5	tgaagacgacgagccacttg
P6	ggaacatatggggcattcg
P7	cagacctcacgatatgtggaaa
P8	gcttcacctgtcttatcactgc
P9	cgcggcgactttggttaaatc
P10	ggcttgacaaacgtcagcttc
P11	tcatctcggtacctgtcgttg
P12	agaggcggatacggaagaag
P13	cataaccgtcgcttggcac
P14	aatgggtgagatgggcttaag
P15	gcacttcgatatttcgcgccaa
P16	gaaccaatgtggcacgaaac
P17	gcaaaacttcgattaacattttcatggcctcctccgagaacg
P18	cgttctcggaggaggccatgaaaatgttaatcgaagttttgc
P19	ggtaccctctagtcaaggcctatagaaaagttgaaatatcagtttttaaaaa
P20	cacgaatcattctctgtctgaaacattcaattg
P21	cagacagagaatgattcgtgtttatttgataattttaatg
P22	cggaggaggccatgaaaatgttaatcgaagttttgc
P23	taacattttcatggcctcctccgagaac
P24	aattactctactacaggaacaggtggtgg
P25	gttcctgtagtagagtaattttgttttccctatc
P26	ggctacgtaatacgactcacagtggctgaaaatttatgc
P27	gagcagcagaatacgagctc
P28	gaaaagttcttctcctttactcatgaaaatgttaatcgaagttttgc
P29	gcaaaacttcgattaacattttcatgagtaaaggagaagaacttttc
P30	ctctcagtacaatctgctctg
P31	gaatacgagctcagaactcg
P32	atgccgcatagttaagccag
P33	atcgacgacgacgacgatcagcagtaaagaagcttgcatgcctgcag
P34	atgttgaagagtaattggacgtcatccatccagcagcac
P35	gtccaattactcttcaacatcccta
P36	ctttactgctgatcgtcg
P37	tctctccctaggcacaacgatggatacgctaac
P38	gagagacctaggcacgatgagcatgatttgacg
P39	atttaggtgacactatagctaccataggcaccacgaggttttagagctagaaatagcaag
P40	gcaccgactcggtgcca
P41	cacttgaacttcaatacggcaagatgagaatgactggaaaccgtaccgcatgcggtgcctatggtag cggagcttcacatggcttcagaccaacagccta

P42 atttaggtgacactatagcaaggcgcatggttctcagttttagagctagaaatagcaag
P43 atttaggtgacactatagcaactttcatgcaataaatgttttagagctagaaatagcaag
P44 ttctttcattcttttcataatctcactcaccatgatattgcatgaaagttgataatgtctactagtactg
P45 aaacaccaacaacgcaatcc
P46 tgacctcatcatctcctccag
P47 tccgaatctgaaccacgaatg
P48 atttaggtgacactatagcattcaatcgagactgcagttttagagctagaaatagcaag
P49 agcctataatctatatcagcattcaatcaaggctacacggttacgatcaggttttgatggaaatgagggt
P50 atttaggtgacactatagcattcaatcaaggctacagttttagagctagaaatagcaag
P51 aagcctataatctatatcagcattcaatcgagactgcacggttacgatcaggttttgatggaaatgaggg
P52 tgaaatatgaaaaaccggat
P53 tcattaatacacgcaaaacttcgattaacattttcatggtcagcaagggagaggcagttatcaaggagttca
tgcgtttcaaggtccaacgagcgttccgagggacgtcactccaccggaggaatggacgagctctacaag
tagagtaattttgttttccctattcgtttcttcatatttcaacttttctcctgcctta
P54 actcggcttcttcggttcc
P55 aacaccagatcactgcgtagag
P56 aaggtccaacgagcgttccg
P57 atggtcagcaagggagagg
P58 cttgtagagctcgtccattcct
P59 attgtgaacctggaaaaatg
P60 tttcactatcagtggcttcacctgtcttatcactgcttcttgtatactgaacgacgttaaacacatctcactttaa
catttagaaattaaaactcctcatcggtttttcatatttcaacttttctcctgccttaatacgtagcccatctctca
tttcttcatgttttaagaactttctgaatctatgtaattagttgg
P61 tttttggcacagtttttgct
P62 ggaattagagactagagctt
P63 cgtgtctctcacaacagccgtttctctaacagaaaaaccttcttttgttgatgtttgtctaaaatcgatttttttcag
caagaaatcgagaaactggaacgagctttggtaagtttttgttcctcgaagtgtaaataattgagtaaaagct
ttcttattgaaaaaaaaaacgaatgttcaaattatgaagattgaaaaatg
P64 tttcccgcgtactcctctc
P65 ctaagaccaacatccaagctcg
P66 tcacatttggcgaggagcca
P67 aatcgaatgactccagcgaa
P68 cagacgtttggctatacgcc
P69 caactggtttcgtcagatcggcttccgcaccatttgccggtgtgatccgtttcgaaaatgatagtttattaatg
gtcagcaagggagaggcagttatcaaggagttcatgcgtttcaagttccgagggacgtcactccaccgg
aggaatggacgagctctacaagtgaattctactacaaaattactaaatcagatgtct
P70 ctgctttgatggccgaatactg
P71 aaacaaaaatatacaaatcg
P72 ccttcgctacattggaaagc
P73 catatgaaatttttaaataaagttgttttctaactgttcccaatattcttaaatcccattgaacagaatttcattttc
aaaaccctgatattttcaggaattttattccaataatatgattttgaaaaactattaatcttacctgtgcatcaata
aagatcttgtgagtatatcatcgatcacagtctccgatttgtctg
P74 ggtcttacccattccaacatcg
P75 ttcgctacattggaaagctgg
P76 cacgcctatgttcccttgtc
P77 ttcatgcgtttcaagttccg

P78	tcgattaacattttctagagtaattttgttttcccaaacaaacaaaggcgcgtcctggattcgtacaaaacata ccagatttcgatctggagaggtgaagaatacgaccacctgtacatccagctgatgagtcccaaataggac gaaacgcgctcaaacaaacaaactatccggtttttcatatttcaacttttctcct
P79	tctcccacttgaatccctctg
P80	ccaaatgttgagccagtcac
P81	ttgaggaaatgcagacgctcgttatcgacctccagatggtctccaagggagagga
P82	tgttattttgagggagccaaatgttgagccagtcagccactacctgatcccttgt
P83	gctgaaggtggatagtgtctc
P84	gagttcggaagtaaaccgtgg
P85	tcaccatctgggaggtgttcacatttggcgaggagccataggtcggctgtcgagccatcgatgtgctcaa
P86	agacgaaagggtgagaactttg
P87	cgcgaggatatgcagttcac
P88	agcattcaatcgagactgca
P89	acaagaaggaaaaaggagaa
P90	aatgcgggacaaaattagaagctttccgttctcccaaacaaacaaaggcgcgtcctggattcgtacaaaac ataccagatttcgatctggagaggtgaagaatacgaccacctgtacatccagctgatgagtcccaaatagg acgaaacgcgctcaaacaaacaaatttttccttcttgtaagaattgcacatccattag
P91	cacatggtccttcttgagtttg
P92	acggtgaggaaggaaaggag
P93	agcattcaatcaaggctaca
P94	cgaagtaaaacaattcatgt
P95	gcttcgatctttaaaaagcgaagtaaaataatttatgtcagaacgggatggagaagatccagagccgaag
P96	tggctcatggacgggaaag
P97	ggaacaggcaacgagatgg
P98	cgtggcacatactttccgttgttg
P99	gtcatctccgacgagcac
P100	ttccgttgttggcttcgttg
P101	tgcacggcgtatcaaactg
P102	ggccattgggagaacttcg
P103	tgacggcctcttctacatatcg
P104	ccgcaagtctctcctgtatg
P105	gctgaaggtggatagtgtctc
P106	attgctccgcaaatgtagtgg
P107	gctgctcaagcaaatcgaatg
P108	ttatcacggtggagaacagc
P109	ttggtagggaatcggctgg
P110	tcaaattgttgaagagatca
P111	cagcagaaaatcaaattgttgaagagatcacagctatggtctccaagggagagga
P112	cggtttccctcttctacgctcgtttcttgattttcgccactacctgatcccttgt
P113	caacgggacatggatttgag
P114	ttgaatttcccggtttccctc
P115	tgttgaagagatcacagcta
P116	cagcagaaaatcaaattgttgaagagatcacagctggtggcggtggatcgggaggaggaggttcggg tggcggaggcagtatggtctccaagggagaggaagataacatggctat
P117	taatacgactcactatagg
P118	cccacactaccatcggcgctac

P119	cactcttactgctaccaacgcttctggaagcgacaaacat
P120	atgtttgtcgcttccagaagcgttggtagcagtaagagtg
P121	tcgttgttccaggagatcagaaaacagcaactgttccaaa
P122	tttggaacagttgctgttttctgatctcctggaacaacga
P123	acccacttcacagtcgattcactcaacaagggagatcatt
P124	aatgatctcccttgttgagtgaatcgactgtgaagtgggt
P125	tagaaaaaatgagtaaaggagaagaacttttcactggagt
P126	actccagtgaaaagttcttctcctttactcatttttcta
P127	agtttgaaggtgataccttgttaatagaatcgagttaaa
P128	tttaactcgattctattaacaagggtatcaccttcaaact
P129	ggattacacatggcatggatgaactatacaaatgcccggg
P130	cccgggcatttgtatagttcatccatgccatgtgtaatcc
P131	acauuccagucaguggugaaccaacuccaacaauuacuuggacuuucgaa
P132	uucgaaaguccaaguaauuguuggaguugguucaccacugacuggaaugu
P133	ugguccuucuugaguuuguaacagcugcugggauuacacauggcauggau
P134	auccaugccauguguaaucccagcagcuguuacaaacucaagaaggacca
P135	5’Atto 565-auccaugccauguguaaucccagcagcuguuacaaacucaagaaggacca
P136	5’Atto 488-ugguccuucuugaguuuguaacagcugcugggauuacacauggcauggau
P137	aggcgacccgtgcggagccagacgtttggctatacgcctgaattcgattcgaaactaccatgaagagtgg
P138	cgtttggctatacgccggg
P139	tccgttgacagaggttacatgc
P140	agcgtcttccagcagaaatg
P141	cttcatggtagtttcgaatcgactt
P142	gctaccataggcaccgcatg